9637

NATIONAL LIBRARY
OTTAWA

CANADA

BIBLIOTHÈQUE NATIONALE
OTTAWA

NAME OF AUTHOR.....ANDRE L. ROLLIN.....

TITLE OF THESIS....."SIMILARITY LAWS AND TURBULENCE STRUCTURE OF DRAG REDUCING FLUIDS"

.....

UNIVERSITY...UNIVERSITY OF ALBERTA, EDMONTON....

DEGREE FOR WHICH THESIS WAS PRESENTED.....Ph.D.....

YEAR THIS DEGREE GRANTED.....1971.....

Permission is hereby granted to THE NATIONAL LIBRARY OF CANADA to microfilm this thesis and to lend or sell copies of the film.

The author reserves other publication rights, and neither the thesis nor extensive extracts from it may be printed or otherwise reproduced without the author's written permission.

(Signed)..André Rollin.....

PERMANENT ADDRESS:

Département de Génie Chimique
Ecole Polytechnique.....
C.P. 501, Snowdon.....
Montréal 248, Québec

DATED. August 31.....1971

NL-91 (10-68)

THE UNIVERSITY OF ALBERTA

SIMILARITY LAWS AND TURBULENCE STRUCTURE OF DRAG REDUCING FLUIDS

by

© ANDRÉ LÉO ROLLIN

A THESIS

SUBMITTED TO THE FACULTY OF GRADUATE STUDIES

IN PARTIAL FULFILMENT OF THE REQUIREMENTS FOR THE DEGREE

OF DOCTOR OF PHILOSOPHY

DEPARTMENT OF CHEMICAL AND PETROLEUM ENGINEERING

EDMONTON, ALBERTA

FALL, 1971

UNIVERSITY OF ALBERTA

FACULTY OF GRADUATE STUDIES

The undersigned certify that they have read, and recommend to the Faculty of Graduate Studies for acceptance, a thesis entitled "SIMILARITY LAWS AND TURBULENCE STRUCTURE OF DRAG REDUCING FLUIDS" submitted by André Léo Rollin in partial fulfilment of the requirements for the degree of Doctor of Philosophy.

.....
Supervisor

.....

.....

.....

Date Aug 23/71..... .....
External Examiner

SOMMAIRE

Des profiles de vitesse et de la fluctuation des vitesses en régime turbulent ont été obtenus experimentallement dans la couche limite et la région central de tuyaux circulaires à l'aide d'une méthode photographique utilisee pour mesurer les vitesses instantanées.

Les données expérimentales ont permis de déceler des erreurs d'interprétation des profiles de vitesse pour des systèmes dans lesquels une réduction de perte de charge est observée, et ont offert un appuie au phénomène d'éjections comme méchanisme responsable de la réduction de la perte de charge.

En particulier, il a été démontré que la correlation empirique présentée par Bogue doit être incorporée au profil semi-logarithmique de vitesse de Seyer-Metzner pour que les données expérimentales soient représentées par des courbes parallelles à l'équation de Prandlt.

Il a aussi été démontré que la fonction B, définie par Seyer and Metzner et présentée à la figure II-12, peut être utilisée dans les limites de faible valeurs de θ^+, mais que la valeur assymptotique de 32 n'est pas unique.

Il est apparu évident que la fluctuation de vitesses des systèmes avec diminution de perte de charge peut être plus grand ou plus petite aux systèmes Newtoniens selon la base de comparaison choisie. Les données expérimentales ont démontré que le paramètre d'échele, définit par Rudd, n'est pas aussi général que désiré.

ABSTRACT

An experimental study, based on streak photograph-determination of instantaneous velocities, was directed at determining the velocity and intensity profiles within the boundary layer and core regions of circular pipes.

The measurements resolve several discrepancies in interpretation of earlier velocity measurements in drag reducing systems by lending support to the ejection phenomena as the mechanism controlling drag reduction. In particular, it is shown that Bogue's empirical correction function must be incorporated in the semi-logarithmic velocity profiles to quantitatively represent the data of drag reducing systems. Failure to do so has led to confusion in determining the proper form of similarity law.

Study of the details of Seyer and Metzner velocity profile intercept function, defined in equation II-12, confirm the function for θ^+ up to approximately 12, but show the estimated maximum value of 32 is not unique.

Turbulence intensities may be viewed as being higher or lower than Newtonian intensities depending on the basis of comparison. The data show that Rudd's scaling factor, which superimposes his data for fixed U^*, does not account for changes in U^* and is therefore not as general as earlier anticipated.

ACKNOWLEDGEMENTS

I wish to express my gratitude and appreciation to:

- Dr. F. A. Seyer for his capable guidance during this research;
- all the technical staff of the Chemical and Petroleum Shop for its suggestions and assistance in the building of the equipment;
- Mr. Peter Smits for his assistance in building the equipment, and for his support during the photographic runs and analysing of the films;
- Mr. A. Chernick of the University of Alberta Photographic Department for his suggestions and assistance in the photographic field;
- the DACS Centre personnel of the Chemical and Petroleum Department for its assistance. Also to Ted Kizior for his helpful suggestions and assistance in computer programming;
- the National Research Council for the financial support which made this study possible;
- the Dow Chemical Company who donated the polymer;
- the personnel of the Department of Chemical and Petroleum Engineering, especially Mrs. Betty Boon and Lynda Masse for the typing.

A very special gratitude to my wife, Solange, and my daughters, Claudine and Martine; without whose understanding and support this work would not have been completed.

TABLE OF CONTENTS

LIST OF TABLES		viii
LIST OF FIGURES		ix
NOMENCLATURE		xii
CHAPTER I	INTRODUCTION	1
I-1	Mechanism of Turbulence	2
I-2	Similarity Laws and Measurement Methods	5
I-3	Proposed Work	12
CHAPTER II	THEORY	13
II-1	Probable Mechanism	13
II-2	Similarity Laws	18
	i) Velocity Profile	18
	ii) Friction Factor	20
CHAPTER III	EXPERIMENTAL	25
III-1	Flow System	25
III-2	Experimental Fluids	32
III-3	Optical System	34
III-4	Operational Procedure	39
III-5	Streak Photographs	40
III-6	Analysis of Streak Photographs	43

CHAPTER IV	RESULTS AND DISCUSSION	48
IV-1	Pressure Drop Measurements	48
IV-2	Instantaneous Velocities and Analysis of Histograms	54
IV-3	Velocity Profiles	65
IV-4	Transitional Flow	70
IV-5	Semilogarithmic Velocity Profiles	77
IV-6	Turbulent Intensities	85
CHAPTER V	CONCLUSION AND RECOMMENDATIONS	102
	BIBLIOGRAPHY	
APPENDIX		
A	RHEOLOGICAL BEHAVIOR OF THE SOLUTIONS	
B	CALIBRATION DATA	
C	ANALYSIS OF ERRORS	
D	SAMPLE CALCULATIONS	
E	TURBULENT SHEAR STRESS AND KINETIC ENERGY DATA	
F	R_o CORRELATION FACTOR DATA	
G	SURVEY ON MIGRATION OF SPHERES	
H	TABLES OF SUMMARY OF RUNS	
I	TABLES OF FRICTION MEASUREMENTS	
	SECOND BOOK WITH VELOCITY DATA	
J	COMPUTER PROGRAMS	
K	INSTANTANEOUS VELOCITY DATA	

LIST OF TABLES

		Page
III-1	Dimensions of Test-Sections	30
III-2	Time Scales of Photographic Runs	36
IV-1	Summary of all the Runs	51
A-I	Viscometric Measurements for Oil and Polymeric Solutions	A-3
A-II	Experimental Viscometric Data for 0.1% Solution	A-4
A-III	Level of Elasticity for 0.01% Solutions	A-5
A-IV	Predicted Drag Reduction	A-7
A-V	Values of B Function	A-8
B-I	Comparison of Recorded Bulk Velocity with Integrated Bulk Velocity for all Runs	B-3
B-II	Axial Magnification Data for Run 15	B-6
B-III	Axial Magnification with Change of Focus	B-6
C-I	Time Scales Versus Dissipative Frequencies	C-10
E-I	Turbulent Properties	E-2
F-I	R_o Calculated Values for all Runs	F-2
H-I	Experimental Runs	H-2
I-I	Pressure Drop Measurements	I-2
L-I	Instantaneous Velocites Data	L-2

LIST OF FIGURES

		Page
Figure II-1	Illustration of 'Bursting Process'	14
II-2	Bogue's Correction Function	21
II-3	Seyer's B Function	24
III-1	Flow System	26
III-2	Calming Section	28
III-3	Optical System	35
III-4	View Section	37
III-5	Typical Streak Photographs (Low Magnification)	41
III-6	Typical Streak Photographs (High Magnification)	42
III-7	Interpretation of Streak Photograph	44
IV-1	Friction Factor - N'_{Re}	49
IV-2	Cumulative Axial Velocities	55
IV-3	Cumulative Intensities	56
IV-4	Histograms of Axial Instantaneous Velocities for Water and Polymer	59
IV-5	Histograms of Radial Instantaneous Velocites	60
IV-6	Axial Histograms	61
IV-7	R_o Correlation Factor	63
IV-8	Velocity Profiles in 1" Pipe	66
IV-9	Velocity Profiles in 1" Pipe	67
IV-10	Velocity Profiles in 2.75" Pipe	68
IV-11	Dimensionless Velocity Profiles	69

IV-12	Velocity Profiles for 0.1% Solutions	71
IV-13	Turbulent Intermittency Factor	72
IV-14	Turbulent Intensity Profiles for 0.1% Solution Run 13	74
IV-15	Turbulent Intensity Profiles for 0.1% Solution Run 14	75
IV-16	Turbulent Intensity Profiles for 0.1% Solution Run 17	76
IV-17	Logarithmic Velocity Profiles	78
IV-18	Estimated B Function	82
IV-19	Turbulent Intensity Profile for Water - Run 4	86
IV-20	Turbulent Intensity Profile for Water - Run 5	87
IV-21	Turbulent Intensity Profile for Water - Run 9	88
IV-22	Turbulent Intensity Profile for Water - Run 11	90
IV-23	Turbulent Intensity Profile for Water - Run 15	91
IV-24	Turbulent Intensity Profile for 0.01% Solution - Run 6	93
IV-25	Turbulent Intensity Profile for 0.01% Solution - Run 10	94
IV-26	Turbulent Intensity Profile for 0.01% Solution - Run 12	95
IV-27	Turbulent Intensity Profile for 0.01% Solution - Run 16	96
IV-28	Comparison of Intensities Relative to Friction Velocity	98
IV-29	Comparison of Intensities Relative to Friction Velocity Rescaled with Rudd's Scale Factor	100

A-1	Flow Curves for Polymeric Solutions	A-2
A-2	Relaxation Time - Shear Stress	A-6
B-1	Flowmeter Calibration	B-2
B-2	Digitizer Calibration	B-5
B-3	Radial Calibration Curve - High Magnification	B-8
B-4	Radial Calibration Curve - Low Magnification	B-9
C-1	Mechanical Error of the Digitizer	C-4
E-1	Reynolds Stress and Kinetic Energy	E-3
G-1	Distribution of Air Bubbles in Pipe	G-2

NOMENCLATURE

A	slope of logarithmic velocity profiles
A	area (Appendix D)
B	intercept of logarithmic velocity profiles
$B(\theta^+)$	Seyer's function
C_3	integration constant in equation II-7
$C_3(\xi,f)$	Bogue's correction function
D	diameter of the pipe
D	Rudd's scale factor (Chapter IV)
e	error in the measured length
f	friction factor defined in equation I-4
f_3	function defined as $-A\ln\xi + C_3(\xi,f)$
$\hat{f}_2$	function defined in equation II-3
$\hat{f}_3$	function defined in equation II-4
$\hat{F}$	function defined in equation II-5
G	function defined in equation II-17
I_x, I_r	dimensionless intensities $\sigma_x/\langle\bar{u}_x\rangle_m$ or $\sigma_r/\langle\bar{u}_x\rangle m$
I_x^*, I_r^*	dimensionless intensities σ_x/U^* or σ_r/U^*
K	constant in equation IV-2
K'	consistency index defined in equation I-7
k_x, k_y	calibration constant for digitizer axis
L	length between pressure taps
M	number of divisions on the 'chopping wheel'
n	total number of observations of instantaneous velocities
n^+	number of positive radial instantaneous velocities
n^-	number of negative radial instantaneous velocities

n'	flow behavior index defined in equation I-7
N_{Re}	Reynolds number
N'_{Re}	generalized Reynolds number defined in equation I-8
p	pressure
ΔP	pressure drop measurement
Q	bulk flow rate
r	radial position from center
R	radius of the pipe
R_o	correlation factor defined in equation II-2
S_x^2, S_r^2	sample variance of the instantaneous velocity distributions
t	time
T	time scale of a streak
u_x, u_r	instantaneous velocity components
u'_x, u'_r	fluctuation term of the velocity components
$\bar{u}_x, \bar{u}_r$	time average velocity components
$\langle\bar{u}_x\rangle$	bulk velocity
$\langle\bar{u}_x\rangle_{max}$	maximum velocity at the pipe center
U^*	friction velocity defined in equation I-2
U^+	dimensionless axial velocity defined in equation I-2
V	volume
W	rotational velocity of the 'chopping wheel'
X, Y	coordinate axis on projection screen of digitizer
y	radial position from the wall
Y^+	dimensionless distance from the wall
Y_1^+	dimensionless boundary layer thickness
Z	dimensionless group defined in equation II-6

α'	parameter defined in equation I-11
γ	intermittency factor
$\dot{\gamma}$	shear rate
δ	boundary layer thickness
θ	relaxation time
θ^+	dimensionless relaxation time defined in equation I-13
μ	Newtonian viscosity
μ_x, μ_r	population mean for statistical distribution
ν	kinematic viscosity
ξ	dimensionless distance from the wall (y/R)
ρ	density of the fluid
σ_x^2, σ_r^2	population variance of instantaneous velocity distributions
τ	shear stress

Subscripts

$(\ )_i$	indicates the ith observation of instantaneous quantity
l	indicates the boundary layer thickness
m	mean value (Appendix C)
max	maximum value
r	radial direction
x	axial direction or direction of flow in pipe
w	referred to the wall

INTRODUCTION

Considerable numbers of theoretical and experimental studies, in the last 10 years, have been focused on the mechanism of turbulence in an attempt to reveal the character at the wall responsible for drag reduction observed in the presence of polymeric additives. In principle a detailed knowledge of the flow in the wall region would aid one in choosing the correct constitutive equation or variables to correlate drag reduction. Many mechanisms, as well as correlations of friction factor and velocity profiles, have been proposed. These correlations represent the available data, but none have been tested very severely over a wide range of variables. In particular the available velocity measurements in drag reducers do not provide a detailed verification of the semi-logarithmic velocity profile. Also great confusion is found from a survey of the measured relative intensities owing to the uncertainty in accuracy of the results and in how to scale or compare them for different systems.

I-1 MECHANISM OF TURBULENCE

Since Prandtl developed the 'Boundary Layer Hypothesis' in 1904, many studies of properties of Newtonian turbulence (19,21,14, 28,45,16,18,38) have indicated that the character of the flow in the wall region was responsible for most of the creation and dissipation of the turbulent energy.

It is only recently that a detailed physical picture of the mechanism was presented, mainly by the work of Bakewell and Lumley (3), Kline et al (20) and Corino and Brodkey (7). Bakewell and Lumley indicated that the dominant large scale structure of the flow in the boundary layer consists of randomly distributed counter-rotating longitudinal eddy pairs of elongated extent in the flow direction. The structure of these eddies was inferred from space-time correlation functions of the fluctuating velocities. The streamlines of these eddies were pictured as to push low momentum boundary layer fluid toward the core region, so that the renewal of fluid was by flow in the circumferential direction.

Qualitatively similar patterns of flow in the wall region were visualized by Kline et al using a dye ejection technique and in more detail from tracer photographs by Corino and Brodkey. Ejections of fluid, originating from a low velocity region adjacent to the viscous sub-layer, were responsible for extracting energy from lumps of fluid originating in the main flow and converting it into turbulent energy. They observed that these ejections were of large scale and moved through the boundary layer until broken down to small scale turbulence by mixing with the main flow.

The simple mechanism of turbulence then is that the turbulent shear stress is generated by the radial transport of low momentum fluid by the large eddies or 'bursts'. The magnitude of the stress is determined by the rate of fluid transported radially as well as its axial momentum. The rate of fluid transported in turn depends on the frequency of occurrence of the eddies as well as their size. The visual studies of wall turbulence provide a starting point for interpreting turbulence measurements in drag reduction.

Many mechanisms have been suggested in order to explain the drag reduction for flow of viscoelastic fluids in pipes (32,39). Generally it is agreed that elasticity of the fluid is responsible for the drag reduction. Furthermore, as emphasized by Wells and Spangler (42) who showed by injection of polymer in the boundary layer that drag reduction is controlled by the flow in the wall region, the elasticity must modify turbulence in the wall region.

From a continuum point of view, Seyer and Metzner (17) have shown that the drag reduction can result from the resistance to flow caused by stretching in the large eddies or 'bursts'. Although their arguments are based on a steady state analysis of eddies as pictured by Bakewell, Denn and Porteous (9) have shown identical ordering parameters appear if a transient analysis of the eddies is carried out. It is difficult to say what the effect of resistance to flow is on the structure of the eddy. For example, the eddies may be increased in size which would appear as a thickening of the boundary layer or they might be reduced in frequency. These points of view also have resulted in dimensionless groups which are the same as for

stretching arguments (24,17) but do not show conclusively what alterations in the structure have occurred.

II-2 SIMILARITY LAWS AND MEASUREMENT METHODS

For drag reducers, apart from completely empirical formulations, most studies have sought to modify the Newtonian similarity laws, so that they described drag reduction. For Newtonian fluids, Millikan (27), for example, has shown from a dimensional analysis that the velocity profile law is

$$U^+ = A \ln Y^+ + B \qquad \text{I-1}$$

where

$$U^+ = \bar{u}_x/U^*$$

$$Y^+ = yU^*/\nu \qquad \text{I-2}$$

$$U^{*2} = \tau_w/\rho$$

$$\tau_w = D\Delta P/4L$$

The generally accepted values for A and B for Newtonian fluids are (5) $A = 2.46$ and $B = 5.6$

Equation I-1 is an accurate representation of all consistent Newtonian data for Y^+ less than 400, but considerable deviation occurs for larger Y^+. Correction factors have been empirically found (18, 5, 27). Bogue's correction factor represents the best fit of available data and is defined as

$$C_3(\xi,f) = 0.05\sqrt{\frac{2}{f}}\, e^{-\frac{(\xi-0.8)^2}{0.15}} \qquad \text{I-3}$$

where $\xi = y/R$

and the friction factor

$$f = \tau_w / \frac{1}{2} \rho \langle \bar{u}_x \rangle^2 \qquad \text{I-4}$$

With Bogue's correction factor the form of the velocity profile for Newtonian fluids is then

$$U^+ = a \ln Y^+ + B + C_3(\xi, f) \qquad \text{I-5}$$

From Equations I-4 and I-5, the friction factor relation for Newtonian fluids follows directly

$$\frac{1}{\sqrt{f}} = A \ln (N_{Re}\sqrt{f}) - 0.4 \qquad \text{I-6}$$

For fluids represented by a power law model in which

$$\tau_w = K' \left(\frac{8\langle \bar{u}_x \rangle}{D}\right)^{n'} \qquad \text{I-7}$$

Dodge and Metzner (10) formulated the friction factor correlation based on the generalized Reynolds number

$$\frac{1}{\sqrt{f}} = \frac{4.0}{(n')^{0.75}} \log \left(N'_{Re}\, f^{1-\frac{n}{2}}\right) - \frac{0.40}{(n')^{1/2}} \qquad \text{I-8}$$

where the generalized Reynolds number

$$N'_{Re} = \frac{D^{n'} \langle u_x \rangle^{2-n'} \rho}{K' 8^{n'-1}}$$

Notice Equation I-8 is simply a generalization of the Newtonian Equation I-6 to account for the non-Newtonian properties. Similarly,

Bogue (5) measured velocity profiles for pseudoplastic fluids and formulated the velocity profile equation such that

$$U^+ - C_3(\xi,f) = 5.57 \log (Y^+)^{1/n'} + I(n',N'_{Re}) \qquad \text{I-10}$$

where I is a weak function of n', N'_{Re}.

Equation I-10 when plotted gives a family of parallel curves to Newtonian fluid with slope A = 2.46 for the core region with intercept higher as n' decreases and N'_{Re} decreases. He also found that turbulent velocity profiles for purely viscous non-Newtonian fluids are essentially the same as those for Newtonian fluids when normalized to the mean velocity.

For drag reducing fluids it is obvious that one of the major effects appears as an increased intercept. Based on Pitot tube measurements, Elata et al (11) modified the law of the wall by incorporating an extra logarithmic term to interpret the higher intercept such that

$$U^+ = A \ln Y^+ + 5.5 + \alpha' \ln \left[\frac{U^{*2}\theta}{\nu_w}\right] \qquad \text{I-11}$$

In this equation, A is assumed the same as for Newtonian fluids and the effect of the elasticity of a solution is expressed by the relaxation time θ which is assumed constant. The parameter α' is an empirical function of the polymer characteristics and the concentration. The equation for the friction factor that follows is then

$$\frac{1}{\sqrt{f}} = \frac{(\alpha'+A)}{\sqrt{2}} \ln (N_{Re}\sqrt{f}) - 0.4 + \frac{\alpha'}{\sqrt{2}} \ln \left(\frac{\theta\nu_w}{D^2}\right) \qquad \text{I-12}$$

For a given flow rate and polymer, equation I-11 plots as a parallel line to the Newtonian curve. A detailed examination of the

data indicate however (especially for large amounts of drag reduction) that the parallel lines are only a crude representation of the data. Alternatively if the best fit straight line is drawn through a given velocity profile an increase of the slope A would be necessary.

A number of other studies, based on Pitot tube readings (49, 11, 26,12) have subsequently shown velocity profiles which are qualitatively similar to Elata's.

In all these, owing to the large quantitative uncertainty in the Pitot readings, it is impossible to determine if the slope is actually different or if modified slope simply reflects errors in the Pitot readings. It has been shown for laminar flows (2) that the Pitot tube measurements in a viscoelastic fluid are made up not only of the kinetic contribution but also largely influenced by normal stresses. The magnitude of the normal stress contribution depends on the local shear rate or radial position and so the Pitot readings may not even determine the correct shape of velocity profile. In turbulent flows the flat velocity profile in the core region would tend to hide the effect of shear rate but would be serious near the wall.

Nicodemo et al (29) have presented velocity profiles using a probe calibrated in a tow tank. It was decided that the velocity profiles could not be interpreted according to Bogue's equation I-5 by a simple increase in intercept. Although the check of integrated and measured flow rates is one of the few studies showing good agreement, this check is a very insensitive one for shape of profile. It should be noted their calibration does not indicate the magnitude of any contributions owing to turbulence.

Similar uncertainties occur in the case of heated probles (25,13,23,33,40). As well indicated by the recent study of Serth and Kiser (40) errors as large as 250% in determination of velocity can occur. Generally these studies indicate directly there is an undetermined quantitative uncertainty in all reported velocity and turbulence measurements utilizing either pitot or heated probes. Qualitatively there may even be errors in shape of profile owing to changes in probe response with radial position.

In 1969 Seyer and Metzner (43) presented experimental velocity profiles obtained from a photographic method which it is significant to note, are free from the uncertainties of Pitot or other probes. A theoretical analysis similar to the arguments of Millikan (27) and Dodge (10) was used to show that

$$U^+ = A \ln Y^+ + B(\theta^+)$$

where $$\theta^+ = \theta U^{*2}/\nu \qquad \text{I-13}$$

and $$\sqrt{\frac{2}{f}} = A(1-\xi)^2 \ln (N_{Re}\sqrt{f}) + (1-\xi_1)^2[B(\theta^+) - A \ln 2\sqrt{2}] - G \qquad \text{I-14}$$

where ξ_1 is the boundary layer thickness (dimensionless) and G is assumed a constant equal to 3.0. Details of this analysis and some modifications will be presented in Cahpter II.

In the limit for ξ^+ and θ_1 going to zero these equations reduce the usual equations for Newtonian fluids (I-1 and I-6). For drag reducers the form of the equations is the same as Elata's with the exception of the intercept function.

Seyer's measurements as well as some later ones in a square tube by Rudd with a Laser Doppler Meter (36), are in excellent agreement with I-13. In each of these studies however a velocity profile was obtained at only one flow rate in a given tube for turbulent flow conditions. Therefore they do not provide a detailed verification of the form of equations I-13 and I-14 nor of the limits of applicability.

Seyer's measurements in a one-inch tube show that transitional flow occurs to Reynolds numbers in excess of 10^5 for what have been termed concentrated or maximum drag reducers. At high Reynolds numbers the function factors seem to approach an asymptote defined by a constant value of $B(\theta^+) = 32$. Virk et al (47) have published a number of papers which consider a different maximum drag reduction asymptote. Based on data from a number of sources of friction measurements it was found that

$$\frac{1}{\sqrt{f}} = 19 \log N_{Re} \sqrt{f} - 32.4 \qquad \text{I-15}$$

Seyer's friction data in transitional flow follow closely to the friction factors defined by equation I-15. The corresponding "ultimate velocity profile" is

$$U^+ = 11.7 \ln Y^+ - 17 \qquad \text{I-16}$$

Notice this is a much higher slope than for Newtonian fluids and has a negative intercept.

The transitional flow velocity profiles suggest the interpretation of I-16 is incorrect. In fact in the final limit the

profiles would be laminar over the entire tube cross section. Laminar (parabolic) profiles on $U^+ - Y^+$ coordinates are easily shown to be a family of parallel curves depending on the Reynolds number. For positions near the center, the curves can be approximated by equations like I-16 with large slope and negative intercept as determined by the Reynolds number. The transition profiles on these plots are qualitatively similar. Thus Virk's constants may simply reflect the transitional nature of the velocity profiles. In the absence of defined limits of transitional flow however, little more can be said about the correct interpretation of the velocity profiles for transitional flow. Clearly these questions are of prime importance in formulating the correct similarity laws and their limits of applicability.

I-3 PROPOSED WORK

In this work it is proposed to extend Seyer and Metzner's optical method of measurements in order to obtain instantaneous velocities, both axial and radial, which will provide a detailed test of the available similarity laws. The wall region as well as the core region will be investigated with different concentrations of polymeric solutions for different pipe sizes.

The statistical properties of the instantaneous velocities will be used to comment on the 'bursting phenomena', and any change in its structure, owing to the presence of polymers.

THEORY

II-1 PROBABLE MECHANISM

As previously mentioned, the recent physical interpretation of turbulence, presented by Corino and Brodkey and based on the observation of a 'bursting phenomena' present in the wall region can serve as a basis to analyse the data collected in this work. Figure II-1 shows schematically a lump of fluid originating in the main flow and entering at a small angle into the boundary layer with an axial velocity component corresponding to the average velocity of its origin. A second lump of fluid located in the boundary layer and possessing a lower velocity is then accelerated by the excursion and shear stresses start to build until one or more ejections occur. Because the origin of the ejections is assumed to be in a region of low momentum situated approximately at a Y^+ of 10, the axial velocity components of the ejections are expected to be smaller than those of the accelerating lumps. Corino and Brodkey observed that the ejected fluid, although accelerated in the axial direction, never reached the axial component of the main flow adjacent to the boundary layer.

ILLUSTRATION OF BURSTING PROCESS

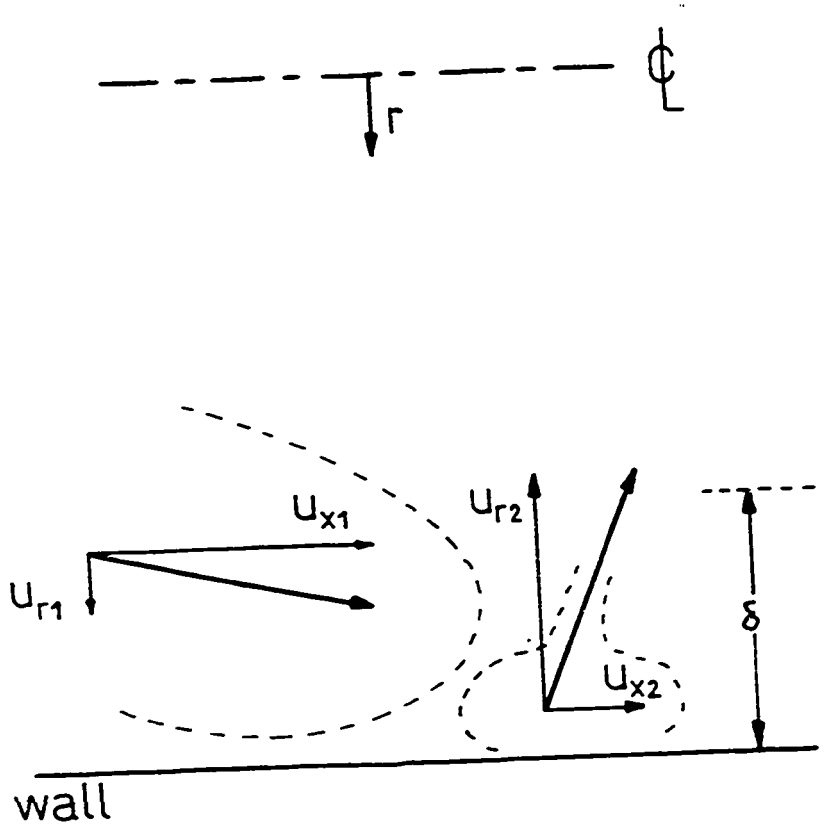

FIGURE II-1

Denoting u_{x1} and u_{r1} as the velocity components of the lump of fluid entering the boundary layer and u_{x2} and u_{r2} for the ejection velocity components, one should expect to find

$$\bar{u}_{x1}(r) > \bar{u}_{x2}(r) \qquad \text{II-1}$$

where

$$\bar{u}_x(r) = \frac{1}{n}\sum_{i=1}^{n}(u_x(r))_i$$

$\bar{u}_x(r)$ can represent the time average velocity at a fixed radial position if sufficient readings are taken (of instantaneous velocities) at random times. Thus a histogram of the axial instantaneous velocities, at a fixed radial position, should be composed of two distributions. Using a flash photolysis method, Popovich and Hummel (33,34) measured velocity profiles which showed a binodal distribution of the axial instantaneous velocities in the boundary layer with the peak of lower axial velocities becoming more pronounced at positions nearer the wall. This simply shows the influence of the velocities of fluid originating near the wall dominates the flow in that region.

The ejection phenomena approach taken in this work can explain, in more detail, the presence of dual distributions than the Popovich analysis, which is based on elements of fluid being directed toward the wall and others directed toward the center.

Each positive (directed toward the wall) radial velocity is associated with a u_{x1} while a negative radial velocity is associated with u_{x2}. The velocity histograms can then be split according to whether the instantaneous radial velocity is positive or negative.

According to the bursting analysis, instantaneous negative radial velocities should be larger than the positive components. Thus to obtain a zero time averaged radial velocity (the sum of all observed components) the positive components must be observed more often than the larger negative components. Defining

$$R_o = n^+/n^- \qquad \text{II-2}$$

where

n^+ is the observed number of u_{r1}

n^- is the observed number of u_{r2}

then R_o is expected to be greater than unity in the boundary layer and approximately equal to unity in the core region. Also if the velocity of ejection is dependent on radial position, as Corino and Brodkey observed, an acceleration of the fluid during the trajectory from its origin to the radial position where it is broken up by the main flow, implies the presence of a peak in the plot of R_o versus dimensionless radial position. This peak should occur in the vicinity of the edge of the boundary layer.

In summary, an analysis of the histograms of axial and radial components of the instantaneous velocities at a radial position in the boundary layer should provide information about the mechanism of ejection. Also it should explain the presence of the binodal distributions in the boundary layer, if these distributions are split according to the direction of the radial component. In the case of drag reducers the available data, although in doubt quantitatively, show that the turbulence is similar to Newtonian turbulence. The

drag reduction, therefore, is probably a result of modifications to the ejection process. For example, if the boundary layer is thickened appreciably, then the peak in R_0 ought to appear at greater values of Y^+ than in the Newtonian case.

In the ejection process, earlier studies (37,43) suggest the increased resistance to stretching causes the radial fluctuations to decrease. Although in the work of Seyer and Metzner, where the ideal case of steady stretching was treated, the same conclusion, that is an increased resistance to stretching, follows from a consideration of the transient motion (8). In Figure II-1 the resistance to sudden deformations would

(i) decrease u_{r_2} at a given point,

(ii) not affect appreciably u_{r_1} and u_{x_1}, because the direction of these larger lumps of fluid are nearly parallel to the flow direction (no stretching in the axial direction),

(iii) implies a lower radial variance from a combination of (i) and (ii) (u_{r_1} not affected, and u_{r_2} decreased).

One cannot predict the change in u_{x_2} but if a decrease results, as might be expected if the sublayer thickens appreciably, then higher axial intensity would result.

Similarly, however, the data of Meak and Baer (24) and Fortuna and Hanratty (15), show the frequency of occurrence of the ejection decreases in polymers. This would also decrease the radial intensity. Unfortunately, the method used in this work cannot distinguish directly which cause is effective in altering the intensity.

II-2 SIMILARITY LAWS

A) Velocity Profiles

Assuming the relaxation time as the characteristic time scale of viscoelastic solutions, Seyer and Metzner (43) introduced the relaxation time as an additional parameter in the wall region where the stretching is assumed to occur. They performed an analysis, similar to Millikan (27), to obtain the logarithmic velocity profile.

The velocity in the boundary layer can be expressed as

$$\bar{u}_x = \hat{f}_2 (\tau_w, y, \rho, \mu, \theta) \qquad \text{II-3}$$

and in the core region as

$$\langle \bar{u}_x \rangle_m - \bar{u}_x = \hat{f}_3 (\tau_w, R, y, \rho) \qquad \text{II-4}$$

so that for the entire section of the pipe

$$\bar{u}_x = \hat{F} (\tau_w, R, y, \rho, \mu, \theta) \qquad \text{II-5}$$

Notice that the fluid parameters should be estimated at the wall shear stress value. Introducing the following dimensionless group

$$Z = RU^*/\nu \qquad \text{II-6}$$

and using those already defined (in Chapter I), the following equations for the core and the wall regions can be found from a dimensional analysis

$$\frac{\langle \bar{u}_x \rangle_m - \bar{u}_x}{U^*} = - A \ln \xi + C_3 \qquad \text{II-7}$$

and

$$\bar{u}_{x_m}/U^* = A \ln Z + B(\theta^+) \qquad \text{II-8}$$

when combined, the expression for the overlapping region is obtained

$$U^+ = A \ln Y^+ + B(\theta^+) - C_3 \qquad \text{II-9}$$

Extensive study was performed by Bogue (5) to find an expression for the C_3 factor. C_3 must be a function of ξ to permit equation II-7 to hold for the entire region. It must be zero at the centerline and contribute approximately 10% to values of the velocity defect for ξ smaller than 0.3 as shown by Bogue. In equation II-9 the correction function may be written in the form

$$C_3(\xi,f) = 0.05\sqrt{\frac{2}{f}}\, e^{-\frac{(\xi-0.8)^2}{0.15}} \qquad \text{II-10}$$

so that the corrected velocity profile becomes

$$U^+ = A \ln Y^+ + B(\theta^+) + C_3(\xi,f) \qquad \text{II-11}$$

and where for Newtonian fluids A = 2.46 and B(0) = 5.6. Assuming, as an approximation, a linear profile in the boundary layer and neglecting $C_3(\xi,f)$ for small ξ, Equation II-11 becomes

$$Y_1^+ = A \ln Y_1^+ + B(\theta^+) \qquad \text{II-12}$$

and serves to define the boundary layer thickness.

Figure II-2 shows the $C_3(\xi,f)$ function increasing with increasing wall distance, ξ. It can be observed that the function increases in value as the friction factor decreases, indicating that, if applicable, the correction becomes more important for drag reducers. Because of the passive role of the core region when drag reduction occurs, as shown experimentally by Wells and Spangler (48) and suggested by the bursting arguments, the same function may apply for viscoelastic fluids.

B) Friction Factor

In order to express the friction factor defined in Equation I-4 , the bulk velocity is obtained from the integrated profile which can be divided into the boundary layer region and the core region

$$\langle \bar{u}_x \rangle = \frac{2}{R^2}\left[\int_0^{\delta} r\, u_{xL}(r)\, dr + \int_{\delta}^{R} r\, u_{xc}(r) dr \right] \qquad \text{II-13}$$

In terms of the dimensionless radial position

$$\langle \bar{u}_x \rangle = 2\int_0^{\xi_1} (1-\xi) u_{xL}(\xi) d\xi + 2\int_{\xi_1}^{1} (1-\xi) u_{xc}(\xi) d\xi \qquad \text{II-14}$$

where

$$\xi_1 = \delta/R$$

Assuming a linear profile in the wall region and using the defect law for the core region, one can obtain

FIGURE II-2

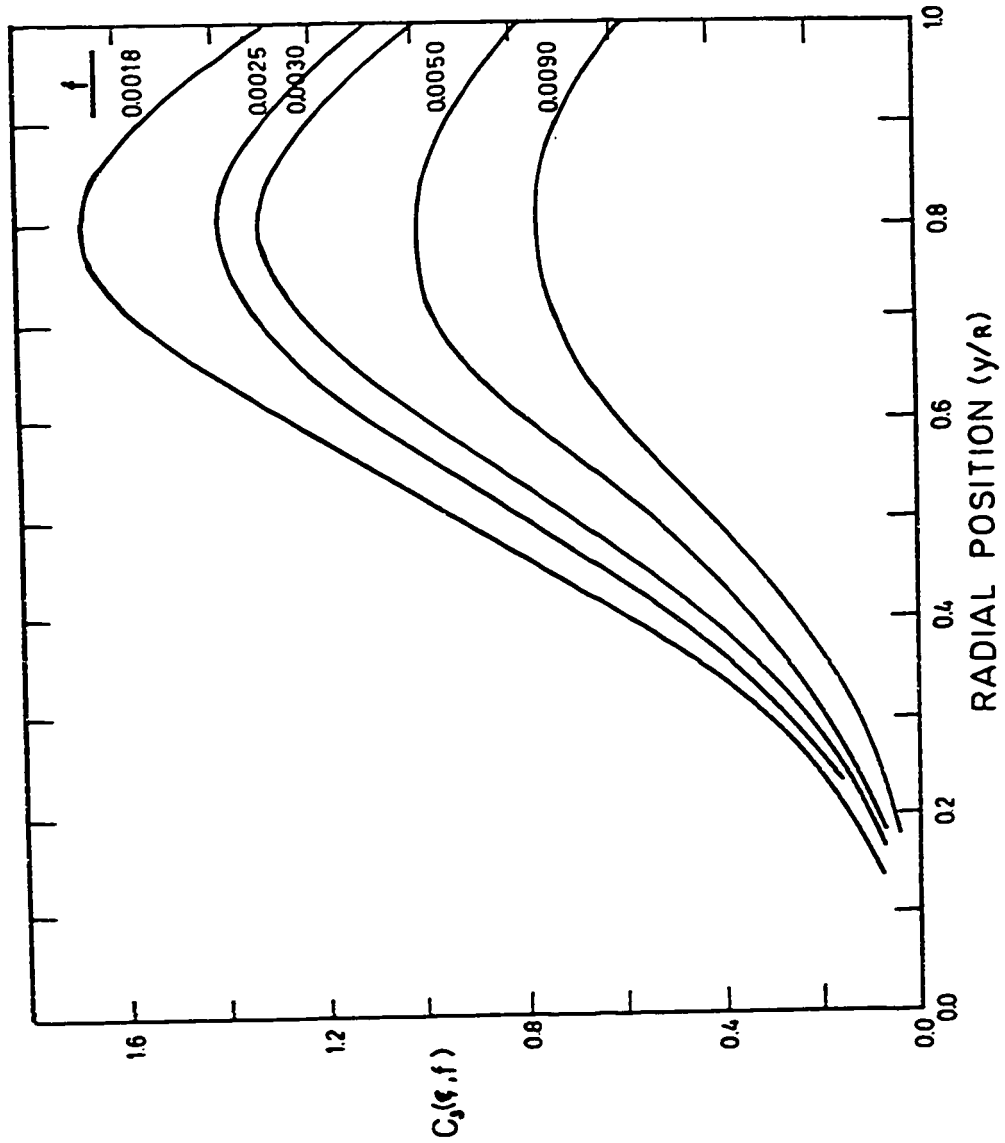

BOGUE'S CORRECTION FUNCTION

$$\frac{\langle\bar{u}_x\rangle}{2} = \frac{RU^*}{\nu}^2\left[\frac{\xi_1^2}{2} - \frac{\xi_1^3}{3}\right] + \frac{\langle\bar{u}_x\rangle_m}{2}(1-\xi_1)^2 - U^*\int_{\xi_1}^{1}(1-\xi)f_3(\xi)d\xi \qquad \text{II-15}$$

Combining Equations I-4 and II-15 and grouping terms, the following expression is obtained

$$\sqrt{\frac{2}{f}} = A(1-\xi_1)^2 \ln(N_{Re}\sqrt{f}) + (1-\xi_1)^2[B(\theta^+) - A \ln 2\sqrt{2}]$$

$$- G(\xi_1, \frac{RU^*}{\nu}, f) \qquad \text{II-16}$$

which is the same as Seyer's equation (41)except that G is now also a function of f. The function G can be expressed as

$$G = 2\int_0^1 (1-\xi)f_3(\xi)d\xi - 2\int_0^{\xi_1}(1-\xi)f_3(\xi)d\xi - \xi_1^2\frac{RU^*}{\nu} \qquad \text{II-17}$$

where

$$2\int_0^1(1-\xi)f_3(\xi)d\xi = -2A\left[\int_0^1 \ln\xi\, d\xi - \int_0^1 \xi \ln\xi\, d\xi\right]$$

$$+ 2\int_0^1 C_3(\xi,f)d\xi - 2\int_0^1 C_3(\xi,f)\xi\, d\xi \qquad \text{II-18}$$

In Equation II-18 with A = 2.46

$$2A\left[\int_0^1 \ln\xi\, d\xi - \int_0^1 \xi \ln\xi\, d\xi\right] = -3.6 \qquad \text{II-19}$$

The curves of Figure II-2 are used to graphically integrate the remaining terms of Equation II-18 involving $C_3(\xi,f)$ giving a value of 0.40 for the case of a very low friction factor of 0.003 where $C_3(\xi,f)$ is

largest. Because the correction factor, $C_3(\xi,f)$ is zero for small values of ξ, the remaining terms of Equation II-17 are not influenced by the correction factor. Therefore, since G is a minor term in Equation II-16, the dependence of G on f, as determined by $C_3(\xi,f)$, is negligible.

Figure II-3 shows the B function evaluated from friction factors and velocity profiles by Seyer (41) for solutions of Separan AP-30 for 1" and 2" pipes at three different concentrations. From Figure II-3 it can be observed that the function reaches an asymptotic value of approximately 32.2 for θ^+ greater than 20. If this function is unique for all viscoelastic fluids and pipe sizes, then maximum drag reduction will be reached whenever θ^+ is greater than 20. The only limitation on the use of Equation II-11 is the dividing point between turbulent and transitional flow.

The limits of transitional flow must be related to the thickening of the sublayer. The definition of sublayer thickness given by Equation II-12 shows how it depends directly on the elasticity of the system. Clearly the sublayer must be less than the tube radius for turbulent flow to occur, but the question of an exact value needs further investigation. In the case of Newtonian fluids the maximum sublayer thickness is approximately $\xi = 0.1$ (at N_{Re} of 2100).

FIGURE II-3

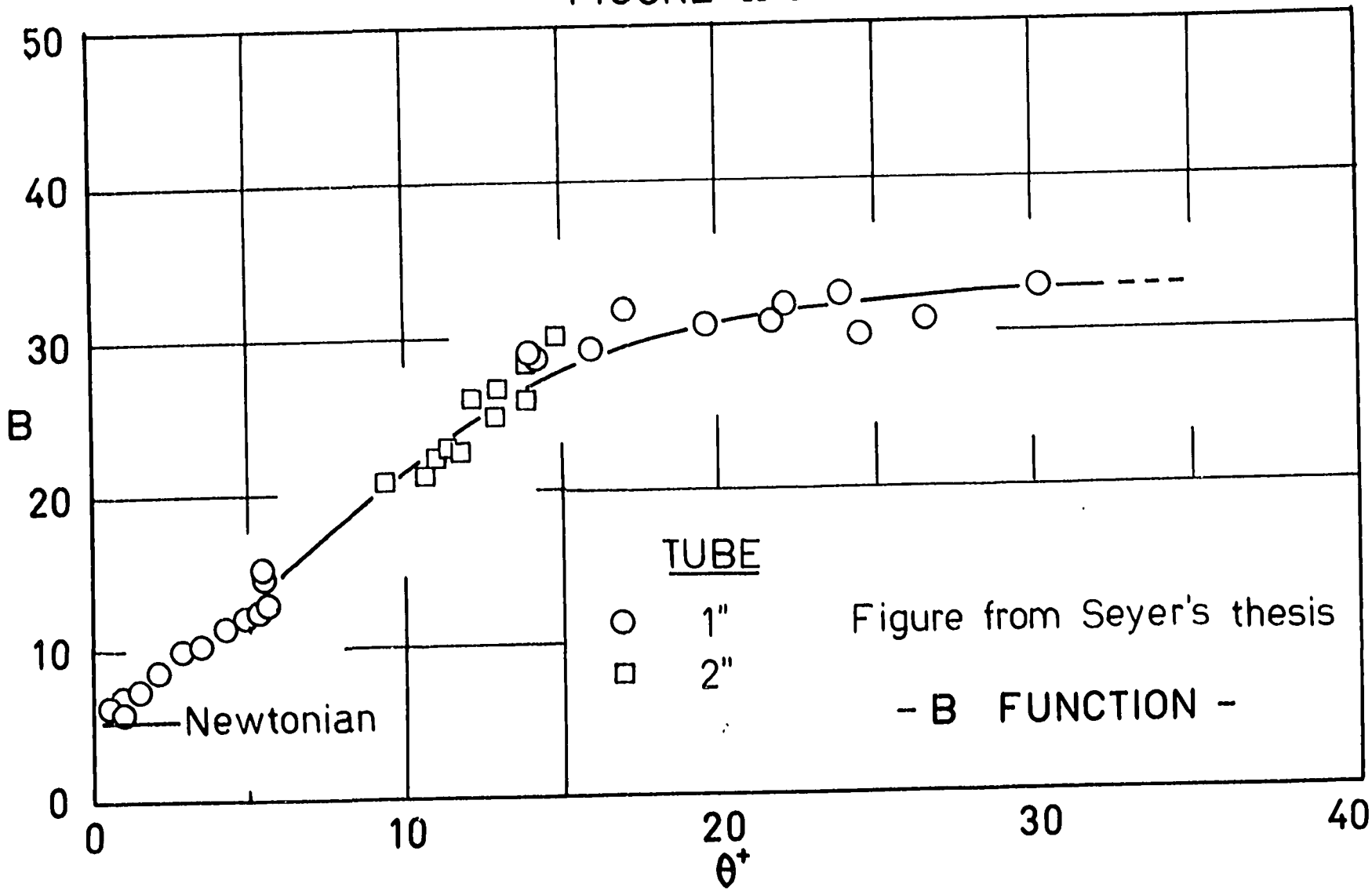
50
40
30
20
10
0
B
0
10
20
30
40
θ+
Newtonian
TUBE
1"
2"
Figure from Seyer's thesis
- B FUNCTION -

EXPERIMENTAL

An optical method of measurement was used to obtain streak photographs of small air bubbles in the water and polymeric solutions in order to measure instantaneous velocities in the boundary layer and core regions. As mentioned before, this method does not suffer from the uncertainties inherent in pitot tube and heated probe measurements.

III-1 FLOW SYSTEM

The flow system, as shown schematically on Figure III-1, consisted of a closed circuit in which the fluid could be pumped through a test section and returned to a 300 gal. stainless steel storage tank. A variable speed Lightnin mixer and a coil were attached to the tank to regulate the level of degradation and the operational temperature of the Separan AP-30 solutions. Two Moyno positive displacement pumps, each with a maximum delivery capacity of 200 gal/min permitted measurement of pressure drop over an extended range of flow rates. A 2" I.D. Foxboro magnetic flowmeter recorded the flow rate passing through the test section.

A variable pressure Desurger following the pump exit damped the flow fluctuations caused by the positive action of these pumps. Nominally the desurger pressure was set for the photographic runs at 75% of the pump discharge pressure. A calming section of 6" I.D. and 6' long containing a baffle plate was inserted before the test section in order to fulfill four requirements:

i) injection point of the tiny air bubbles used as tracers,

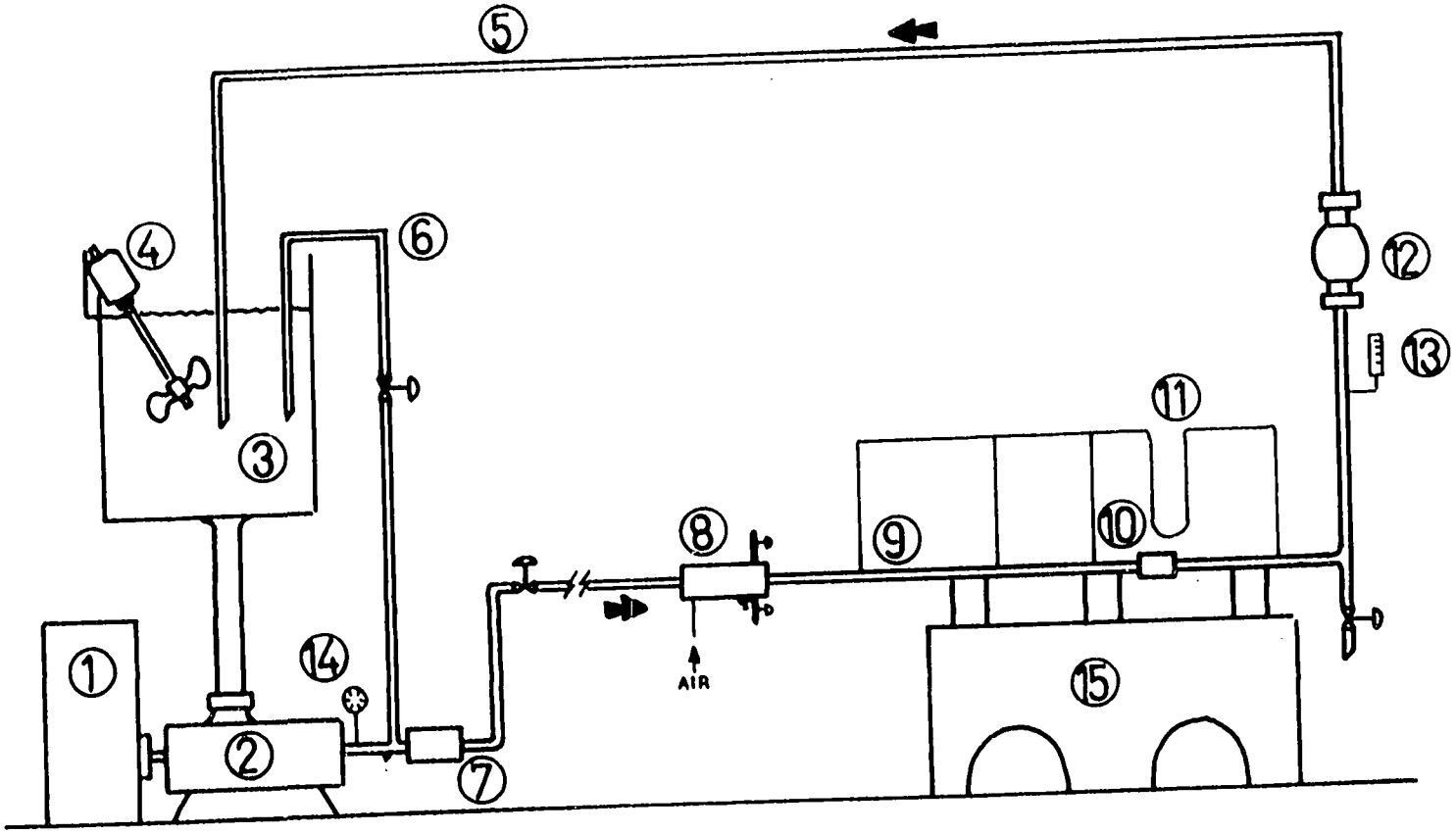

- FLOW SYSTEM -

FIGURE III-1

ii) trapping of the dirt particles in the system,

iii) trapping of large air bubbles,

iv) calmed the fluid and uniformly distributed the tracers in the fluid.

Air bubbles injected into the fluid flow were used as tracers. The injection point was situated in the calming section in front of the baffle plate (see Figure III-2). The number and size of the air bubbles were adjusted by a needle valve and a porous chamber located inside the calming section. This variable-position porous chamber allowed the bubbles to be mixed completely in the flow by locating it in the large eddies formed at the front of the plate. Additionally, since the velocity of the flow was very small in this 6" section, large air bubbles migrated to the top where they could be purged from the system. Simultaneously, dirt and rust particles, which caused a loss of contrast in photographs, could be collected at the bottom.

These variables were adjusted to obtain an average diameter of the bubbles of approximately 0.002". The maximum observed diameter of photographed bubbles was 0.0041" in diameter, which is smaller than the smallest turbulence scale. In all cases, however, readings of the large bubbles (0.004") were rejected.

The maximum percentage volume of air in the fluid was calculated using photographs obtained at an exposure time of 1/1000 second for run 14. On the average, 18 bubbles appeared per frame, between the wall and the center of the pipe. A percentage of air by volume, the maximum relative to the size of the bubbles and to the

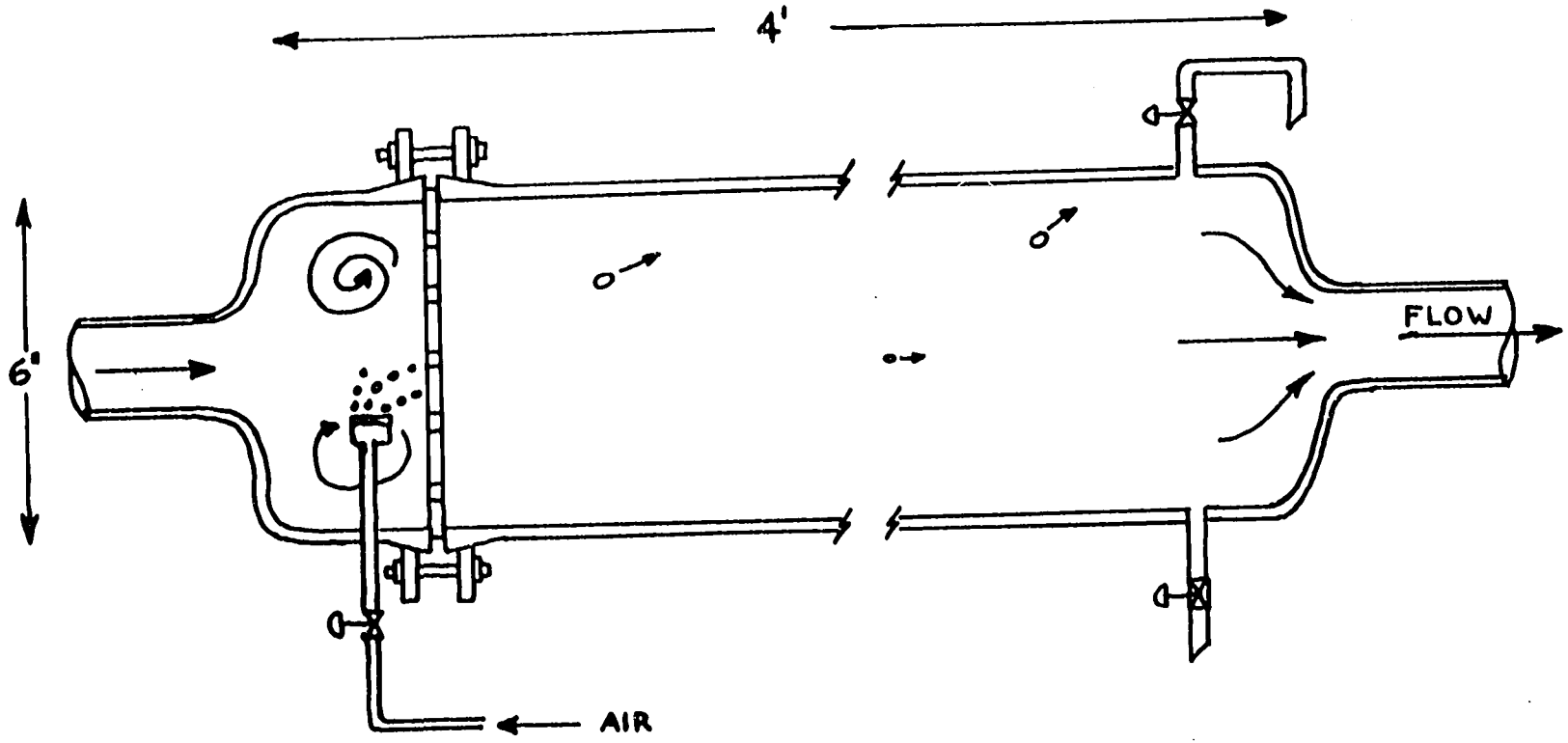

- CALMING SECTION -

FIGURE III-2

estimated volume of fluid, was then calculated, using 0.004" as the diameter of the bubbles. Thus all bubbles are assumed to be of maximum size in the photographed volume of

$$V_{fluid} = 0.5" \times 0.752" \times 0.0592" = 0.0222 \text{ in}^3$$

The volume of air is

$$V_{air} = 18(0.524 \times 0.004^3) = 604 \times 10^{-9} \text{ in}^3$$

and therefore

$$\% \text{ volume of air} = (604 \times 10^{-9}) \times 100/0.0222 = 0.00272$$

which is considered negligible. It is interesting to note that, at the position where photographs were obtained, the air bubbles were found to be unevenly distributed in the illuminated cross section of the pipe. A maximum concentration occurred at a radial position r/R = 0.890 (see Appendix G for the experimental distribution curves of radial concentration).

Two different systems of test section were designed in order to study the diameter effect present with drag reduction. The first system consisted of precision bore pyrex tubes of 1" inside diameter and the second system consisted of standard plexiglass pipes of 2.75" inside diameter (dimensions of these systems can be found in Table III-1). It may be noted in Table III-1 that, in the case of the second system, part of the 1" tube was used and connected as a bypass, in order to measure pressure drops and determine the level of degradation of the solutions being used in the 2.75" pipe.

TABLE III-1

TEST SECTIONS

	System I	System II	
Nominal diameter (inch)	1	1	2.75
Material	pyrex bore	pyrex bore	plexiglass
Inside diameter (inch)	1.0 ± 0.0015	1.0 ± 0.0015	2.75 ± 0.005
Total length (ft)	28	21	36
Entry length to optical box L/D	187	--	114
Entry length to first pressure taps L/D	54	66	60
Pressure taps-hole diameter (inch)	0.025 ± 0.005	0.025 ± 0.005	0.020 ± 0.005
Length between pressure taps (in ft)			
(1)-(4)	22	--	23.60
(2)-(4)	16	12	17.50
(3)-(4)	11	6	11.69

Four sections of precision bore 1" tubes 7 feet in length were connected and clamped on a lathe bed in order to cut down vibrations originating mainly from the pump. Great care was taken to ensure that the upstream joints presented no discontinuity to disturb the flow. This was done by inserting a Teflon plug, 0.995" in diameter and 3" in length, inside the tubes at the joint before connecting two sections together. Four pressure taps were used and connected to two 60" manometers containing Mercury and O-Dichloro Benzene of density 1.305.

Similarly, in replacing the 1" system, the 2.75" sections were carefully jointed and clamped to the lathe bed. Three pressure taps were connected to the same manometers. The justification for the many pressure drop measurements along the pipe was to check the reproducibility of the measurements and also to verify that the large entry length (δ) had been exceeded at the optical section.

III-2 EXPERIMENTAL FLUIDS

The drag reducing fluid chosen for the entire work was a polyacrylamide product of Dow Chemical Co., named Separan AP-30. This granular white powder, of an estimated molecular weight between 2 and 3 million, possesses elastic properties when in solution with water. It was preferred to other polymers because of its known level of drag reduction which can be found in previous works (30,43).

Two different weight concentrations were used: the 0.01% (dilute) and the 0.10% (concentrated). Physical properties of these solutions are presented in Appendix A. The viscous properties of the 0.01% solutions showed that their behavior can be assumed to be Newtonian with a kinematic viscosity of 1.2×10^{-5} ft^2/sec at room temperature.

To ensure the same degradation level for all of the final data, a new solution was prepared for each run and the following procedure was used. A mechanical degradation by shearing in the 1" pipe at a high flow rate was followed until the recorded pressure drop measurements reached the drag reduction level desired. The desired level was determined arbitrarily by a master curve of pressure drop versus flow rate in the 1" pipe which had been determined so that enough drag reduction could be obtained in the 2.75" pipe. Then the photographic run was started with a check of pressure drop before, in the middle, and at the end to assure that negligible degradation occurred. A slightly different procedure was followed for the determination of the level of degradation of the solutions used in the 2.75" pipe. Here the solutions were degraded in the 1"

pipe to the desired level, the flow was then diverted to the 2.75" pipe for readings of pressure drop and photographs taken. This ensured that drag reduction and velocity measurements in the 2.75" pipe would be at the same level of degradation as measurements in the 1" pipe. Friction measurements were also checked at the end of a photographic run in the 2.75" pipe by additional measurements in the 1" pipe.

III-3 OPTICAL SYSTEM

The main features of the optical system shown in Figure III-3 are

i) a light source which illuminated a thin horizontal portion of the pipe cross section,

ii) a chopping disk for the determination of the time scale,

iii) an optical box,

iv) a camera assembly.

The instantaneous velocities of the fluid in the pipe were determined by photographing the air bubbles sweeping through the narrow light beam located at the center of the pipe. A three phase 'Christie' transformer of D.C. maximum output of 3300 watts at 100 amps operated a 'Christie' Xenon arc-lamp. The converging mirrors in the lamp-housing, No. BSF 50, were positioned to direct the light beam through the view section of the pipe. An adjustable slit was placed immediately in front of the lamphousing lens to produce a narrow beam, and converging lenses used after to adjust the light beam to a thickness smaller than the slits on the chopping disk.

Aluminum disks of 15" in diameter and 1/8" thick were assembled on three phase motors to obtain constant rotational speed. In order to interrupt the light and provide streaks of known duration, each wheel was divided into an equal number of radial slits and spokes. The rotational speed of the motors and the number of slits on the wheels were determined in order to obtain time scales smaller than the reciprocal of the estimated frequencies of turbulence. Table III-2 represents the different combinations used for the various runs.

FIGURE III-3

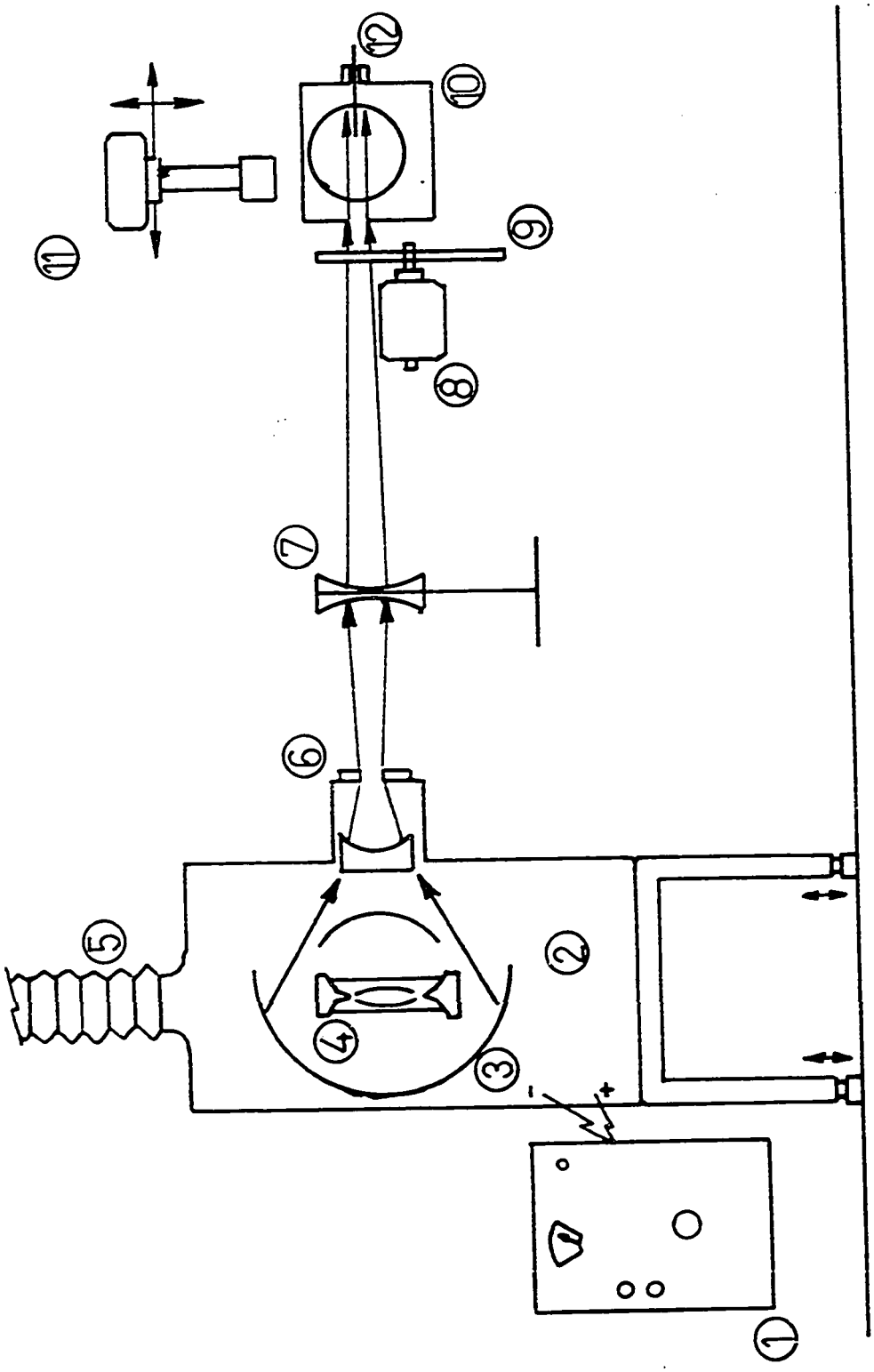

- OPTICAL SYSTEM -

These time scales also provided convenient streak lengths on the films.

TABLE III-2

Motor rpm	Number of Divisions on the wheel	Time Scale sec.	Run Number
1790	40	0.001675	4,5,6,7
3577	40	0.000837	9,10
3575	60	0.00056	11,12,13,14
1790	60	0.001118	15,16,17

The chopping disks were placed perpendicular to the light beam in front of the view section with the axis of the motor in the plane of the light slit. Optical boxes placed around the test sections were slightly different in construction. For the 1" pipe, the view section consisted of a plexiglass box filled with a mineral oil of approximately the same index of refraction as glass. The second type consisted of a polished cylinder of 2.75" I.D. in a cubic piece of plexiglass which was inserted between two sections of pipe. The upstream joint was then polished to remove any discontinuity.

Figure III-4 shows a scheme of the optical box used for the 2.75" pipe. A slit of 0.0592" in height and 2" in width was placed on the view section to assure the illumination of a volume of fluid of nearly the same X-section. The outside of the optical box was painted black in order to cut down possible reflections.

A needle of 0.020" in diameter, inserted in the test section through a partially sealed hole, could be moved across the illuminated portion of the fluid. A cylindrical guide was attached to the rear portion of the view section to properly align the needle. This

- VIEW SECTION -

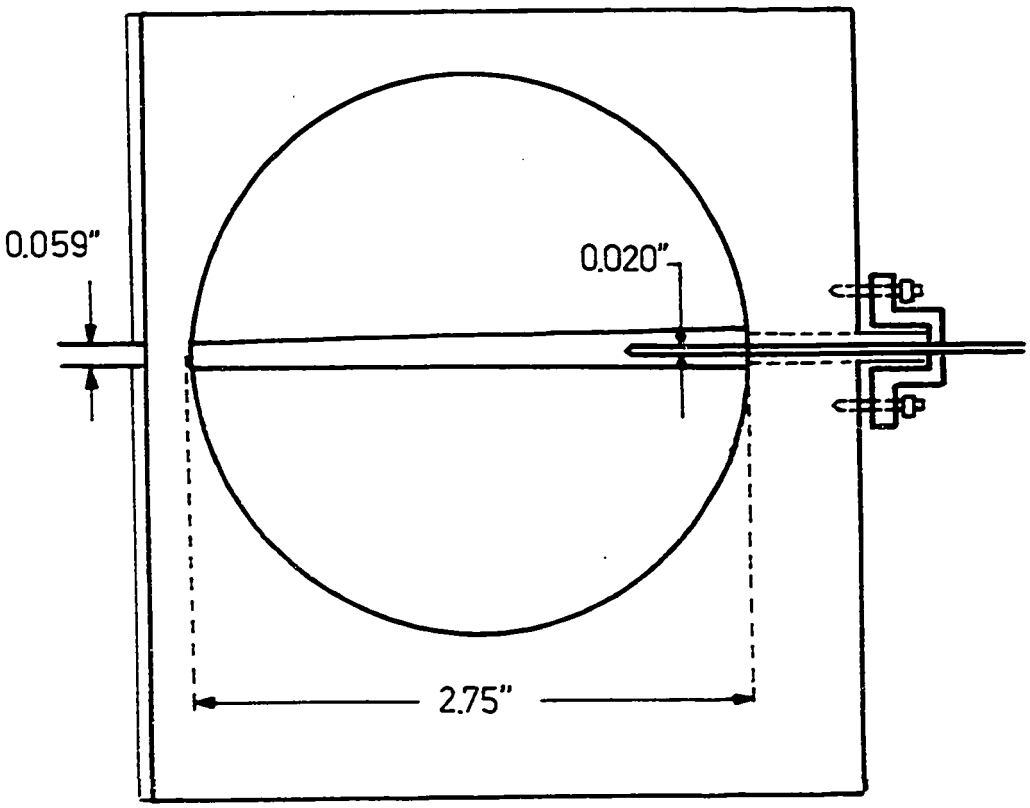

FIGURE III-4

needle served to obtain the radial calibration curves (see Appendix B)

A Miranda 35 mm camera, located perpendicular to the light beam, was attached to Setco Building Blocks equipped with micrometer handwheels graduated in 0.001" increments. Real magnifications of approximately 8X and 2X were obtained from different combination of extension tubes and lenses. A 1:1.9/50 mm lens with a depth of field of 0.077" was used for the runs in the 1" pipe while a 1:3.5/80 mm lens with a depth of field of 0.65" was used in the 2.75" pipe. Thirty-five mm Tri-X films with ASA speed of 400, were used in this study.

The best exposure times and shutter openings were determined by a trial and error procedure;

a) obtaining a maximum number of streaks per frame (one streak per radial position if possible) to cut down the labor of analysing the films and to economize on film. This necessitated a long exposure time.

b) alternatively, a long exposure time meant that the illuminated curvature of the wall would appear very dark and would mask the streaks near the wall. This necessitated closing the shutter opening.

c) finally the air bubbles used as tracers had to appear very sharp on the films.

Experimentally, it was found that an exposure time of 1/15 of a second with a shutter opening of f:4 gave the best results.

III-4 OPERATIONAL PROCEDURE

After a solution was found to be at the desired level of degradation, it was pumped through the system at a very high flow rate for a few minutes to enable the air to escape from the apparatus. The light source was turned on and the optical system adjusted. Then the flow rate was adjusted to the desired value and the tracers were introduced into the system. When the flow rate and the other variables of the run were found to be steady (as indicated by the magnetic flow meter, the thermometer, etc.) photographs were taken. The photographic runs took 3 to 4 hours for the first few runs, but only between 1 and 1.5 hours for all other runs due to the amelioration of the procedure to obtain calibration curves (see section on Analysis of Streak Photographs).

III-5 STREAK PHOTOGRAPHS

Typical streak photographs are shown on Figures III-5 and III-6 for the case of four different runs at four different magnifications. Figure III-5a indicates an instant in time in which all of the streaks are parallel to the wall. This streak pattern is observed on a portion of the photographs during the photographic runs of the concentrated solutions and indicates a patch of laminar flow. Other photographs which show large radial components indicate a patch of turbulent fluid. Identical streak photographs can be found in Seyer's work (43). In contrast, Figure III-5b shows the presence of radial components and represents a fully turbulent flow. Those radial components as it is emphasized from an enlarged view, as shown on Figure III-6a for a water (run II), were observed on every photograph.

Figure III-6b shows three streak patterns located in an illuminated region (from illumination of the curved inside wall of 0.059' width), to indicate how close to the wall photographs of tracers could be obtained at high magnification. The closest streak pattern is located at radial position approximately 200 microns from the wall.

FIGURE 5

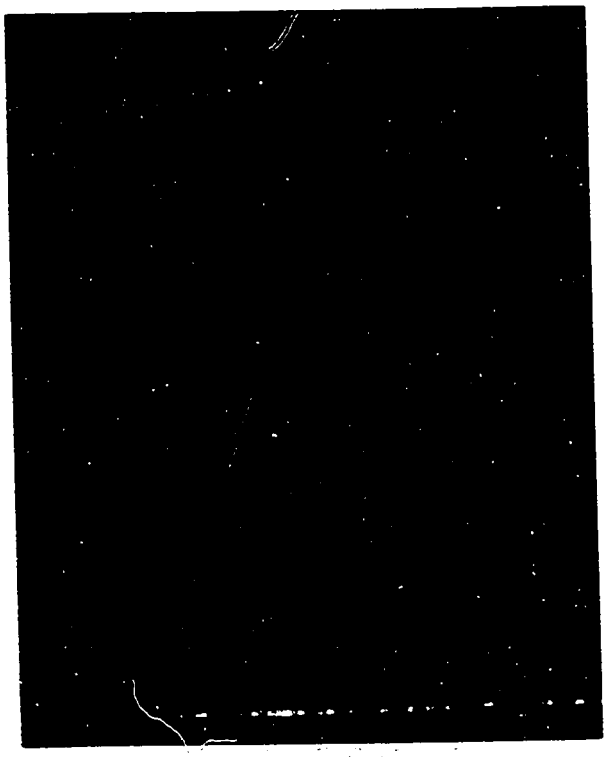

a RUN 14 $\langle \bar{U}_x \rangle = 33.64$ FT/SEC

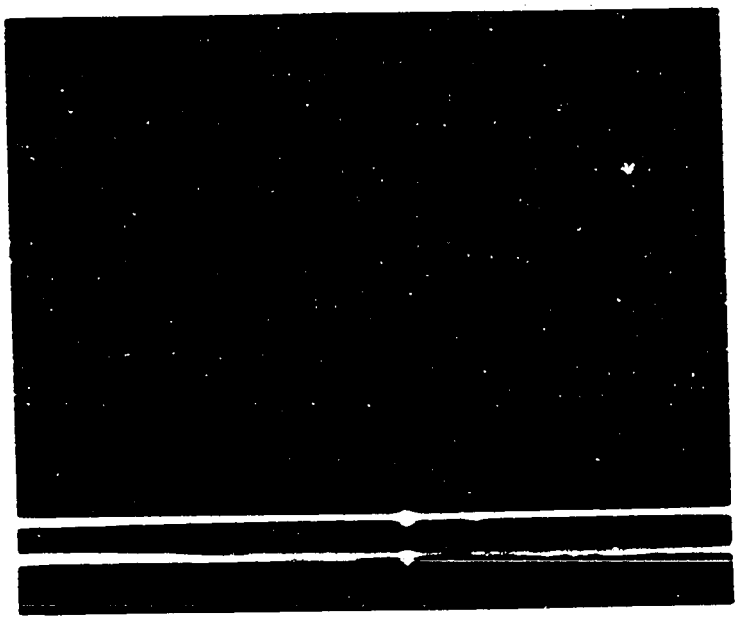

b RUN 16 $\langle \bar{U}_x \rangle = 5.09$ FT/SEC

FIGURE 6

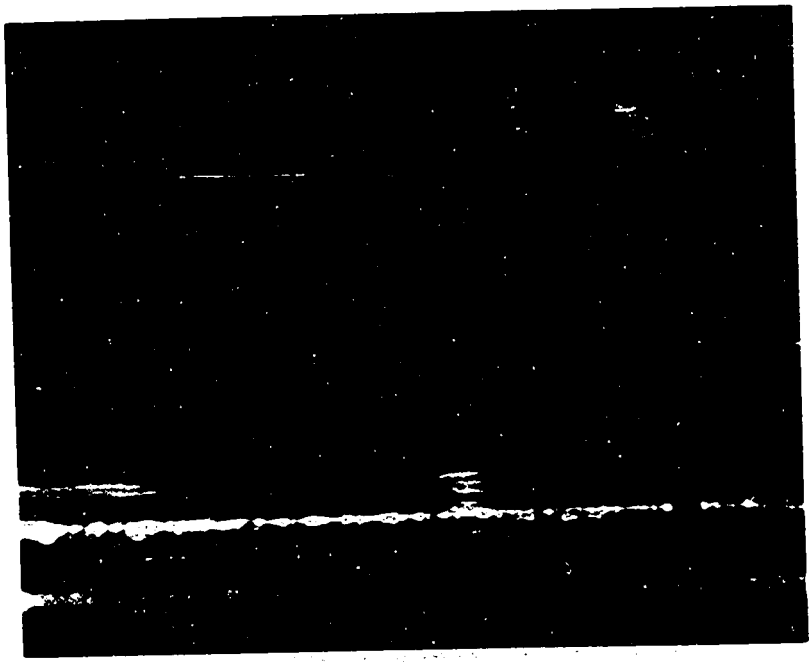

a RUN 11 $\langle \bar{U}_x \rangle = 13.67$ FT/SEC

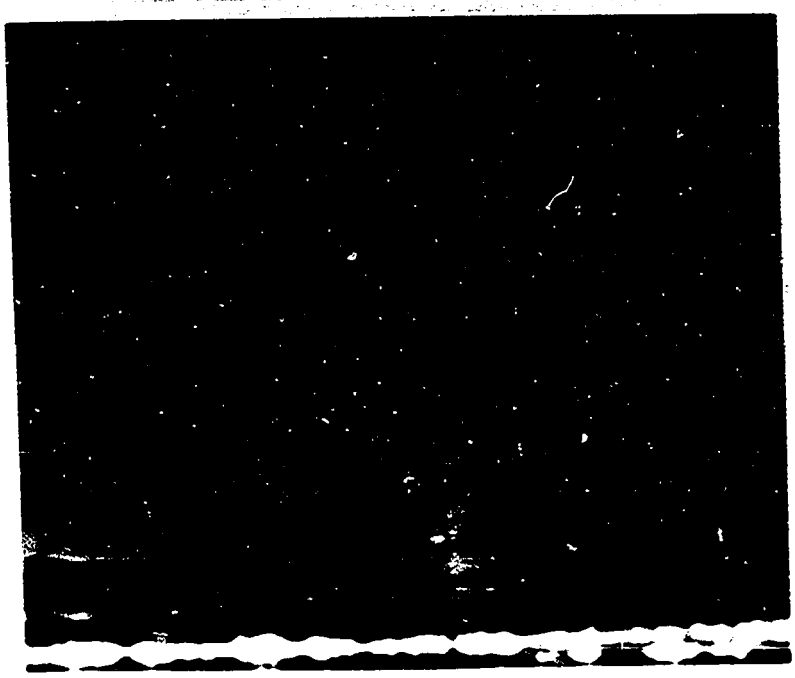

b RUN 13 $\langle \bar{U}_x \rangle = 21.62$ FT/SEC

III-6 ANALYSIS OF STREAK PHOTOGRAPHS

All photographs were analysed using a 'digitizer' which determines the X-Y coordinates of a picture projected onto a glass screen. The projection provides an additional magnification of approximately 20X. The 'digitizer' automatically provided an IBM punched card containing the X-Y coordinates, in volts, of points relative to the 'digitizer' frame. The X-Y frame of the digitizer (22.9" x 21.7" in full scale) consisted of a cross hair device connected to two variable resistances. A power supply coupled to the variable resistances provided a reading of 10.000 ± 0.005 volts for the full trajectory of the axis. Six voltages were then punched on a card and two extra numbers were added in order to define the number of streaks-spokes read and the radial position.

Figure III-7 shows, schematically, a projected photograph containing a single streak pattern. The large arrows represent the interrupted streak and its direction for a period corresponding to the time taken by three spokes of the timing wheel to cut the light. The small lines represent the axial and radial components of the streak and spoke for one time period.

In order to determine the streak length in the axial and radial directions for a known time period, readings of four coordinates relative to the fixed frame of the digitizer were needed. Points 1 and 2 represent the beginning and end of a streak-spoke, respectively, and points 3 and 4 locate the line determining the pipe wall and consequently the axial direction in the pipe. With these readings and appropriate calibrations which convert the voltages to actual distances,

FIGURE III-7

INTERPRETATION OF STREAK PHOTOGRAPH

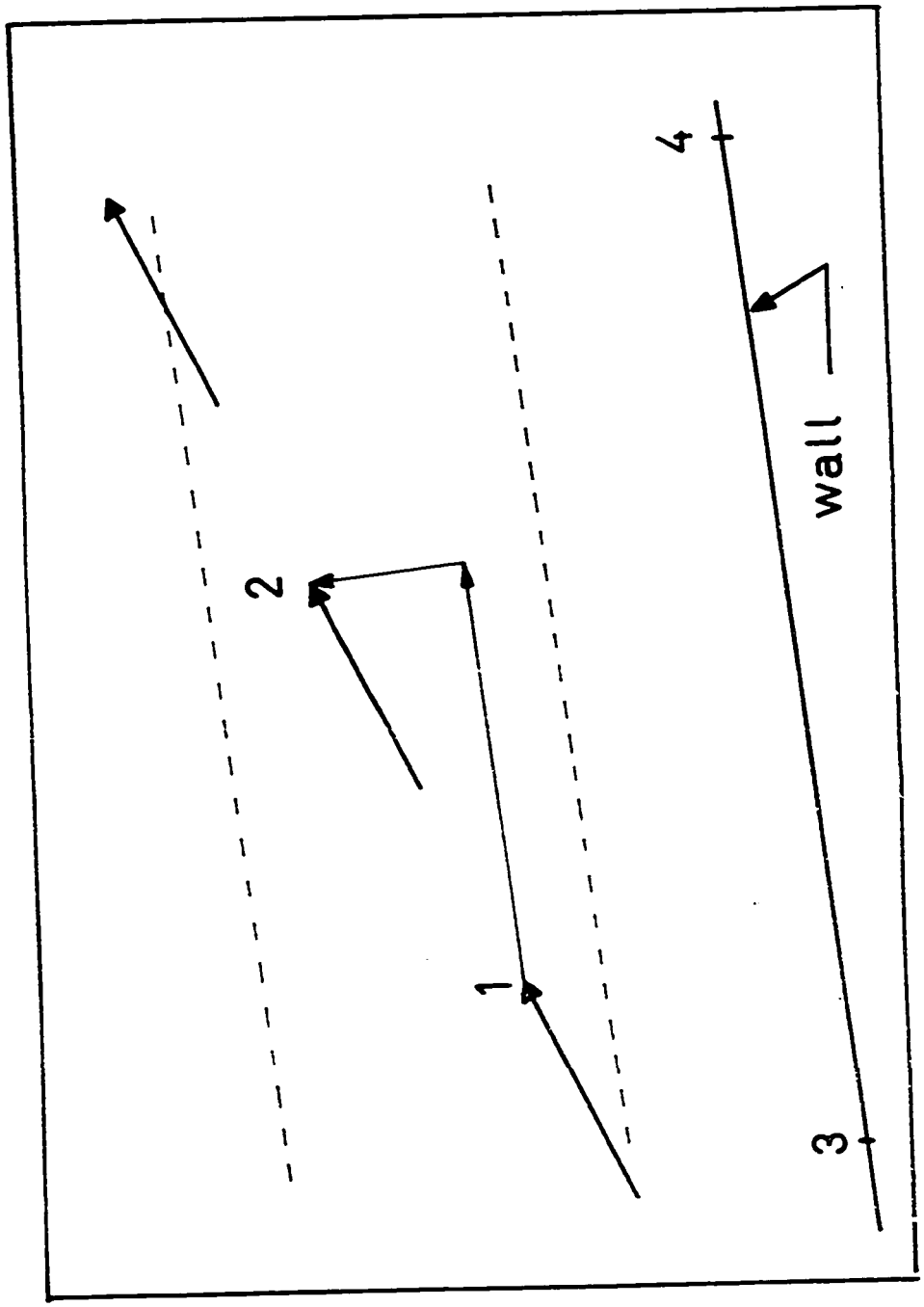

the resolution of a streak into a radial and an axial component follows directly.

The dashed lines represent the band defining a radial position where the streaks were classified as acceptable. The true radial position for each acceptable streak was taken to be the location of the center of the band. In the core region, where the velocity and intensity gradients are small, the width of the band is of little consequence. However, this is not true very near the wall. For the average velocity near the wall, since the profile is essentially linear over the width of the band, the average is not changed. However, the calculated intensity will be slightly higher than the actual intensity.

Generally, if two or more correlated streak patterns were observed in the band, only one reading of velocity was taken. This tends to eliminate the bias of too many readings of the same instantaneous velocity.

The reproducibility of readings and mechanical errors involved in the use of the 'digitizer' are presented in Appendix C. The instantaneous velocities were calculated on the IBM 1800 facilities in this department. Programs used in this work are presented in Appendix J which can be found in Book II.

To determine the axial magnification, pictures of a Keuffel and Esser ruler were taken outside the tube at identical camera focus (with respect to the photographic runs) and projected on the 'digitizer' screen where measurements of the scale were obtained. Trial runs have shown that identical magnifications were obtained with the ruler inside and outside of the pipe (see Table B-II).

The technique developed to find the radial magnification and the radial positions was complicated by the non-linearity of the curves due to wall curvature. A needle of 0.020" in diameter was positioned perpendicular to the camera and located at the center of the pipe or light beam (see Figure III-4). This needle was attached to a micrometer head with a smallest division of 2 microns and mounted on a sliding block. The needle was then moved to the wall of the pipe (where it could be photographed) and a sequence of pictures were taken as the needle was retrieved, one position at a time. The fine adjustment micrometer head provides accurate positions in the wall region and the handwheels, graduate in 0.001" increments, provided subsequent measurements to the center of the pipe. For most of the runs, this set of pictures was checked by a second set which was obtained with the needle moving from the center of the pipe toward the wall. Appendix B presents typical data for the calibration curves obtained and shows a typical example of the third order polynomial radial calibration curves. The knowledge of both axial and radial magnifications and the radial positions permitted the voltages to be transformed into instantaneous axial and radial distances, whereby Δx and Δr, could be calculated.

Knowing the time scale and length scale for each streak-spoke, the axial and radial instantaneous velocities could be found

$$u_x(r) = \Delta x/T$$

$$u_r(r) = \Delta r/T$$

where $T = 60/(M)(W)$ --- (sec)

M = number of slit-spoke on the chopping wheel

All the instantaneous velocities are presented in Appendix K, which can be found in Book II.

The mean velocities could then be calculated, at a radial position, from

$$\bar{u}_x = \frac{1}{n} \sum_{1}^{n} (u_x)_i$$

$$\bar{u}_r = \frac{1}{n} \sum_{1}^{n} (u_r)_i$$

and the Root Mean Square values calculated from

$$\sigma_x = \sqrt{\frac{\sum_{1}^{n} (\bar{u}_x - u_x)_i^2}{n-1}}$$

$$\sigma_n = \sqrt{\frac{\sum_{1}^{n} (\bar{u}_r - u_r)_i^2}{n-1}}$$

RESULTS AND DISCUSSION

IV-1 PRESSURE DROP MEASUREMENTS

Figure IV-1 represents the friction factor - generalized Reynolds number data obtained for both water and polymeric solutions in the 1" and 2.75" diameter pipes. These data are tabulated in Appendix I.

The experimental values of the friction factor for water were obtained in order to check the experimental equipment as well as the Newtonian form of the friction similarity law. All the Newtonian data representing the curve labelled water, in Figure IV-1, are obviously in close agreement with the accepted Newtonian curve.

In Figure IV-1 considering the 0.01% solution first, the data represent a certain level of degradation of the polymer. As shown by comparison of friction factors, the amount of degradation in this work is somewhat less than the amount of degradation in Seyer and Metzner's work with equivalent solutions. The somewhat 'fresher' solutions used were necessary in order to get significant drag reduction in the 2.75" tube. If the solutions were too fresh however, it was found that they would degrade significantly over the period of a photographic run. In Figure IV-1, runs were made from low to high flow rates and back, as a check, over which period little degradation occurred. Thus the set of data is not influenced by any changes in shape owing to degradation.

In the photographic work the data in the figure were used as a reference for obtaining a consistent amount of degradation. Data

FIGURE IV-1

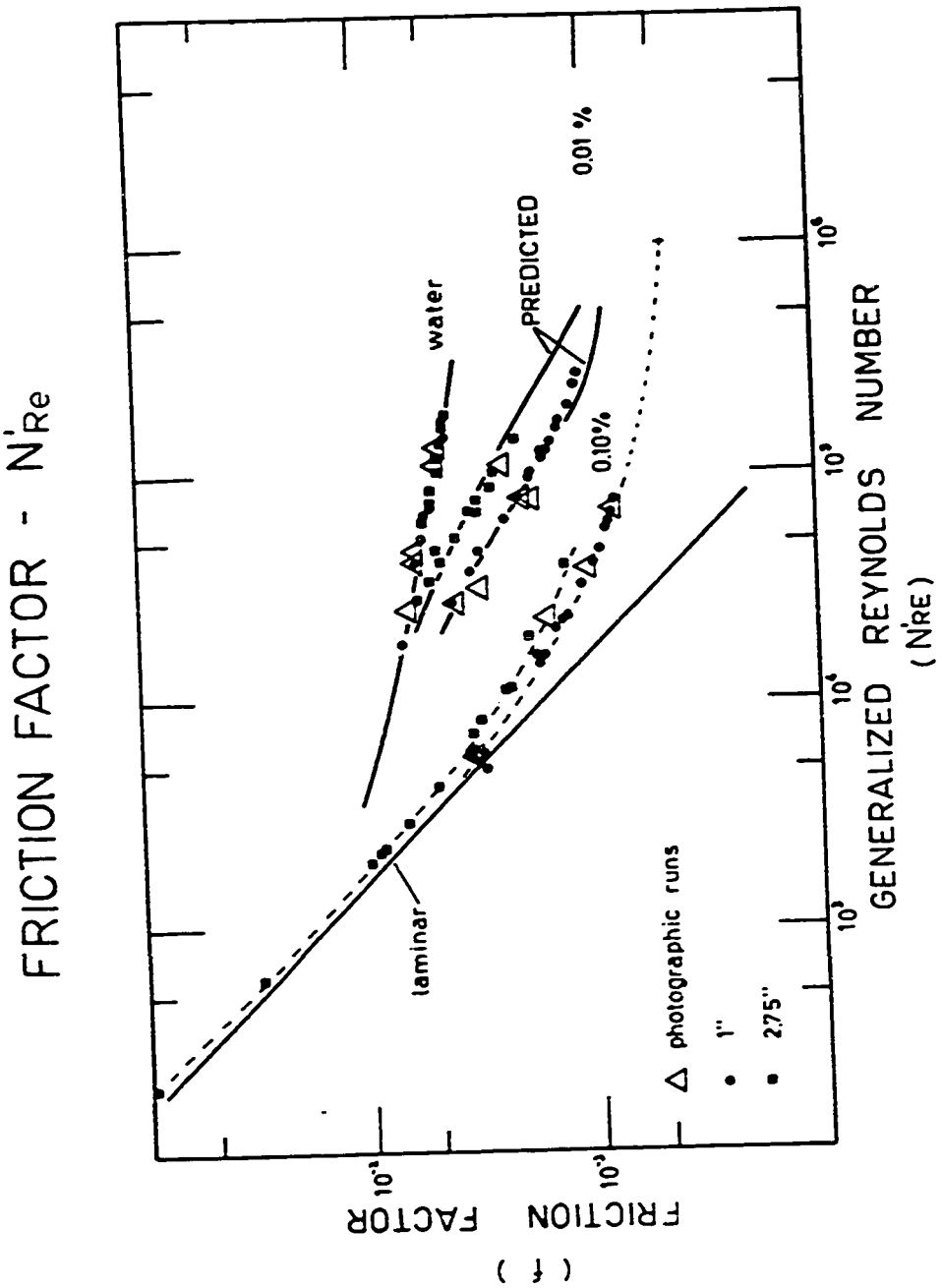
FRICTION FACTOR - N'Re
water
PREDICTED
0.01 %
0.10%
laminar
photographic runs
1"
2.75"
GENERALIZED REYNOLDS NUMBER
(N'RE)
FRICTION FACTOR
(f)

points obtained during the photographic runs are indicated by the large triangles. Table IV-1 summarizes the photographic runs. Except for run 10 and 12, it can be observed that no apparent large degradation occurred during the photographic runs from the reported range of friction velocities calculated from pressure drop measurements. However, the friction velocities of run 12 show a significant degradation occurred during the period of the run, and consequently run 12 was split into two separate entities: run 12a and run 12b. The degradation occurred simply because of the inordinate length of time necessary to complete the photographs for this particular run at high shear rate. For run 10 an average friction velocity was used.

As noted from the triangles, drag reduction of up to 60% could be obtained for the photographic runs in the 1" pipe and of 44% in the 2.75" pipe for the dilute solutions. The maximum of flow rate of the system prevented the photographic runs at higher N'_{Re} in the 2.75" pipe while degradation caused by high shear with vibration of the system limited readings in the 1" pipe.

The prediction of drag reduction in the 2.75" pipe from the 1" pipe data points, using Equation II-16 and the Seyer and Metzner B function, agreed well with the experimental friction data as shown on Figure IV-1. These predicted lines were obtained from an estimated relaxation time function $\theta \propto \tau_w^K$ obtained from the 1" pipe friction data (see Appendix A). At the highest Reynolds number (highest shear stress) there is a small disagreement between the data points and the curves, however, essentially exact agreement would have been found using point values of θ obtained from the 1" pipe friction data.

TABLE IV-1

SUMMARY OF ALL RUNS

Run No.	Fluid	Pipe I.D. in	$\langle \bar{u}_x \rangle$ ft/sec	U^* ft/sec	N'_{Re}	f 10^5	% drag	n'	$\%\Delta\langle \bar{u}_x \rangle$ ft/sec	$\langle \bar{u}_x \rangle_{max}$ ft/sec
4	water	1.00	4.83	0.259-0.259	38123	550	0	1.000	+0.48	5.65
5	water	1.00	3.07	0.175-0.175	23785	620	0	1.000	--	3.80
6	0.01%	1.00	4.38	0.189-0.189	20133	380	34.5	1.000	-1.76	5.35
7	0.10%	1.00	4.98	0.020-0.020	5192	320	64	.686	--	--
9	water	1.00	4.98	0.261-0.261	42229	540	0	1.000	-2.15	6.23
10	0.01%	1.00	4.98	0.183-0.195	34377	297	48.3	1.000	-1.97	6.12
11	water	1.00	13.26	0.624-0.624	104299	450	0	1.000	-2.49	16.40
12A	0.01%	1.00	11.62	0.346-0.346	80354	179	62	1.000	-4.18	13.80
12B	0.01%	1.00	11.62	0.361-0.361	80354	193	61.2	1.000	-4.18	13.80
13	0.10%	1.00	22.02	0.487-0.496	37600	110	82.7	.705	+1.87	30.50
14	0.10%	1.00	33.40	0.666-0.666	64850	80	83.8	.715	-0.72	49.80
15	water	2.75	5.00	0.233-0.233	114083	435	0	1.000	-2.79	6.29
16	0.01%	2.75	5.07	0.183-0.183	97774	258	43.7	1.000	-0.43	5.87
17	0.10%	2.75	8.77	0.234-0.234	121905	146	77.2	.679	+1.08	11.38

measurements.

These calculations quantitatively support the intercept function determined by Seyer and Metzner using solutions that are significantly more elastic and for a moderately larger tube than they used. In the calculations, however, the parameter θ^+ (see Appendix A) is limited to values less than 12 so that the calculations do not provide a test of the maximum drag reduction asymptote as noted in Chapter II (B = 32). For larger tubes at equivalent Reynolds number, however, θ^+ will generally be less than 12 so that predictions outside this range are of little consequence.

In Figure IV-1, the friction measurements of the concentrated solutions show the characteristic slow departure from the laminar curve relatively to Newtonian fluids. These solutions were prepared and degraded similarly to the dilute 0.01% solutions. The data serve to extend the previous measurements (41) for concentrated drag reducers which are known to exhibit transitional flow at surprisingly high Reynolds numbers. As with the 0.01%, these data show a bit more drag reduction than the same concentration studied by Seyer and Metzner. It is important to notice that the experimental curves for both the 1" and 2.75" pipes are reasonably close to the predicted maximum drag reduction asymptote of Virk et al (47) if plotted according to N_{Re}.

In order to check the asymptotic value of the B function, the 1" pipe data curve was extended, as indicated by the dashed line, to a Reynolds number of 10^6, where, as shown later, fully turbulent

flow is estimated to exist (estimation based on the calculated intermittency factor presented in Figure IV-13). The calculated value of B at a N'_{Re} of 10^6 was calculated to be 43. This value is significantly larger than the asymptotic value of 32.2 obtained from Seyer and Metzner's work. It should be noted that the data do not prove the existence of an asymptote, but merely show that previous asymptotes are not unique.

IV-2 INSTANTANEOUS VELOCITIES AND ANALYSIS OF HISTOGRAMS

The data for all runs of the calculated values of velocity and turbulence intensity at a given point in the tube can be found in Appendix H. These runs correspond to those summarized in Table IV-1. The instantaneous velocities are available in tabulated form in Appendix K enclosed in book II.

In order to show that the number of instantaneous velocities used to estimate the mean velocities was adequate, the cumulative mean of axial and radial velocities were considered for each run. Figure IV-2 shows, as an example for different radial positions in the 1" pipe, the levelling of the axial velocities for run 6. Large fluctuations of the cumulative mean are observed when less than 10 velocities are used, but the curves level rapidly for 30 or more observations. It is apparent from the figure that with 30 observations or more, random fluctuations in velocity have negligible influence on the calculated mean. Similar results are predicted from simple statistical analysis.

Similarly, the typical cumulative axial and radial intensities (relative to the maximum velocity) are shown in Figure IV-3. For these calculations, particularly for the axial intensity, some of the curves tend to a stationary value rather slowly. This is shown best by the top curve in Figure IV-3, which does not become stationary until about 70 observations are used. Consideration of other runs with as many as 200 observations show that any change in intensity after 70 observations is insignificant. Again, simple statistics show that many more observations are necessary to estimate a variance than a mean. Uncertainty limits on the statistical quantities are considered

FIGURE IV-2

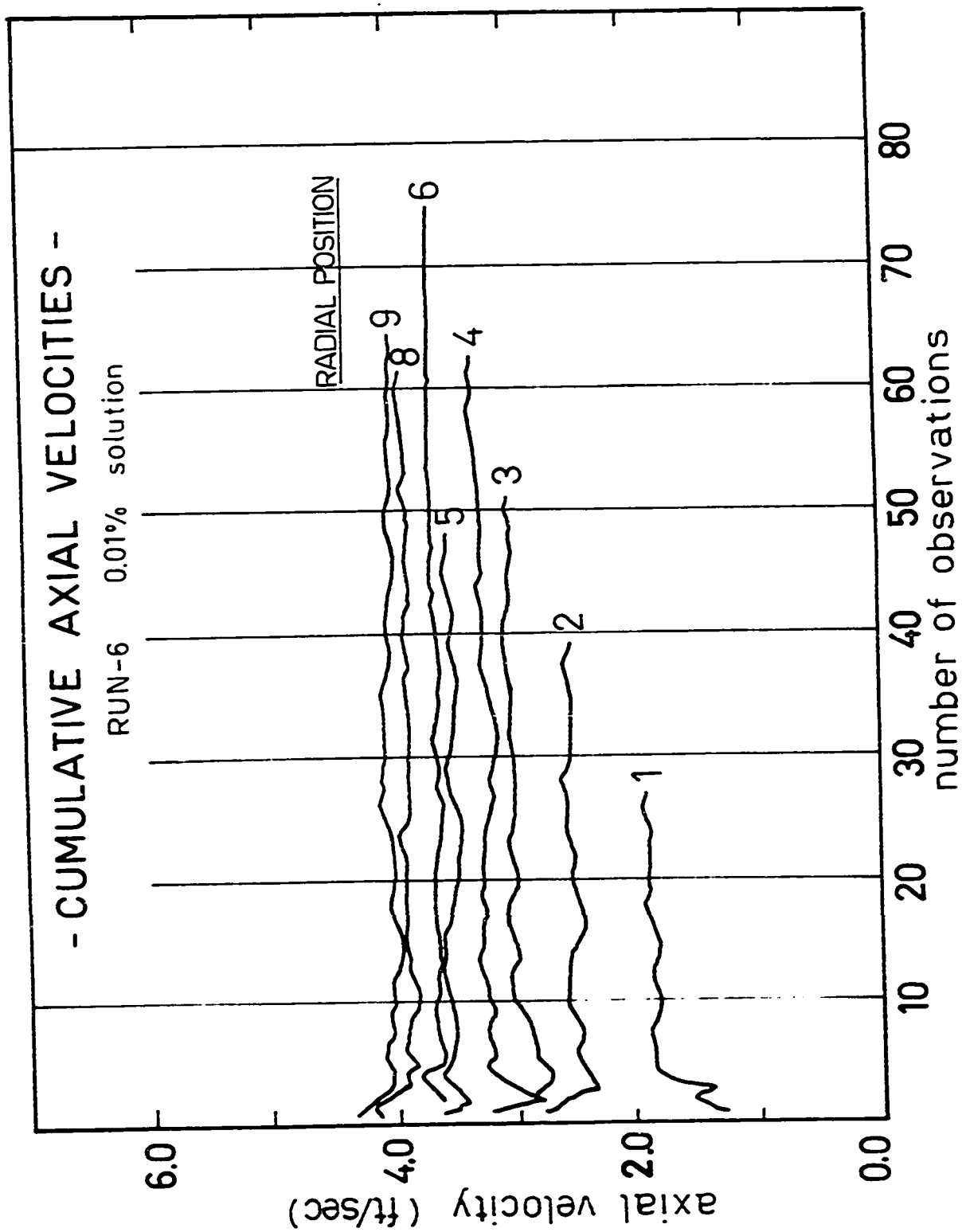
- CUMULATIVE AXIAL VELOCITIES -
RUN-6 0.01% solution
RADIAL POSITION
1
2
3
4
5
6
8
9
6.0
4.0
2.0
0.0
axial velocity (ft/sec)
10
20
30
40
50
60
70
80
number of observations

FIGURE IV 3

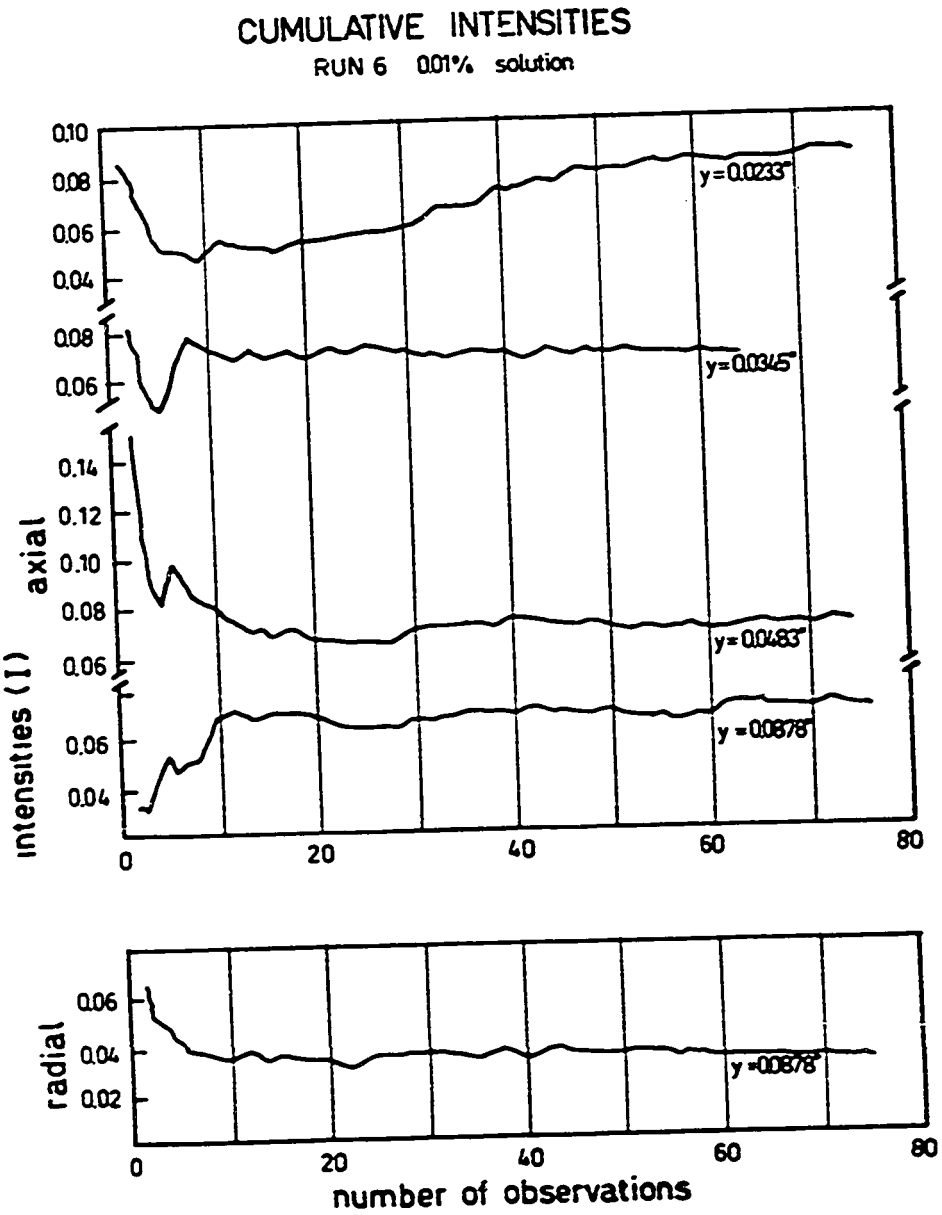
CUMULATIVE INTENSITIES
RUN 6 0.01% solution
intensities (I)
axial
radial
y=0.0233"
y=0.0345"
y=0.0483"
y=0.0878"
y=0.0878"
0.10
0.08
0.06
0.04
0.08
0.06
0.14
0.12
0.10
0.08
0.06
0.06
0.04
0.06
0.04
0.02
0
20
40
60
80
number of observations

in Appendix C. As illustrated by the figure, the axial intensity was found to be more sensitive than the radial intensity.

Histograms of instantaneous velocities for both water and 0.01% solution (run 9 and run 10), at approximately the same Reynolds number, are given in Figures IV-4 and IV-5 for axial and radial velocities respectively. The gross features of these histograms are in qualitative agreement with earlier independent studies and offer support for the bursting phenomena.

Except for the histograms of radial velocity for polymer, the presence of binodal instantaneous velocity distributions, similar to those presented by Popovich (33), can be observed on Figures IV-4 and IV-5 where the histograms consistently show a dip near the center of the plot. These are typical of all the histograms obtained in or near the boundary layer. As noted in Chapter 2, this suggests that the velocities, inside the boundary layer, are composed of two different distributions depending on the origin of the fluid. The lower peak can be identified with the mean axial velocity of lumps of ejected fluid, while the higher mean axial velocity or peak results from lumps of fluid originating from the flow outside the boundary layer. Double peaks in the core were not observed.

In Figure IV-5, the histograms of the radial velocities for the 0.01% are markedly different than the Newtonian ones and show no indication of two peaks. This is viewed as a consequence of the resistance to stretching in the radial direction destroying the large fluctuations or peak in the histograms. From the radial distributions it is clear that the magnitude of the largest fluctua-

FIGURE IV-4

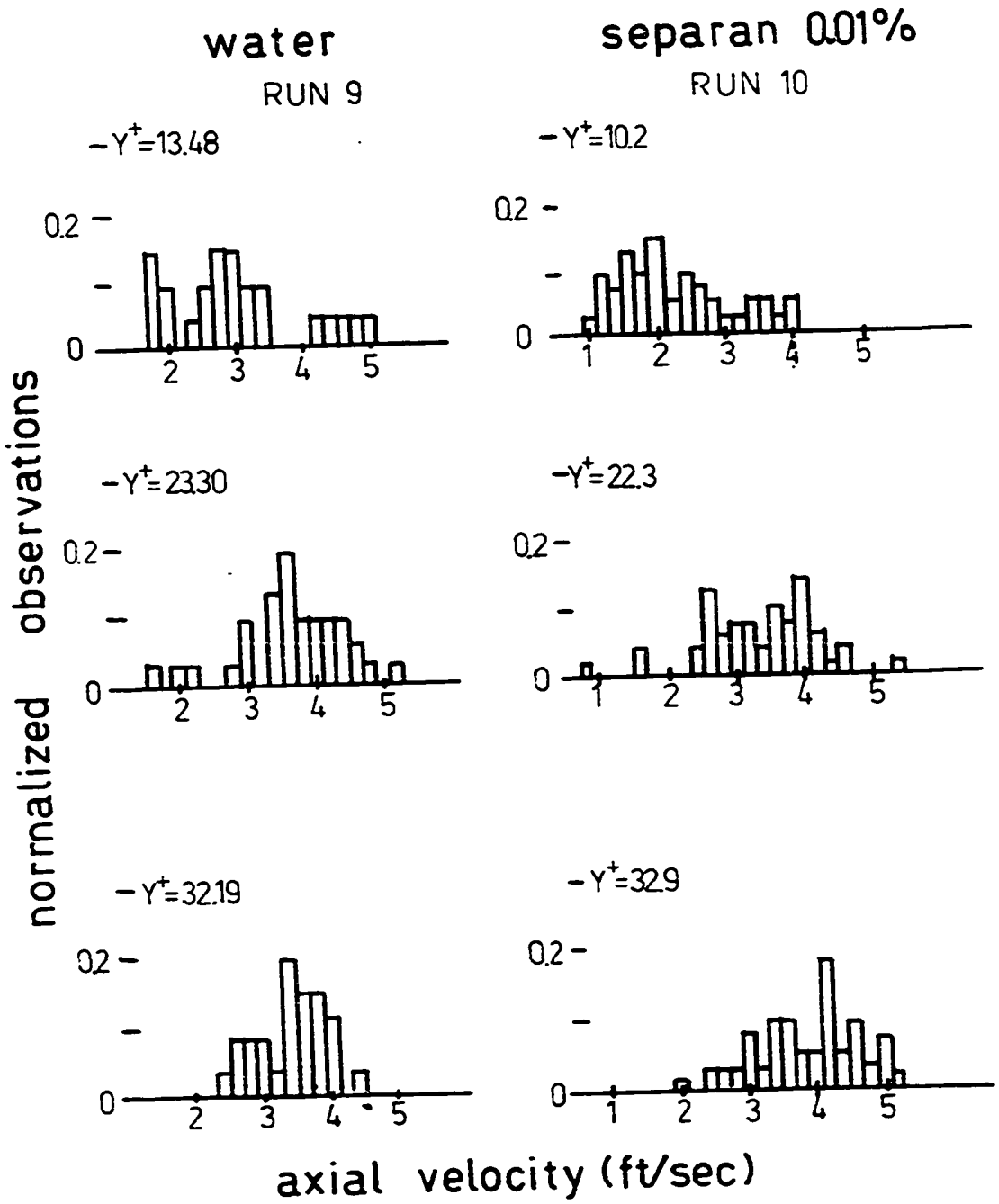

HISTOGRAMS OF AXIAL INSTANTANEOUS VELOCITIES

FIGURE IV-5

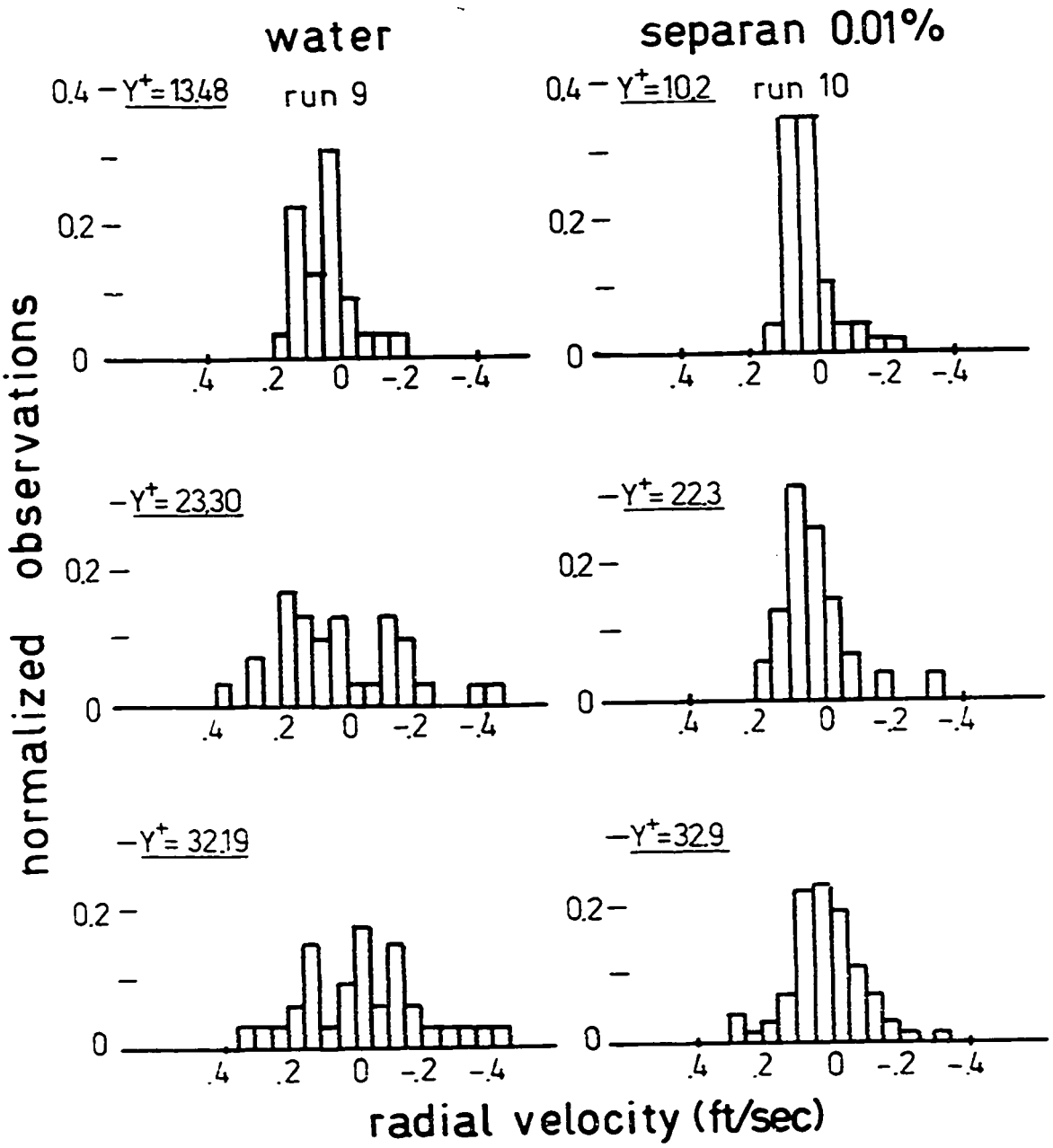

HISTOGRAMS OF RADIAL INSTANTANEOUS VELOCITIES

FIGURE IV-6

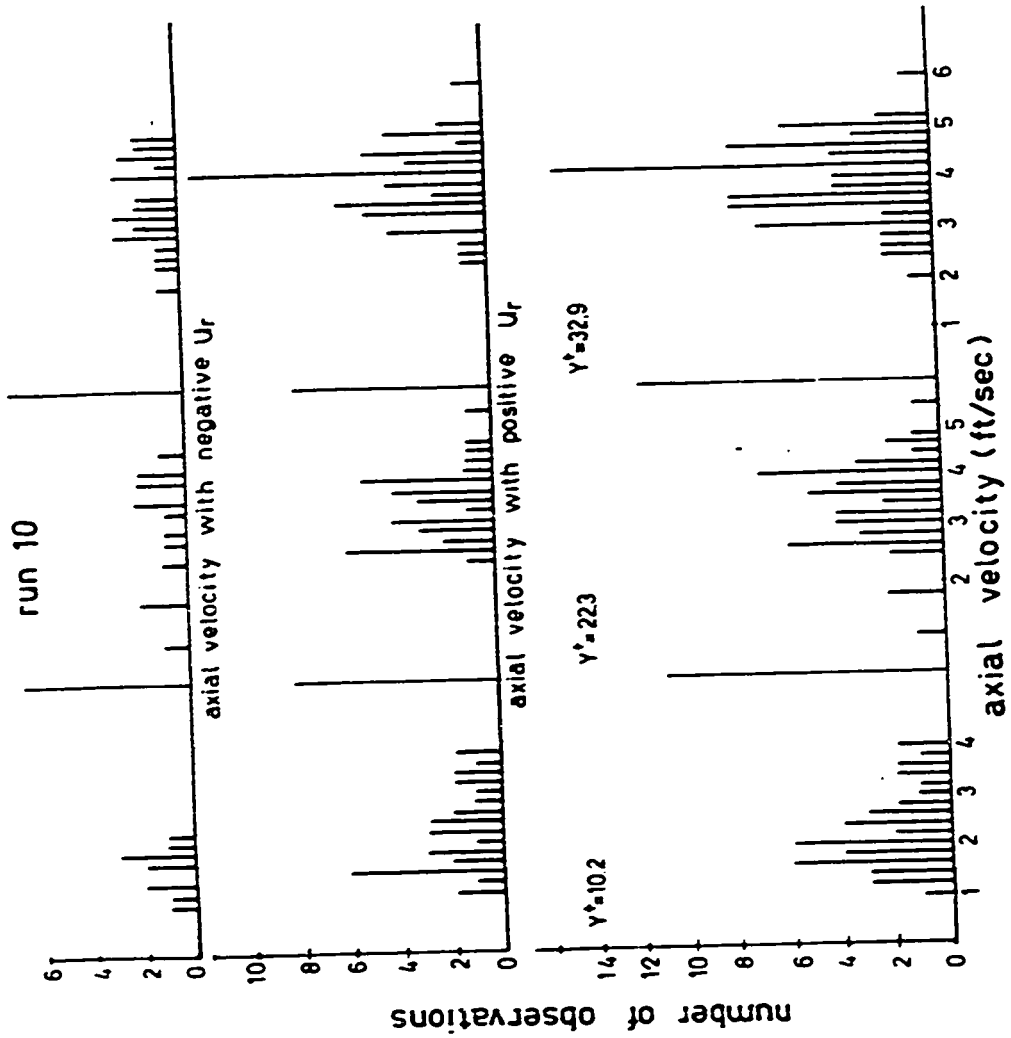

AXIAL HISTOGRAMS

tions is reduced relatively to water. It is difficult to make a statement regarding the frequency of large fluctuations and whether they have been reduced or not, as noted by Meek and Baer for example (2[illegible]), owing to the small number of large fluctuations observed.

In order to show in more detail the nature of the axial instantaneous velocity distributions, inside the boundary layer, the distributions of Figure IV-4 have been split according to the sign of the radial component and are presented in Figure IV-6 for run 10. The mean values of axial instantaneous velocity with positive radial component were found larger than the ones associated with negative radial components. This shows that the ejections must originate from a region of low momentum, and is in agreement with Kline et al (20), Corino and Brodkey ([illegible]), Klebanoff (19). Qualitatively the mean for each side of the distribution corresponds to each of the peaks in the binodal. Splitting of the histograms for flow in core did not show that a significant difference existed between means of axial velocity associated with plus and minus radial velocities. The splitting of distributions is tabulated in Appendix F.

Comparisons were also made at identical friction velocity, as suggested by previous work (15,36,[illegible],[illegible]), and are presented later as intensity profiles. In any event, the radial fluctuations of the velocity were found to be identically lower than the Newtonian fluids in the boundary layer when normalized to the wall parameters, but the same outside the boundary layer.

Values of the correlation factor R_o, defined in Equation II-2, are presented as Figure IV-7 for runs 6 and 10 of the dilute

polymer and run 9 for water. Data for the other runs, which have been omitted to clarify the figure, show similar behavior. Although there is considerable scatter in the data, there are distinct trends with radial position. As discussed earlier, the bursting arguments coupled with simple continuity considerations, imply R_0 should be greater than unity in the vicinity of the edge of the sub-layer. The data points for the water connected with the dashed line, although not extending deeply enough into the sublayer, suggest this trend. To map the trend completely, one would like measurements for $Y^+ < 10$ or to positions, as indicated previously (7), where the ejections originate. For example for water, the data point closest to the wall, at a $Y^+ \approx 14$, has R_0 of approximately 3. Equivalently, at this position positive radial fluctuations are observed three times as often as the larger negative fluctuations, while the mean of all the observed fluctuations is zero within the statistical uncertainty of the calculations.

For the polymer solutions, runs 6 and 10, there is a distinct peak in values of R_0 at ξ of about 0.05. The values become constant at about $\xi = 0.1$. Consideration of the dimensionless velocity profiles shown later in Figure IV-16, indicates, as expected, this peak is within the sublayer and the end of the peak ($\xi \approx 0.1$) coincides with the outer edge of the sublayer which has been shifted to about $Y^+ \approx 100$ for the polymer. Qualitatively the bursting arguments suggest that R_0, in addition to being greater than unity, should show a peak owing to the acceleration from small to large radial velocity as the element of fluid moves through the sublayer. The values should decrease to

FIGURE IV-7

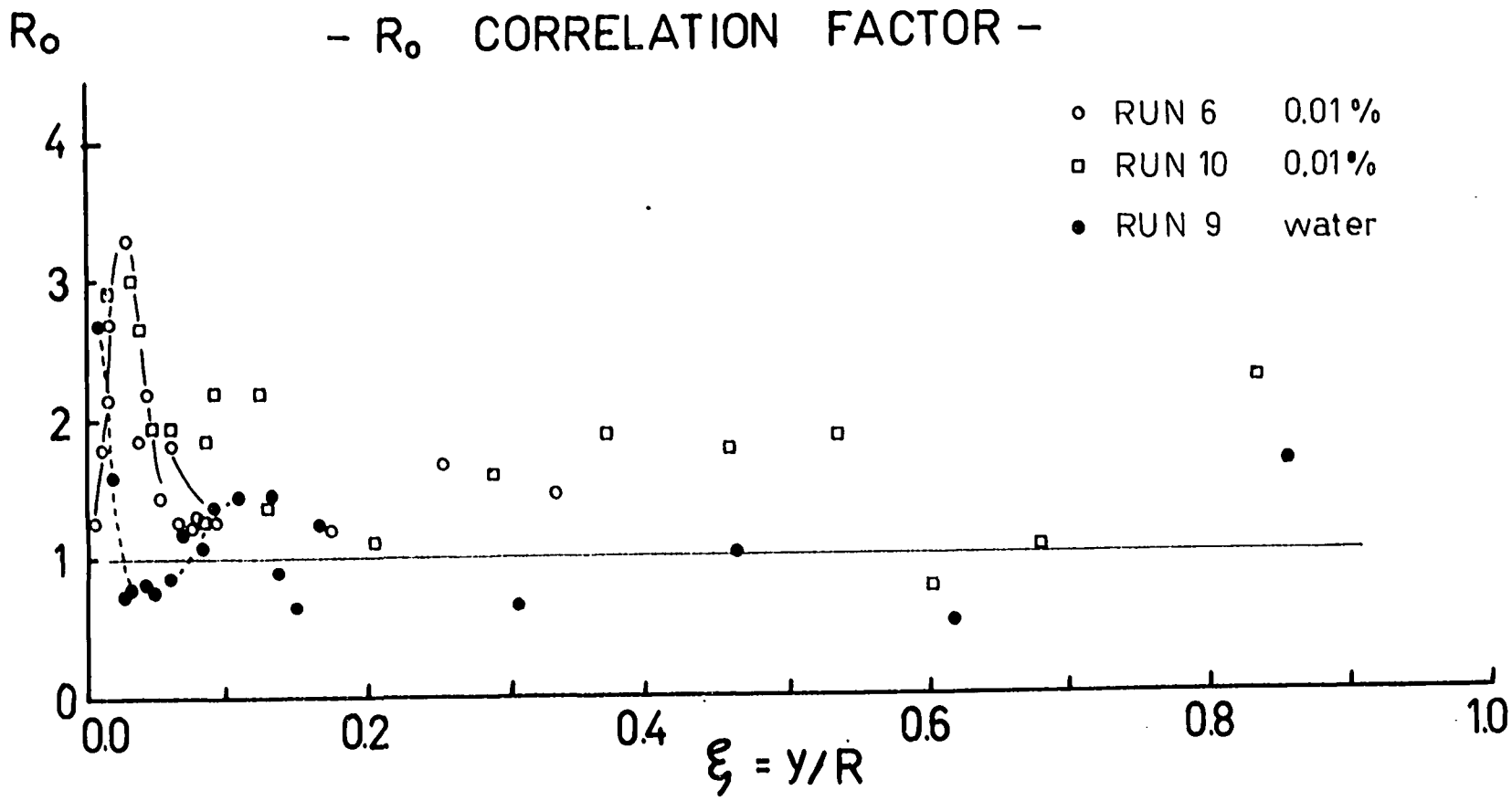
R_o
- R_o CORRELATION FACTOR -
RUN 6 0.01 %
RUN 10 0.01 %
RUN 9 water
4
3
2
1
0
0.0
0.2
0.4
0.6
0.8
1.0
$\xi = y/R$

unity at the edge of the sublayer as the fluid mixes with the core fluid.

For the remainder of the cross section, for all the runs, R_0 scatters around unity, except over a narrow range of radial positions near to $\xi \approx 0.65$ where it is consistently less than unity. Seyer's earlier data ([illegible]) show exactly the same trends, however, no explanation can be offered for this behavior.

IV-3 VELOCITY PROFILES

Figures IV-8 to IV-10 represent actual time average velocity profiles for all the runs in the 1" and 2.75" pipes. The mean or bulk velocities obtained by integrating these profiles (using actual data points and not smoothing the profiles) agreed within 2% of the recorded bulk velocities, except for run 12 which was 4% in error (see Table IV-1). Owing to the small amount of scatter, these data show the usefulness of the streak photograph method over a wide range of conditions. It should be noted that no discontinuity appears in the curves owing to different magnifications used during a run.

More information about the nature of the profiles is found in Figure IV-11 where dimensionless velocity profiles are compared to predictions using Bogue's equation for turbulent flow and the Newtonian laminar equation. The water data are in excellent agreement with the predicted curve while the 0.01% profile which is at the highest Reynolds number for the dilute solutions is markedly flatter in the core. For the other runs at lower Reynolds number where less drag reduction is occurring, the flattening is not so large and the curves approach Newtonian behavior.

FIGURE IV-8

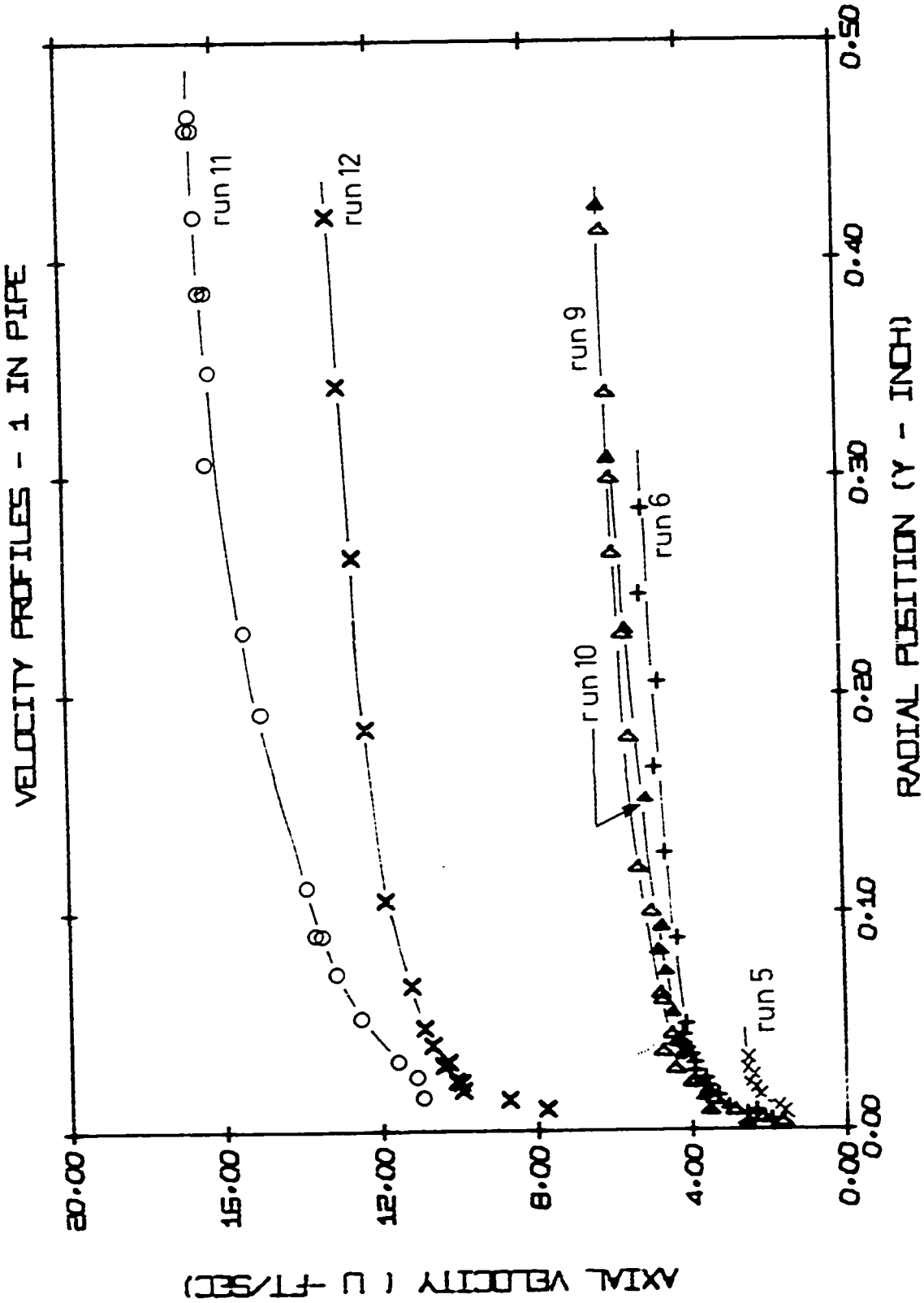
VELOCITY PROFILES - 1 IN PIPE
run 11
run 12
run 9
run 6
run 10
run 5
20.00
16.00
12.00
8.00
4.00
0.00
0.00
0.10
0.20
0.30
0.40
0.50
RADIAL POSITION (Y - INCH)
AXIAL VELOCITY (U -FT/SEC)

FIGURE IV-9

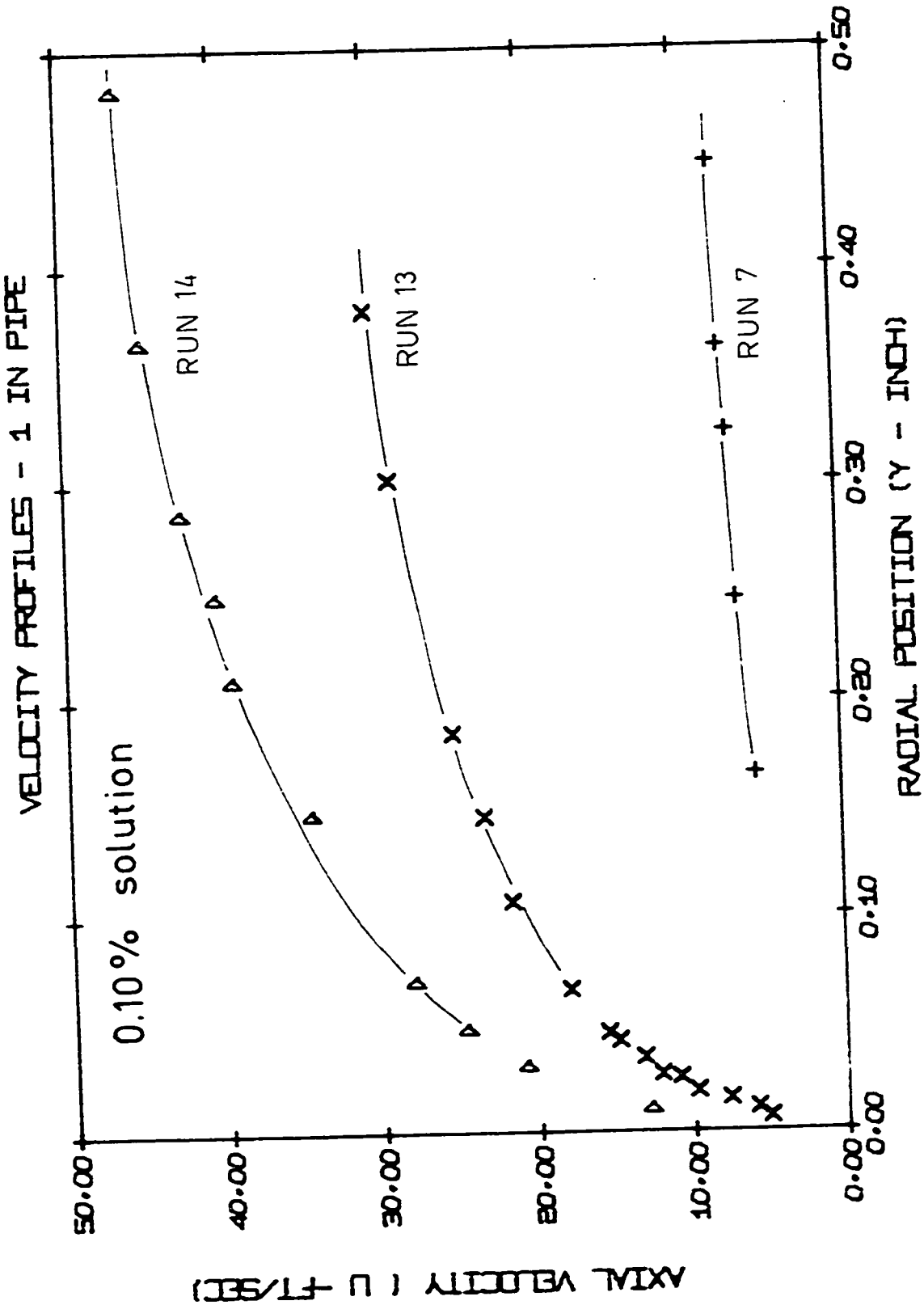
VELOCITY PROFILES - 1 IN PIPE
0.10% solution
RUN 14
RUN 13
RUN 7
AXIAL VELOCITY (U -FT/SEC)
RADIAL POSITION (Y - INCH)
50.00
40.00
30.00
20.00
10.00
0.00
0.00
0.10
0.20
0.30
0.40
0.50

FIGURE IV-10

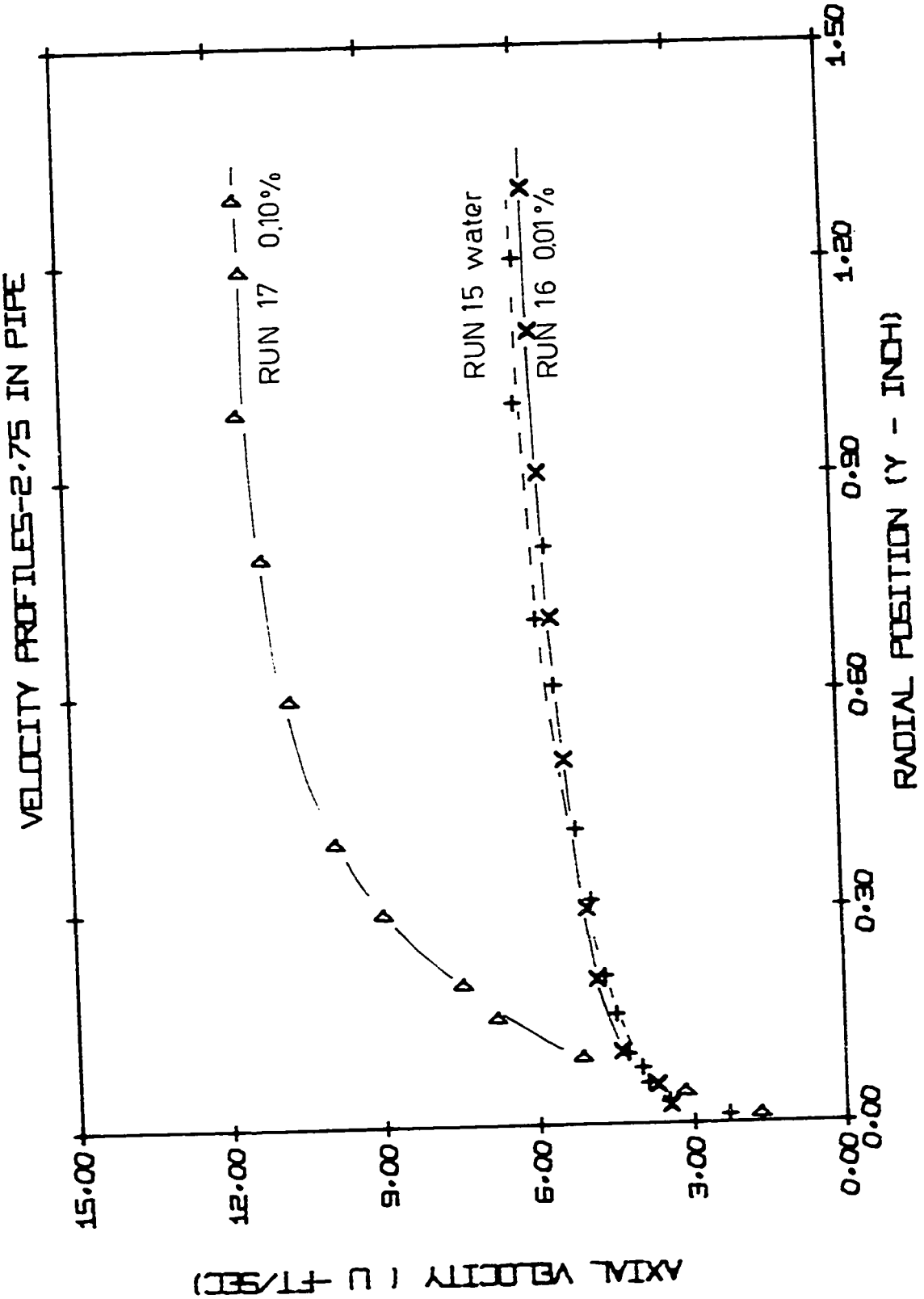
VELOCITY PROFILES-2.75 IN PIPE
RUN 17 0.10%
RUN 15 water
RUN 16 0.01%
AXIAL VELOCITY (U -FT/SEC)
RADIAL POSITION (Y - INCH)
15.00
12.00
9.00
6.00
3.00
0.00
0.00
0.30
0.60
0.90
1.20
1.50

FIGURE IV-11

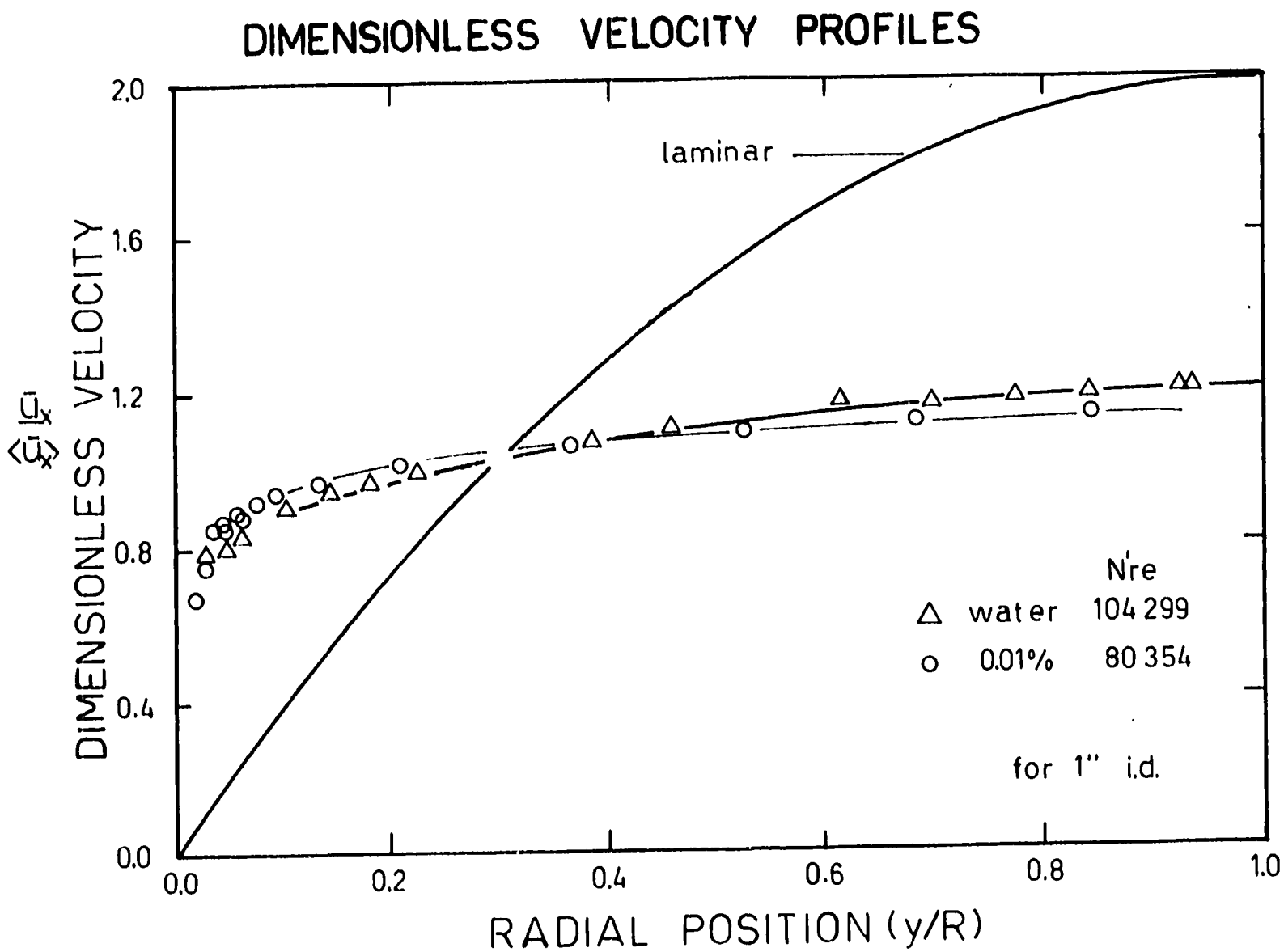
DIMENSIONLESS VELOCITY PROFILES
laminar
N're
water 104 299
0.01% 80 354
for 1" i.d.
DIMENSIONLESS VELOCITY
$\bar{u}_x / \langle \bar{u}_x \rangle$
RADIAL POSITION (y/R)
0.0
0.4
0.8
1.2
1.6
2.0
0.0
0.2
0.4
0.6
0.8
1.0

IV-4 TRANSITIONAL FLOW

Figure IV-12 is a plot of the velocity data for the 0.10% solutions which serve to extend Seyer's earlier data (41) for transitional flow. The fact that these profiles reflect transitional flow has been documented in detail before. Briefly, the transitional flow consists of alternating patches of turbulent and laminar fluid. The relative number of each is described by the intermittency factor, γ, defined as the fraction of the time the flow is turbulent. Thus γ equal unity is fully turbulent while γ of zero reflects laminar flow. Furthermore, it has been shown (35) that the intermittency, at the center of the pipe, is given simply by the position of the velocity profile relative to the fully turbulent and fully laminar profiles.

Figure IV-13 represents the intermittency factors calculated from the velocity profiles at the center line of both 1" and 2.75" pipes and are compared with Rotta's data points for water (35). The 1" pipe intermittency factor curve indicates how slowly γ increases with the Reynolds number for the concentrated drag reducer as compared to the Newtonian curve (see Rotta (35) and Patel and Head (31)). This curve indicates also that the fully turbulent flow will be reached at a $N'_{Re} = 10^6$. Although there is some uncertainty in locating the point of zero intermittency, it is clear that the Reynolds number where turbulence first appears is not significantly different from 2100. From the frictional data curve on Figure IV-1, it was not so evident that the transitional flow existed at that N'_{Re}.

The velocity measurements indicated that the intermittency factor depends strongly on the tube diameter where a 39% increase

FIGURE IV-12

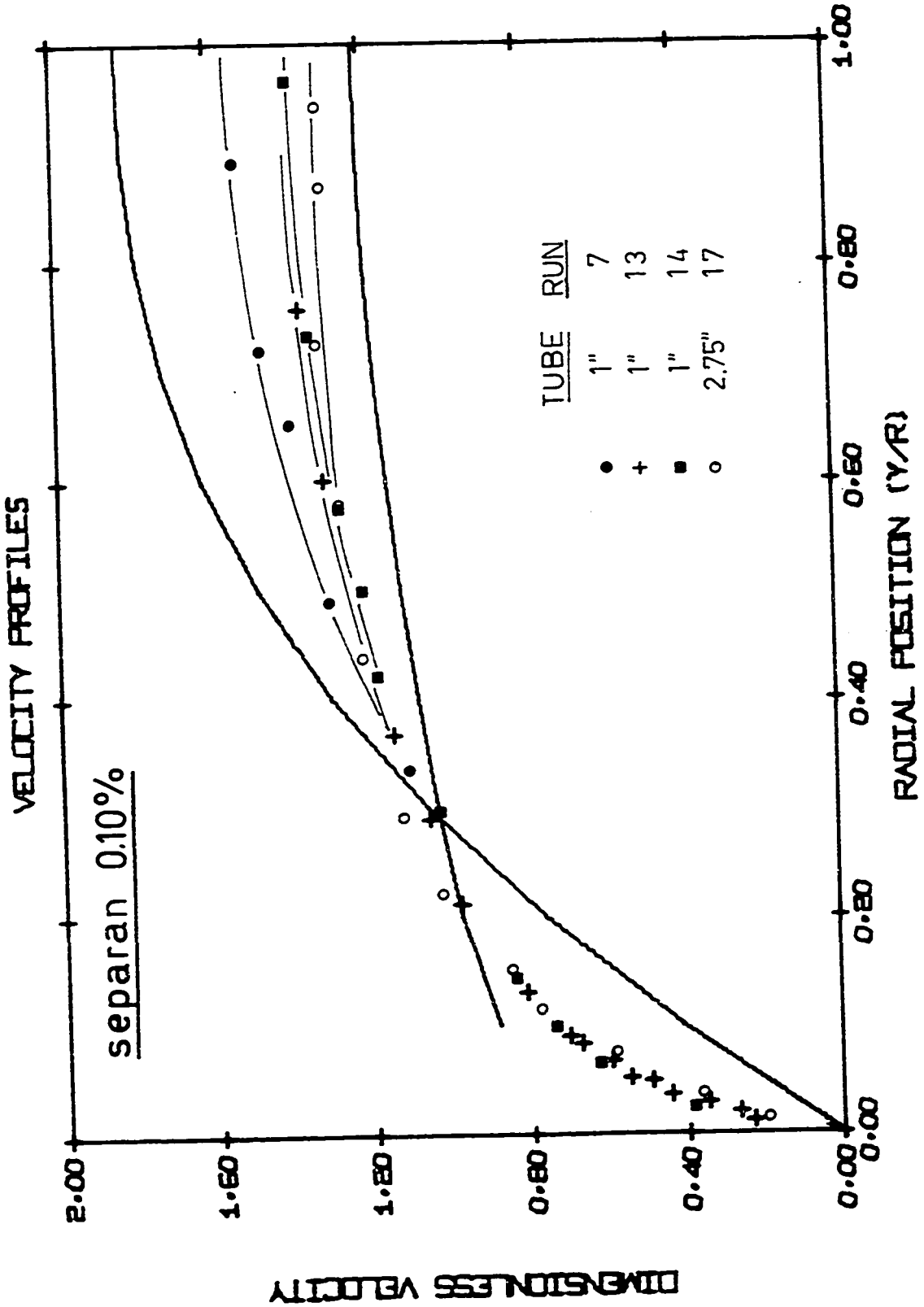
VELOCITY PROFILES
separan 0.10%
TUBE RUN
1" 7
1" 13
1" 14
2.75" 17
DIMENSIONLESS VELOCITY
RADIAL POSITION (Y/R)
0.00
0.40
0.80
1.20
1.60
2.00
0.00
0.20
0.40
0.60
0.80
1.00

FIGURE IV-13

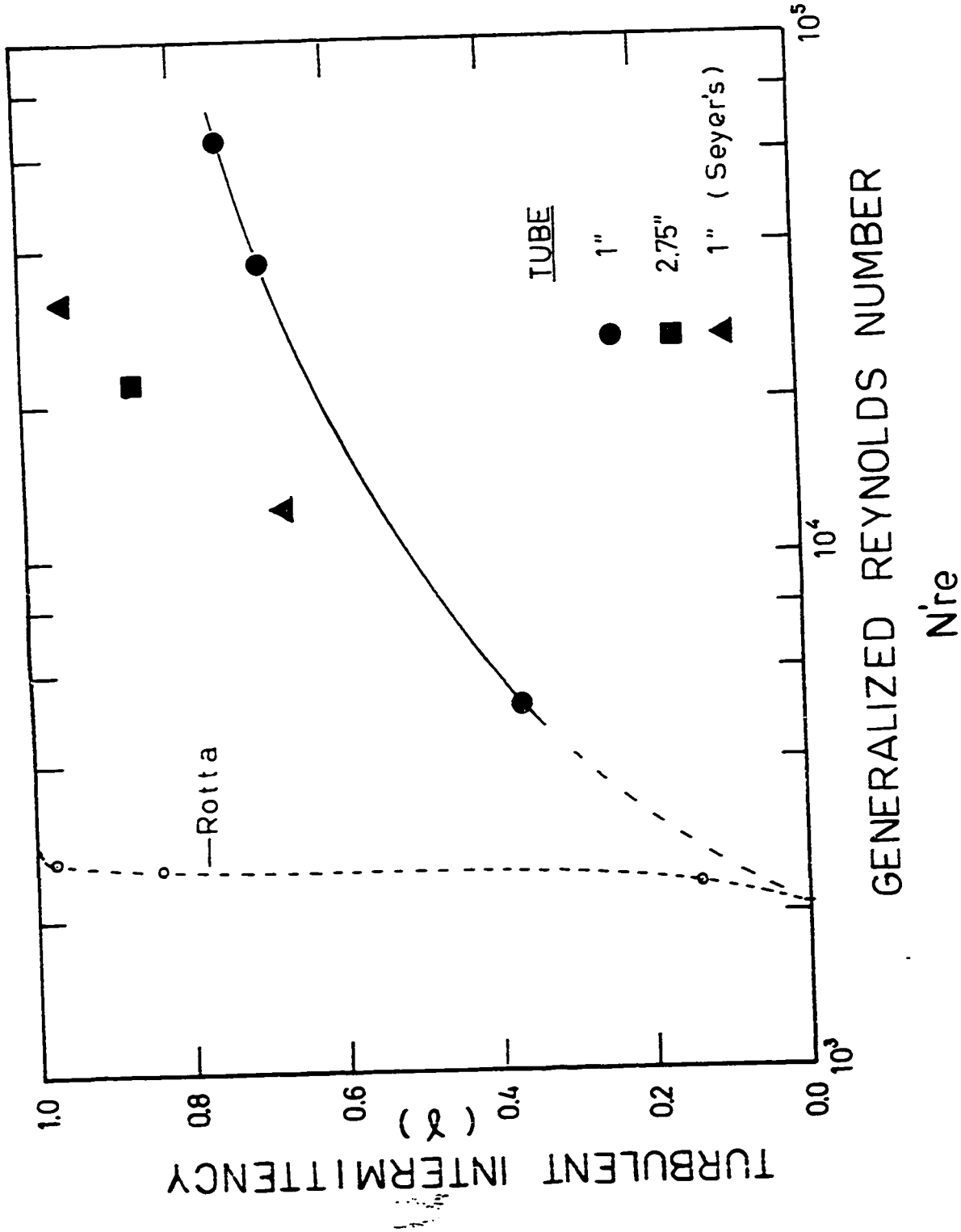
TURBULENT INTERMITTENCY
(γ)
1.0
0.8
0.6
0.4
0.2
0.0
—Rotta
TUBE
1"
2.75"
1" (Seyer's)
10^3
10^4
10^5
GENERALIZED REYNOLDS NUMBER
N'_{re}

relative to the 1" pipe curve was recorded for the 2.75" pipe at a N_{Re} of 2×10^4. Similarly the intermittency factors determined from Seyer's profiles in a 1" pipe are significantly larger than the ones in this work and suggest a Reynolds number of about 10^5 is necessary for fully turbulent flow. Thus the intermittency, at high Reynolds number is very sensitive to the level of degradation of the polymer.

Figures IV-14 to IV-16 give the corresponding intensities for the transitional flow. These simply confirm Seyer's earlier data (41) which shows a very small radial intensity but an apparently large axial intensity. The radial fluctuations decrease rapidly to zero, because they can only occur γ of the time; however, large axial fluctuations still occur because of the profile alternating between fully laminar and fully turbulent profiles.

These measurements make it apparent that the limits of transitional flow should be investigated in order to determine the range of applicability of the similarity laws for drag reducers. The limits must be related to the thickening of the boundary layer as defined by Equation II-12 for example, and clearly must be less than the tube radius. Currently the true upper limit of stable boundary layer thickness is unknown; however, for Newtonian fluids at Reynolds number of 2100 the thickness is approximately $\xi = 0.1$.

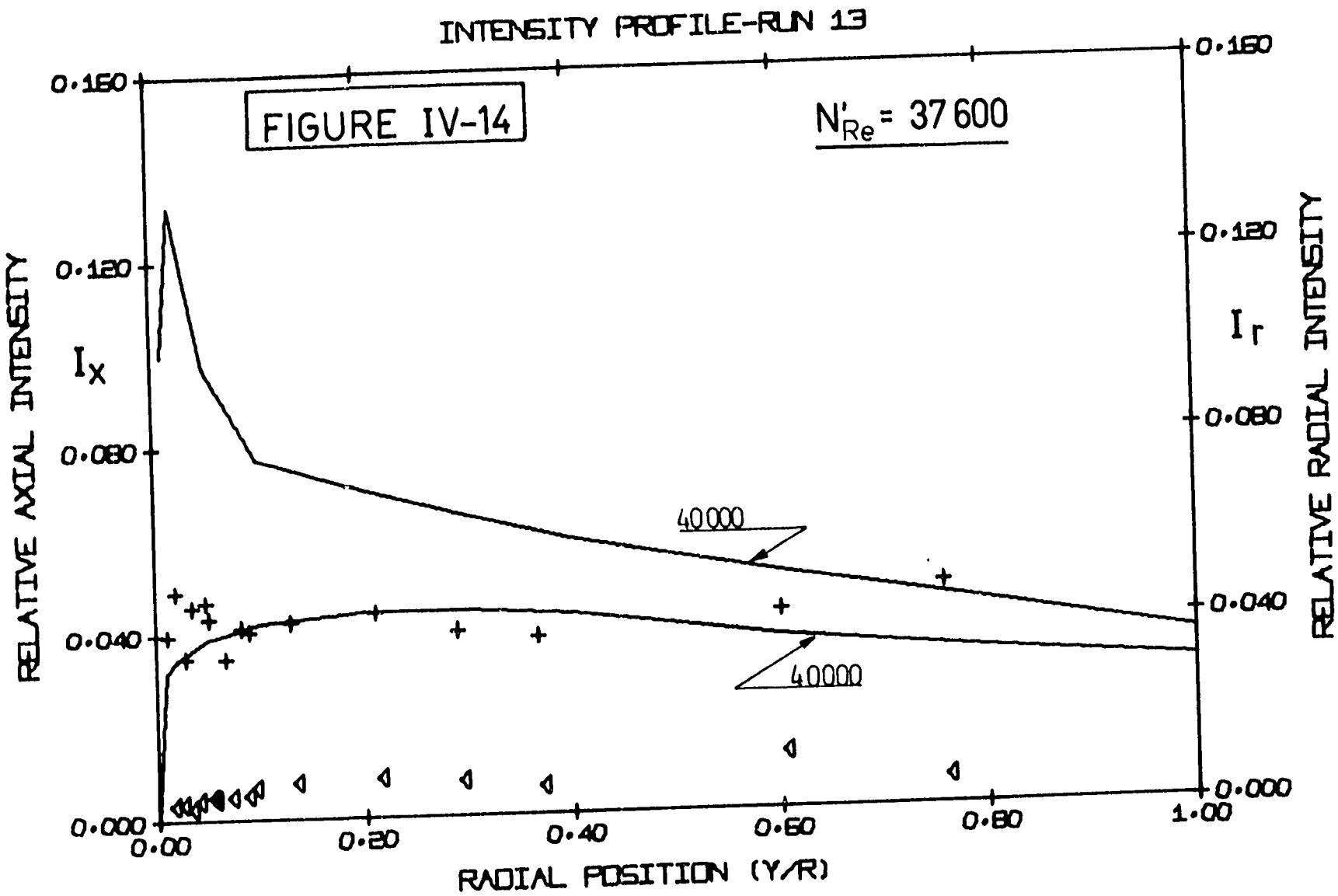
INTENSITY PROFILE-RUN 13
FIGURE IV-14
N'Re = 37 600
RELATIVE AXIAL INTENSITY
Ix
RELATIVE RADIAL INTENSITY
Ir
40000
40000
0.160
0.120
0.080
0.040
0.000
0.00
0.20
0.40
0.60
0.80
1.00
RADIAL POSITION (Y/R)

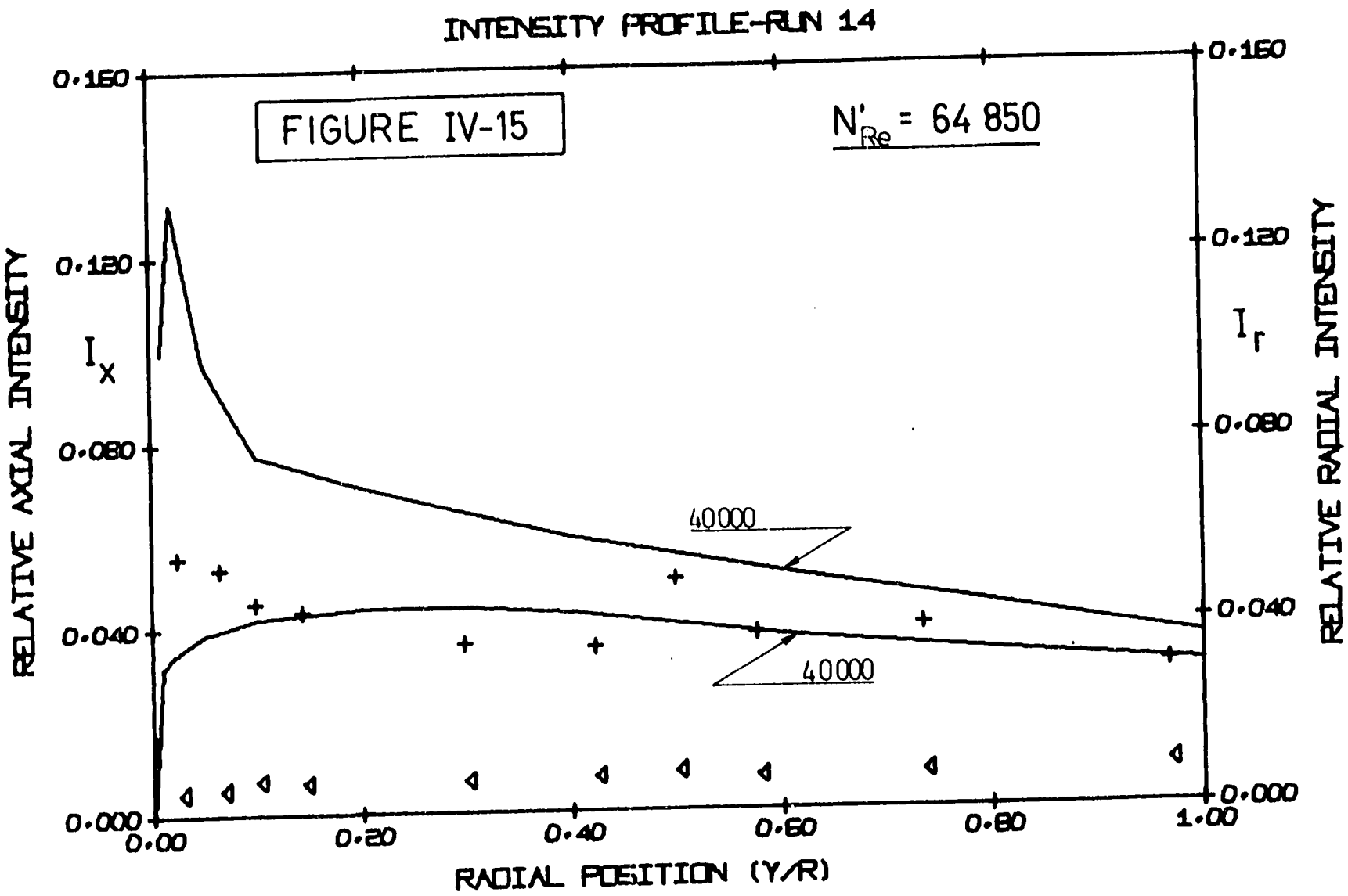
INTENSITY PROFILE-RUN 14
FIGURE IV-15
N'_{Re} = 64 850
RELATIVE AXIAL INTENSITY
I_x
RELATIVE RADIAL INTENSITY
I_r
0.160
0.120
0.080
0.040
0.000
40000
40000
0.00
0.20
0.40
0.60
0.80
1.00
RADIAL POSITION (Y/R)

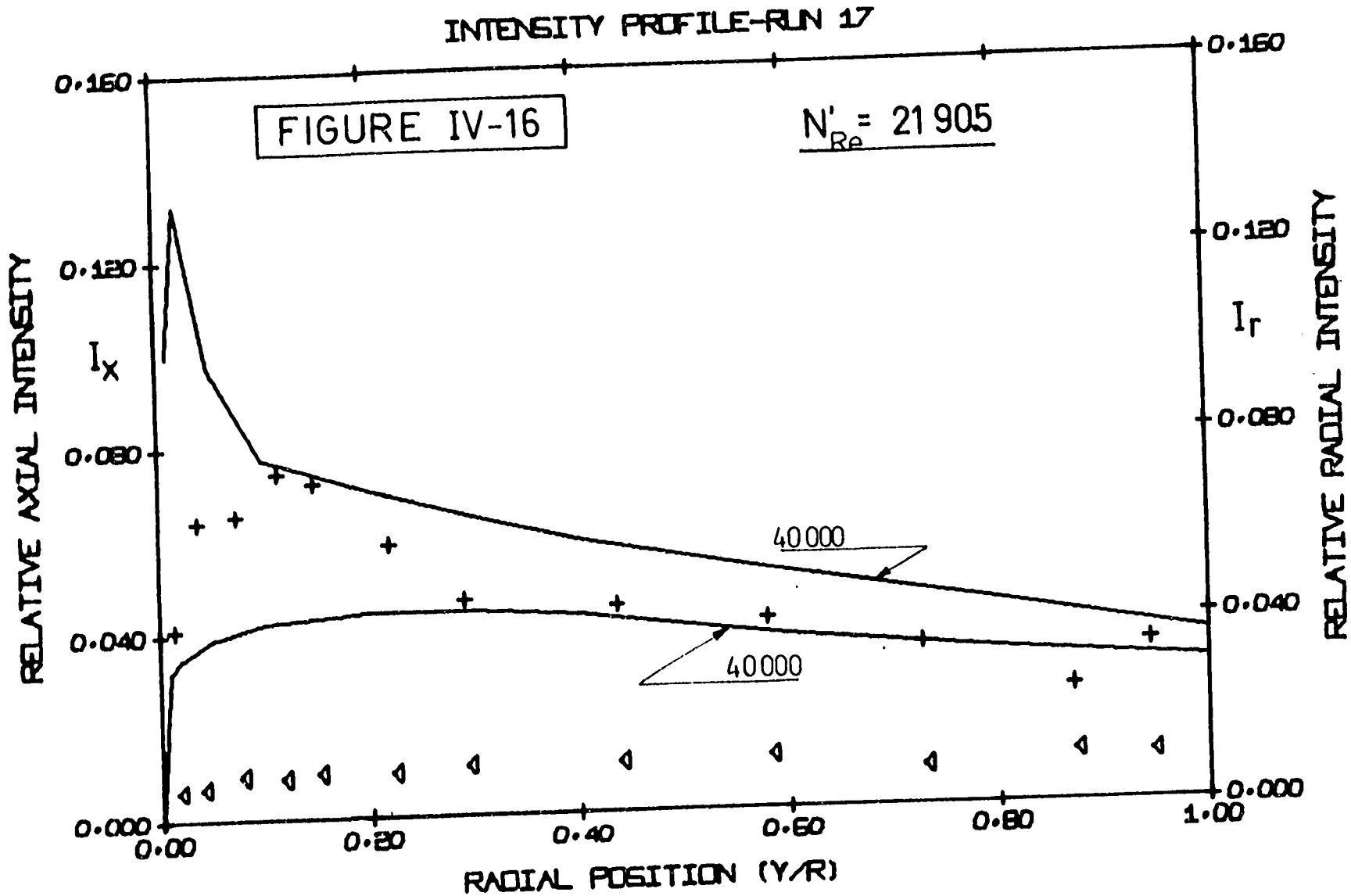
INTENSITY PROFILE-RUN 17
FIGURE IV-16
N'Re = 21 905
RELATIVE AXIAL INTENSITY
Ix
RELATIVE RADIAL INTENSITY
Ir
40000
40000
0.160
0.120
0.080
0.040
0.000
0.00
0.20
0.40
0.60
0.80
1.00
RADIAL POSITION (Y/R)

IV-5 SEMILOGARITHMIC VELOCITY PROFILES

Velocity profiles for the dilute drag reducer and water, plotted on U^+ - Y^+ coordinates are given by Figure IV-17. For the polymer solution the solid lines represent eyeball estimates of the best curve through the data. The curve through the water data has been determined using Equation II-11. At Reynolds number of 80354 in the 1" tube there is a considerable shift in the data points for $30 < Y^+ < 100$. The upper points which form a continuous curve to Y^+ about 90 were obtained at high magnification while the remaining points were obtained with a lower magnification. As noted before and in Table IV-1 with runs designated 12a and 12b this run suffered from a significant amount of degradation. Thus the shift simply reflects the increase in U^* that occurred between the high and low magnification portions of the run. In the other runs where a change in U^* was noted the average was used in Figure IV-17 and one cannot distinguish between data obtained at high and low magnifications.

In all cases the data correspond roughly to Equation I-1 but not in detail. In particular the Newtonian data have a constant intercept B and slope A up to Y^+ about 400 but deviate considerably at higher Y^+. This behavior is quantitatively equivalent to that observed in the number of other studies reporting turbulent velocity profiles of Newtonian fluids (18).

The velocity profiles for the 0.01% polymer solutions show a marked similarity to the Newtonian data at high Y^+ suggesting the same correction $C_3(\xi,f)$, may be applicable. From the figure it is evident that the velocity profiles could be interpreted in a number of

FIGURE IV-17

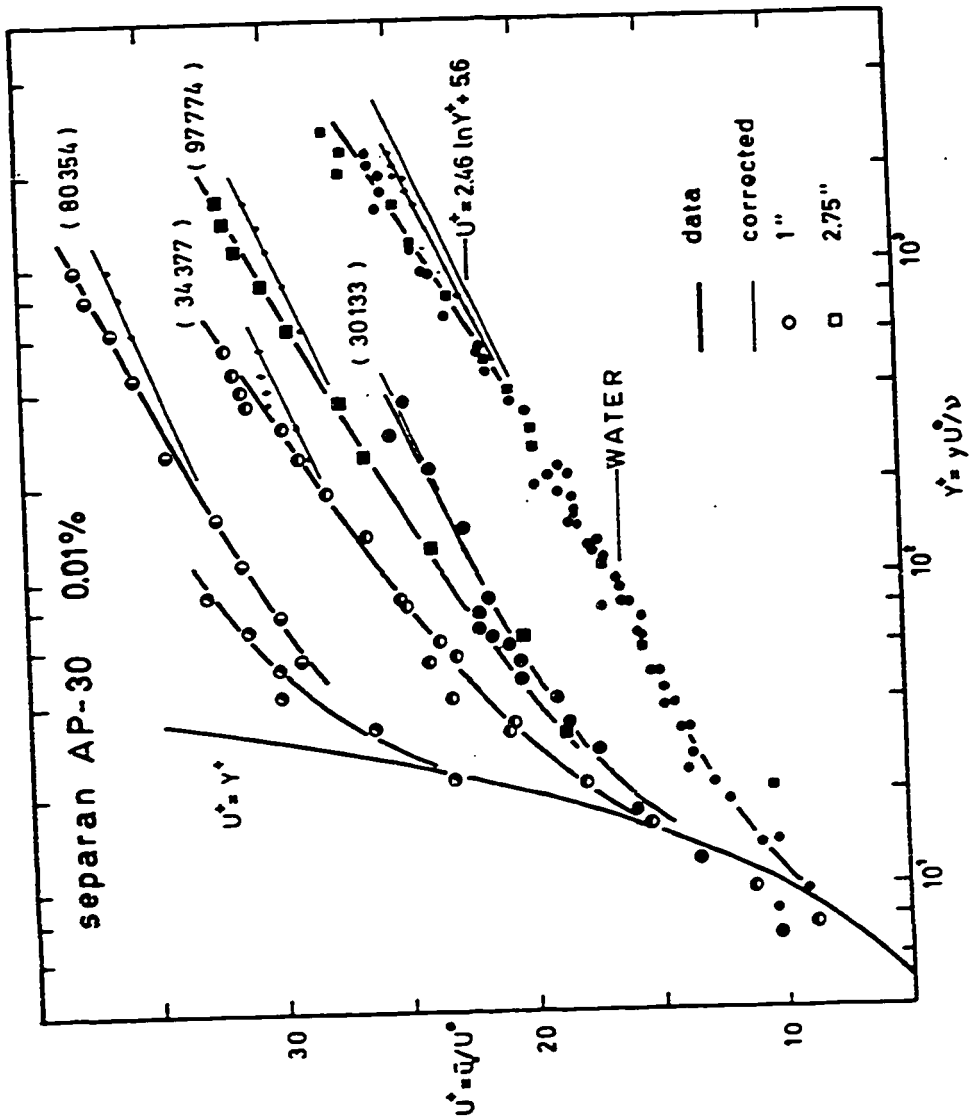

LOGARITHMIC VELOCITY PROFILES

ways:

(i) using Equation I-1 the best fit line through the data would clearly have a slope somewhat higher than the value 2.46 for Newtonian fluids.

(ii) using Equation I-1 with A = 2.46 would fit the data poorly, at least at the higher Reynolds numbers, and would result in a large uncertainty in vertical location of the line.

(iii) using Equation II-11 and assuming Bogue's correction function, at least as a first approximation, is applicable to the drag reducers.

It is emphasized that each of the above yield different values of the intercept function B. In the extreme case the data in Figure IV-17 shows that the discrepancy between (i) and (iii) above could be as large as 20%. In the case of predictions for small amounts of drag reduction in large tubes an error of 20% in B can be shown to cause significant discrepancies in predicted pressure drops.

For drag reducers apparently only one study has applied Bogue's correction function to velocity profiles. As mentioned earlier Nicodemo et al (29) have measured velocity profiles in typical drag reducers using a Pitot probe calibrated in a circular tow tank filled with the polymer solution under consideration. Based on the observation that the data on a semilog plot are linear over only a small portion of the tube near the center, they conclude the profiles cannot be interpreted according to Equation II-11 without major modification. In contrast the velocity profile obtained by Seyer (41)

from streak photographs is in good agreement with Equation II-11. A detailed examination of the profile however, indicates the data are really inconclusive and could be just as well interpreted with or without the function $C_3(\xi,f)$. This being mostly because $C_3(\xi,f)$ is negligible for Seyer's data.

In Figure IV-17 Bogue's correction function has been applied to the smoothing curves drawn through the polymer data. The resulting corrected velocity profiles are given by the lines located below the data points of the various runs. For all of the runs the correction applied to the smoothed curve yields a line that is parallel (within the uncertainty of locating the smoothed curve) to the corrected Newtonian curve showing that (a) Bogue's correction function is adequate for the drag reducers, and (b) the constant A is the same as for Newtonian fluids.

Examination of the resulting velocity profiles shows that the difficulty in interpreting the uncorrected profiles results from the greatly thickened transition portion of the profile merging with the high Y^+ data approximately where the correction function becomes significant. For Newtonian fluids there is a large range of $Y^+(30 < Y^+ < 400)$ separating these two regions.

Figure IV-17 shows quantitatively the marked thickening of the sublayer region. For the highest Reynolds number the influence of the wall extends to $Y^+ = 200$ whereas for Newtonian fluids $Y^+ = 30$ is about the upper limit of the wall region. It is interesting to note that the buffer region is somewhat larger in the 2.75" than that in the 1" tube.

If the correction factor is ignored significant errors may result in the determination of the intercept $B(\theta^+)$ and uncertainty in the intercept function may be serious in prediction of drag reduction particularly in large pipes.

Since no elasticity measurements were made in this work it is not possible to determine B as a function of the parameter θ^+ as is suggested by Seyer (43). However, for a given polymer and concentration θ^+ depends on U^* and therefore it is equivalent to plot B as a function of U^*.

The function B as determined from friction measurements and corrected velocity profiles is given by Figure IV-18. The agreement from the velocity profiles of the two tubes as well as that from friction measurements supports in some detail, and over a significant range of variables, the velocity profile and attendent analysis given by Equations II-1 to II-11. The largest disagreement occurs for the point designated as run 10. As indicated by the somewhat lower friction factor for this point in Figure IV-1, the polymer had not been degraded sufficiently and so the higher value of B is expected. Alternatively, if the function were plotted against the relaxation time parameter the higher elasticity of the material at conditions of run 10 would cause this point to shift to the right relative to points 6 and 16, and would fall much nearer to the curve.

FIGURE IV-18

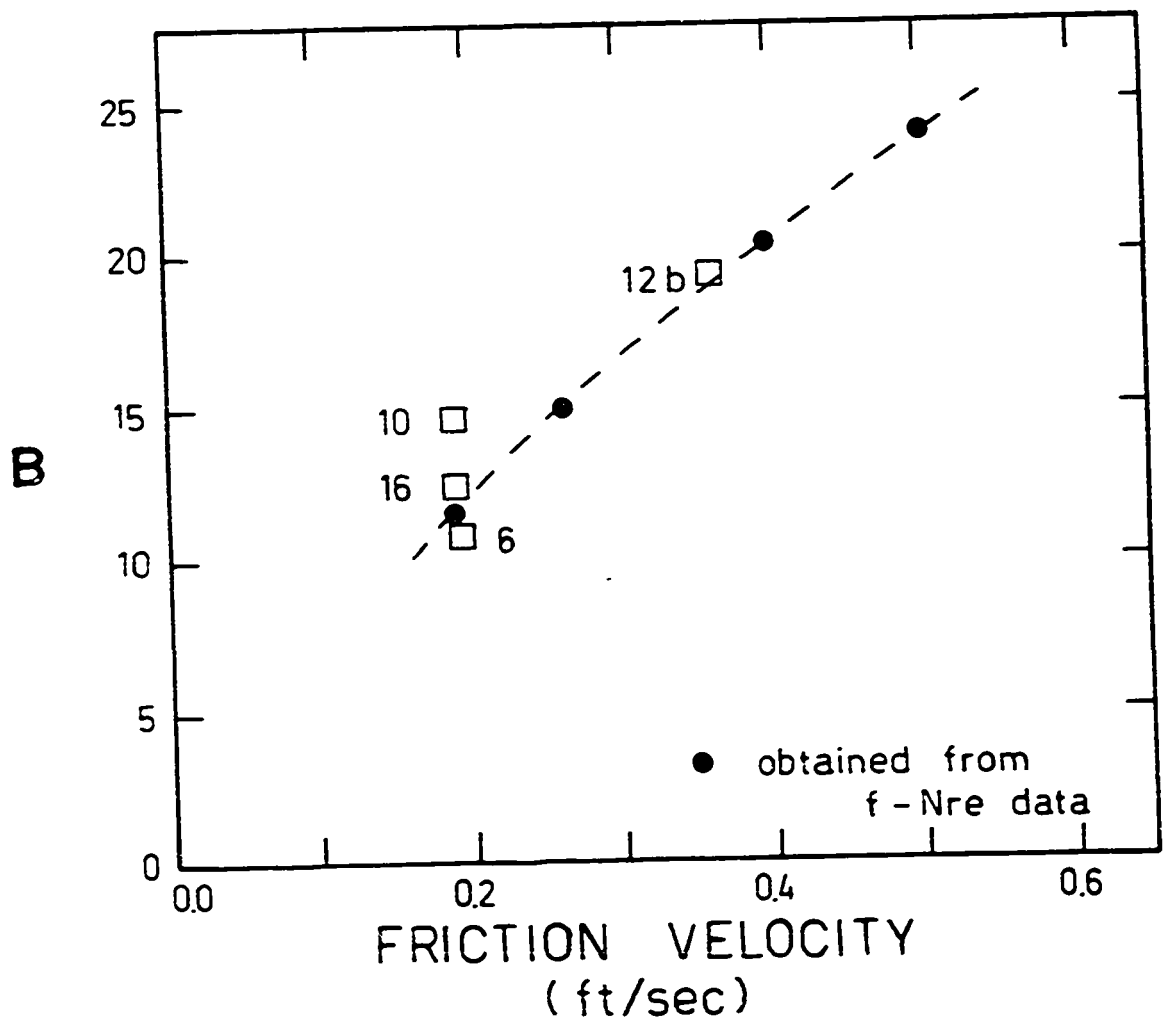
B
25
20
15
10
5
0
0.0
0.2
0.4
0.6
12 b
10
16
6
obtained from
f - Nre data
FRICTION VELOCITY
(ft/sec)

Rudd (37) indicated that if Schubert and Corcos theory of the wall turbulence is considered and modified for the case of viscoelastic fluid, then the similarity laws can be rescaled to take account of the viscoelastic terms so that the parameters for drag reducers can be predicted from the Newtonian values. From his development and experimental determination of the scale factor, he obtained the following expression for the B function

$$B = 12\ D - 2.44\ \ln D - 6.5 \qquad \text{IV-1}$$

where

$$D^2 = 1 + K\ \theta^+ \qquad \text{IV-2}$$

is the scale factor with $K \approx 0.5$ as found from Rudd's data. This scale factor should, if calculated for each run, rescale all turbulence parameters (velocity and distance) to bring them on a single curve, the Newtonian case. From his work the predicted values of B with θ^+ were compared to the experimental results of Seyer and Metzner. The B functions are in agreement for θ^+ lower than 17 but Rudd's estimated asymptote is higher with value of 40 for θ^+ of 37. This is in reasonable agreement with the extrapolation of the friction data in this work.

It is interesting to use his correlation to estimate the boundary layer thickness and the value of B for run 12b of this work. The estimated relaxation time obtained from the friction data of run 12b and using Equation II-16 was used in Equation IV-2 to evaluate the scale factor D. It was found that $\theta = 8.8 \times 10^{-4}$ sec and D = 2.4. The estimated dimensionless thickness of the boundary was $Y^+ = 84$

($Y^{+}_{1_{water}}$ x D) and the value of B was found to be 20.61. From Figure IV-17 the intercept is 19.1 for this run and the boundary layer extends to something in the order of 100. This is surprisingly good agreement.

IV-6 TURBULENCE INTENSITIES

The RMS values obtained for each set of the axial and radial instantaneous velocities are used to estimate the relative turbulence intensities. As indicated in Chapter I, great confusion is found from a survey of the measured relative intensities in the drag reducers owing to the uncertainty in accuracy of the results and in how to scale or compare them for different systems.

The sample histograms for polymer in Figure IV-5 when compared to water have already indicated a significant lowering of radial fluctuations or intensity occurs for the dilute drag reducer at a given Y^+.

Figures IV-19 to IV-23 show all of the Newtonian intensity data obtained in this work. The curves on the figures represent Sandborn's data for air at the indicated Reynolds numbers. Runs 4 and 5 on Figures IV-19 and IV-20 do not extend over an appreciable portion of the tube but are considered to be in excellent agreement with the curves at the smallest radial positions. Reference to Appendix H shows these data are based on a small number of instantaneous readings relative to the other runs in this work.

In Figure IV-21 for run 9 the circled points form a group of data which are consistently lower than the curves. These data which have been circled are from a separate set of photographs (the high magnification portion of the run) than the remaining points and apparently reflect some mistake in determining calibration constants. If they are ignored the data show excellent agreement with Sandborn's curves over the entire section.

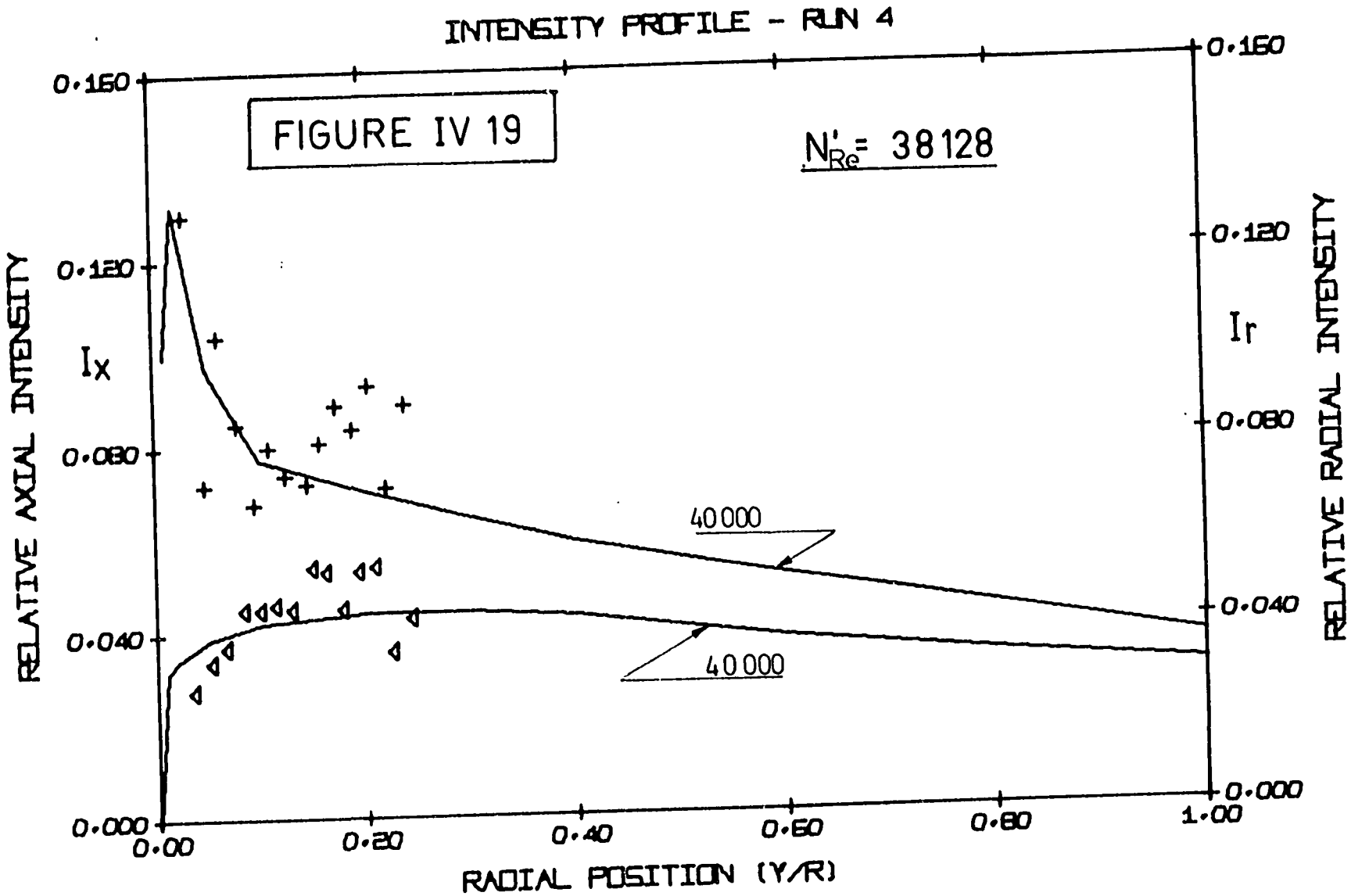
INTENSITY PROFILE - RUN 4
FIGURE IV 19
N'_{Re}= 38128
RELATIVE AXIAL INTENSITY
Ix
RELATIVE RADIAL INTENSITY
Ir
40000
40000
0.160
0.120
0.080
0.040
0.000
0.00
0.20
0.40
0.60
0.80
1.00
RADIAL POSITION (Y/R)

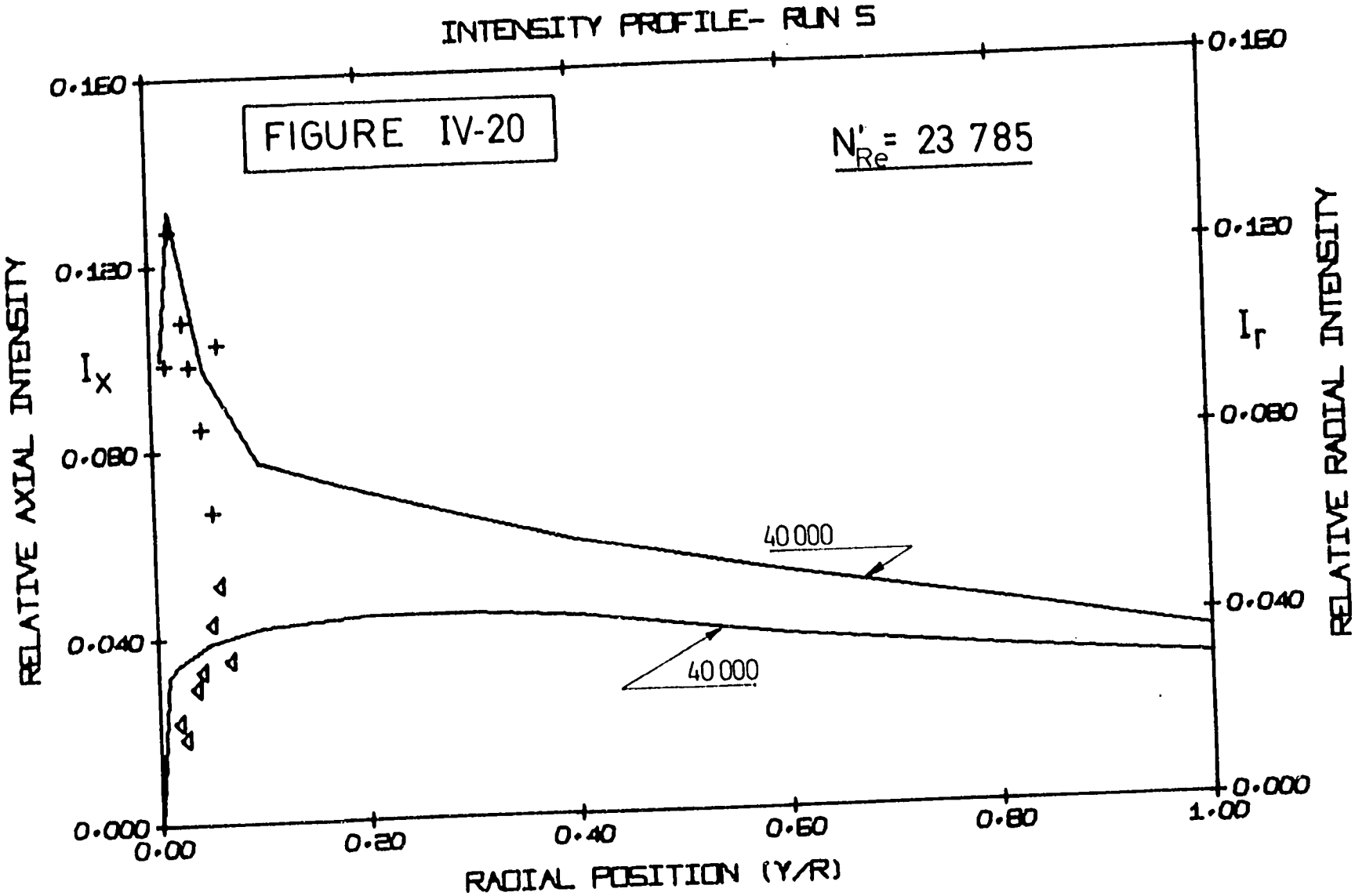
INTENSITY PROFILE- RUN 5
FIGURE IV-20
N'_{Re} = 23 785
RELATIVE AXIAL INTENSITY
I_x
RELATIVE RADIAL INTENSITY
I_r
40 000
40 000
0.160
0.120
0.080
0.040
0.000
0.00
0.20
0.40
0.60
0.80
1.00
RADIAL POSITION (Y/R)

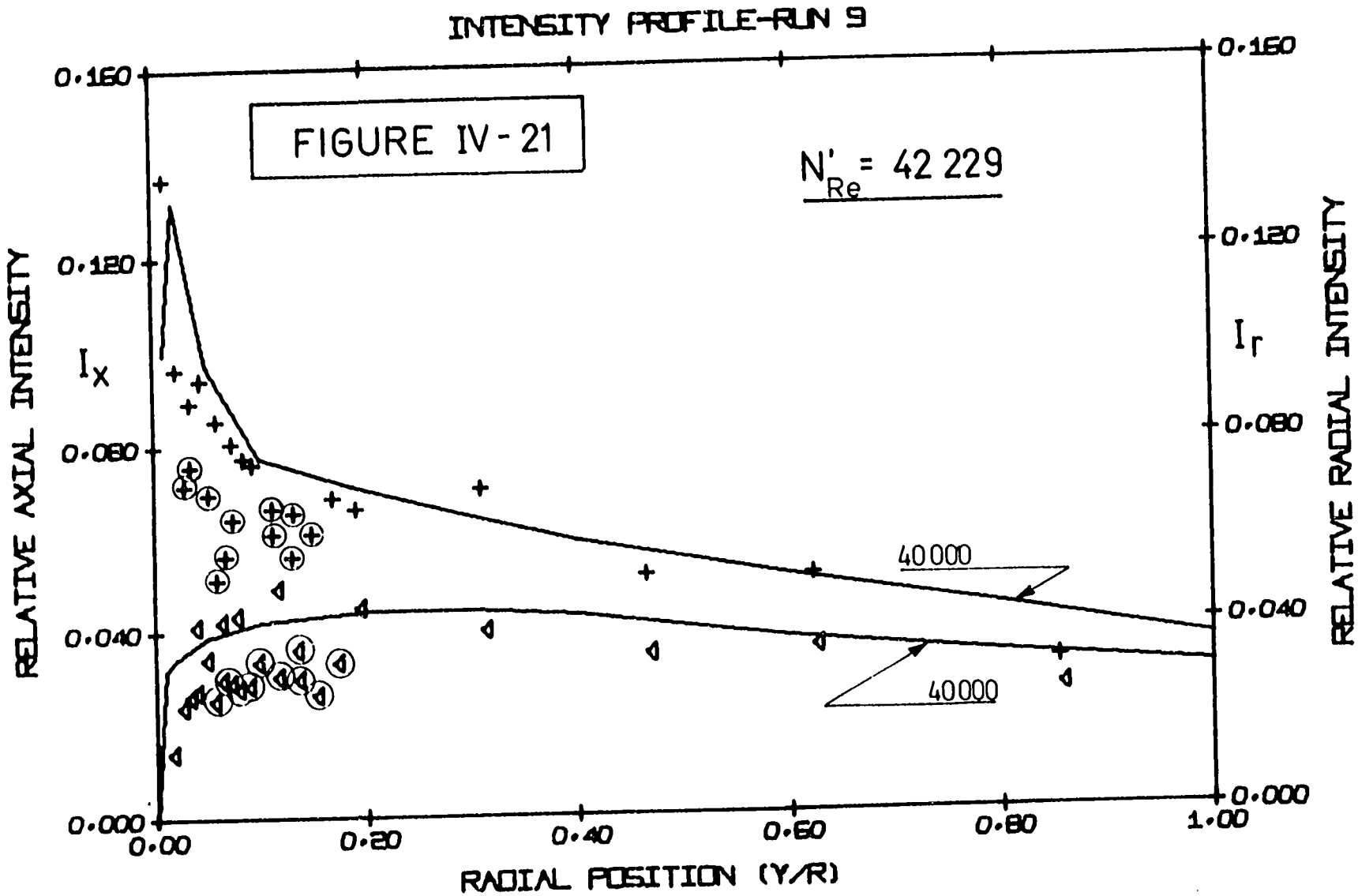
INTENSITY PROFILE-RUN 9
FIGURE IV-21
N'Re = 42 229
RELATIVE AXIAL INTENSITY
Ix
RELATIVE RADIAL INTENSITY
Ir
40000
40000
0.160
0.120
0.080
0.040
0.000
0.00
0.20
0.40
0.60
0.80
1.00
RADIAL POSITION (Y/R)

The data in Figures IV-22 and IV-23 for the remaining runs which are at the highest Reynolds numbers are again in excellent agreement with the curves over most of the section. Near the centerline the data are somewhat higher than the curves, however, it is not clear what the origin of this discrepancy is. As shown in Appendix E, calculations of the Reynolds stress by forming the product $\overline{U_x'U_r'}$ and the kinetic energy $\overline{U_x'U_x'}$ for run 11 are in excellent agreement with the measured Reynolds stress and Laufer's (21) kinetic energy. Thus it is not clear that the intensities are seriously in error.

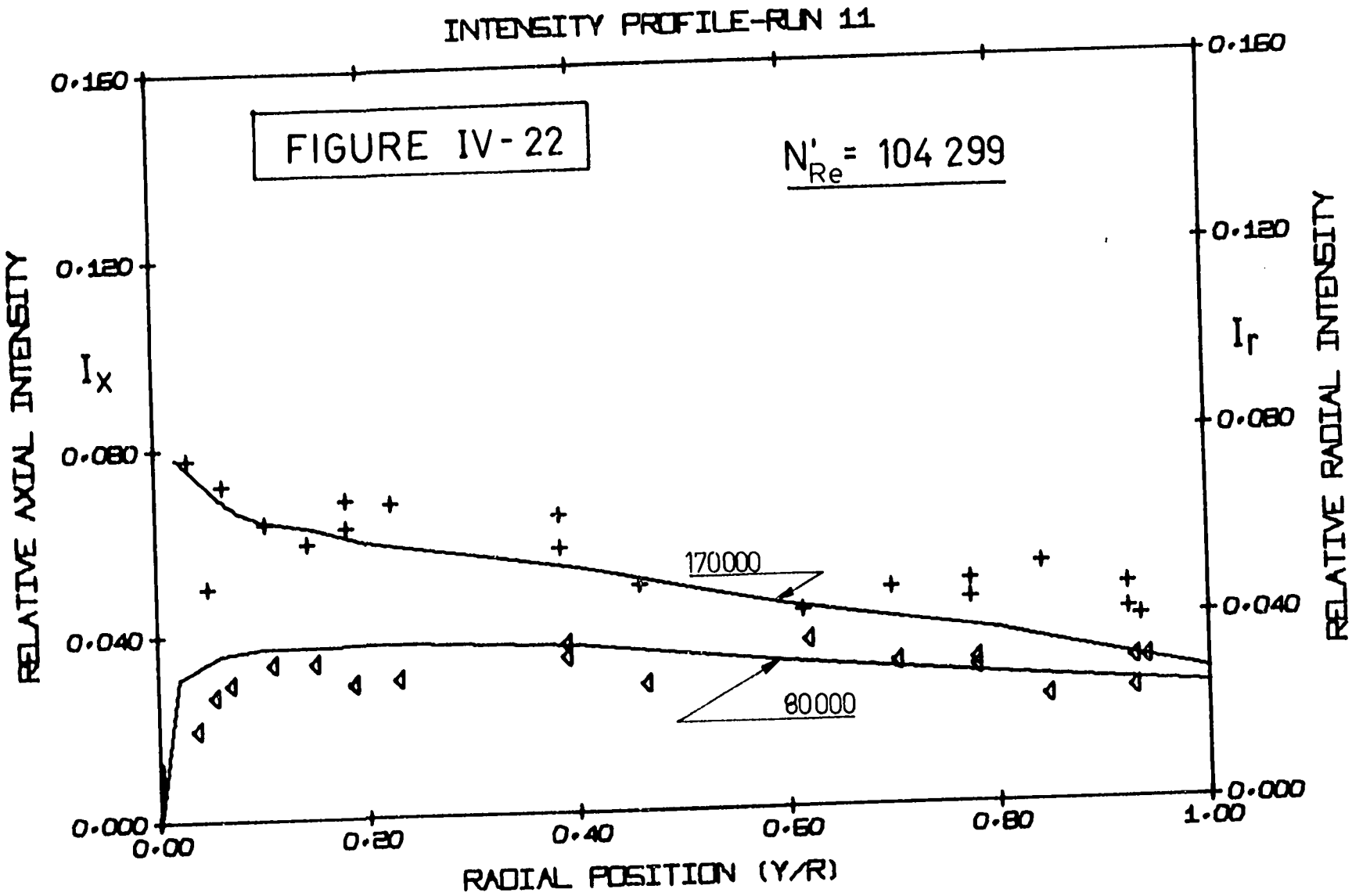
INTENSITY PROFILE-RUN 11
FIGURE IV-22
N'_{Re} = 104 299
RELATIVE AXIAL INTENSITY
I_x
RELATIVE RADIAL INTENSITY
I_r
170000
80000
0.000
0.040
0.080
0.120
0.160
0.00
0.20
0.40
0.60
0.80
1.00
RADIAL POSITION (Y/R)

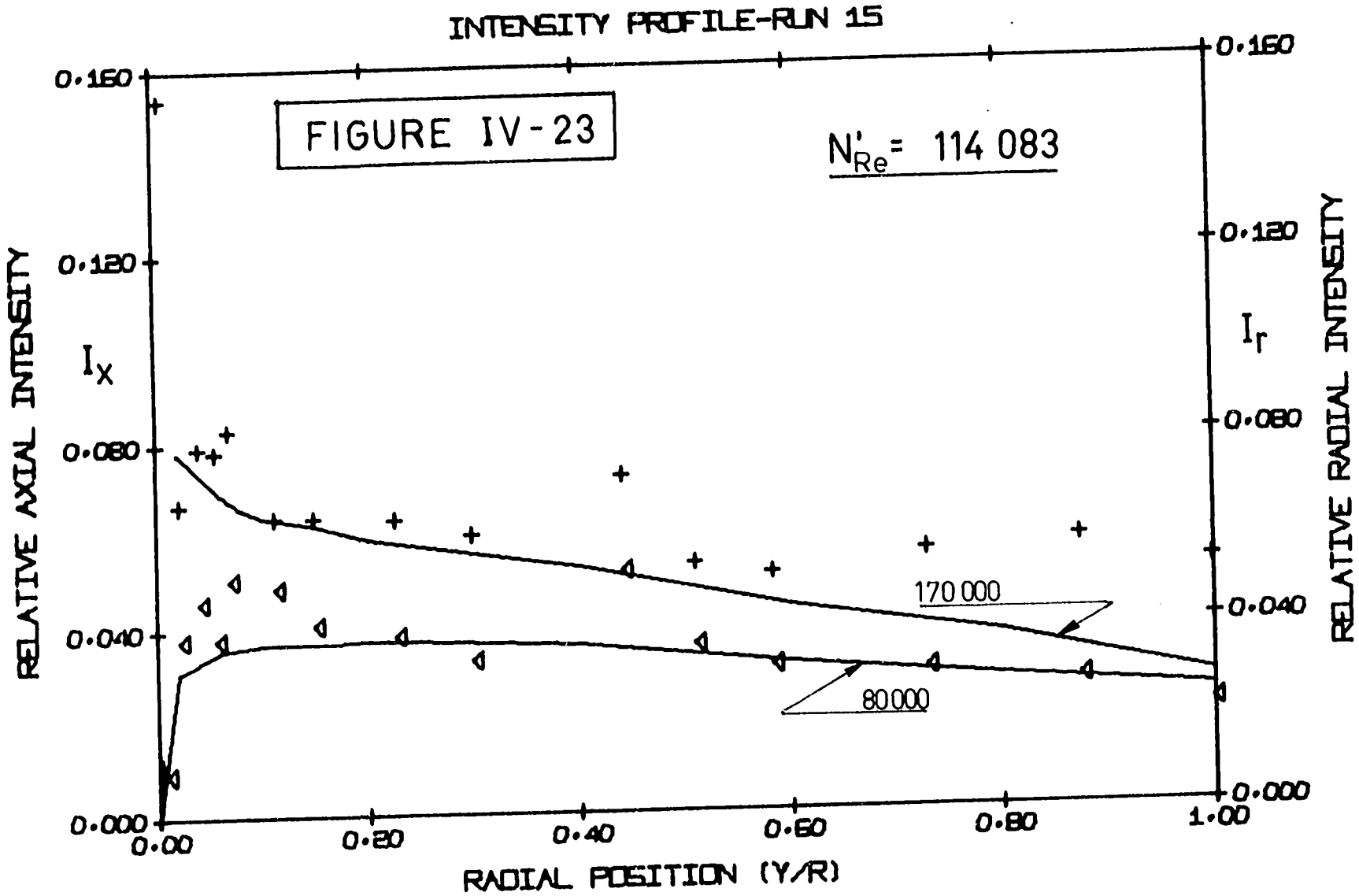
INTENSITY PROFILE-RUN 15
FIGURE IV-23
N'_{Re}= 114 083
RELATIVE AXIAL INTENSITY
I_X
RELATIVE RADIAL INTENSITY
I_r
0.160
0.120
0.080
0.040
0.000
170 000
80 000
0.00
0.20
0.40
0.60
0.80
1.00
RADIAL POSITION (Y/R)

The .01% intensities relative to maximum velocity for runs 6, 10 and 12 in the 1" tube and run 16 in the 2.75" tube are compared to the air curves in Figures IV-24 to IV-27. These figures provide a comparison of the intensity calculated relative to maximum velocity at approximately equal Reynolds number. Since the water and polymer viscosities are about the same the comparison could also be viewed as one at the same flow rate or bulk average velocity.

In each run the radial intensities are markedly lower at all radial positions than the intensities for Newtonian fluids. The amount of lowering of the intensities is ordered according to the amount of drag reduction; thus the radial intensities for the 2.75" pipe are somewhat higher than those in the 1" pipe at an equivalent Reynolds number.

Axial intensities for the low Reynolds number runs, run 6 and run 10 are not altered significantly from the Newtonian values. At high Reynolds number however, they are significantly lower in the core. Notice that the Newtonian curves of axial intensity in Figures IV-26 and IV-27 are for Reynolds number of 170000 and that a curve for Reynolds number coinciding with the data points would be above this curve.

In all cases the rapid increase in intensity, usually associated with the edge of the boundary layer, is shifted toward larger radial positions. This suggests, as do the velocity profiles, a thickening of the boundary layer occurs.

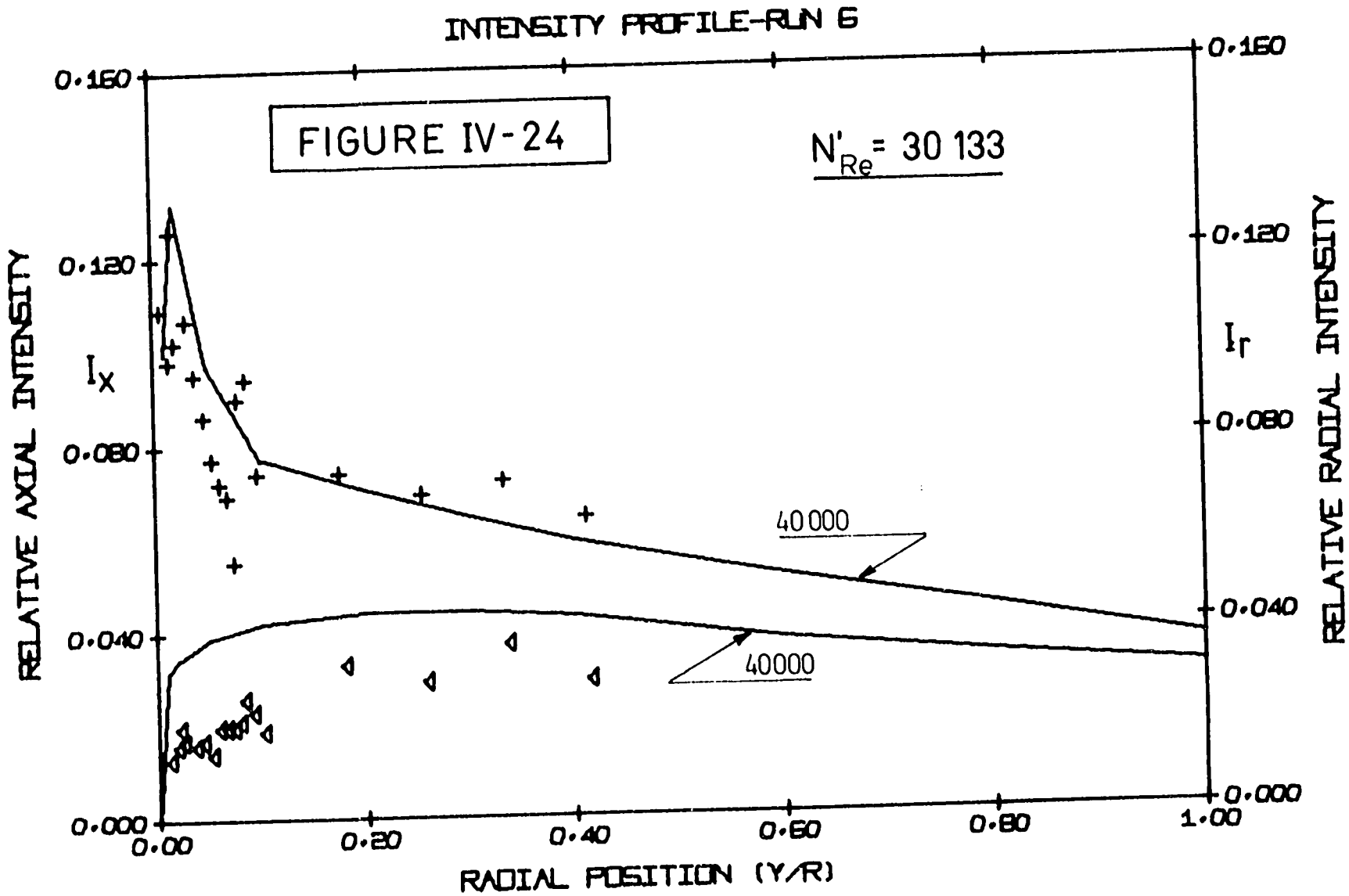
INTENSITY PROFILE-RUN 6
FIGURE IV-24
N'Re = 30 133
RELATIVE AXIAL INTENSITY
Ix
RELATIVE RADIAL INTENSITY
Ir
40 000
40000
0.160
0.120
0.080
0.040
0.000
0.00
0.20
0.40
0.60
0.80
1.00
RADIAL POSITION (Y/R)

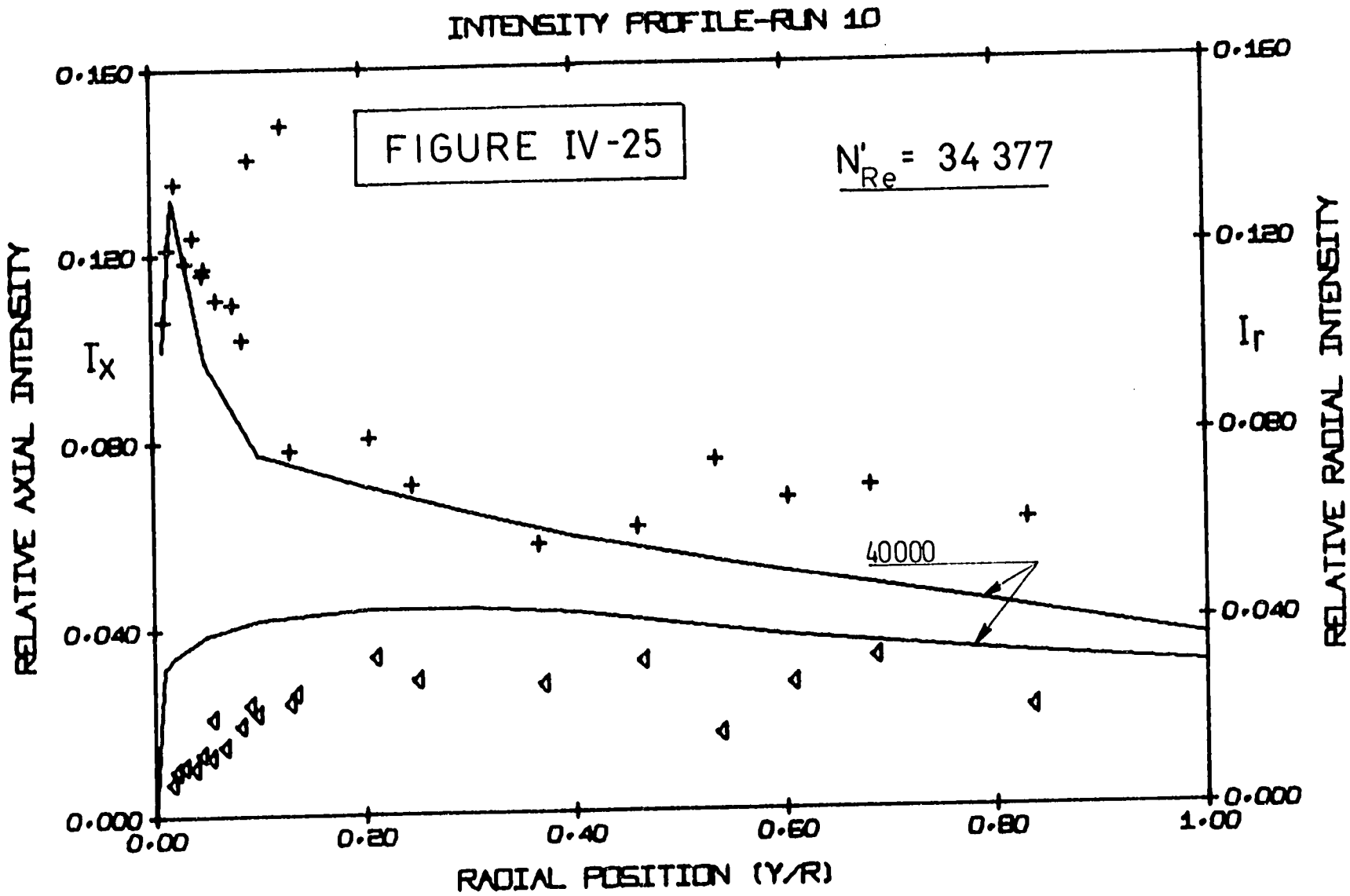
INTENSITY PROFILE-RUN 10
FIGURE IV-25
N'Re = 34 377
40000
Ix
Ir
RELATIVE AXIAL INTENSITY
RELATIVE RADIAL INTENSITY
RADIAL POSITION (Y/R)
0.000
0.040
0.080
0.120
0.160
0.00
0.20
0.40
0.60
0.80
1.00

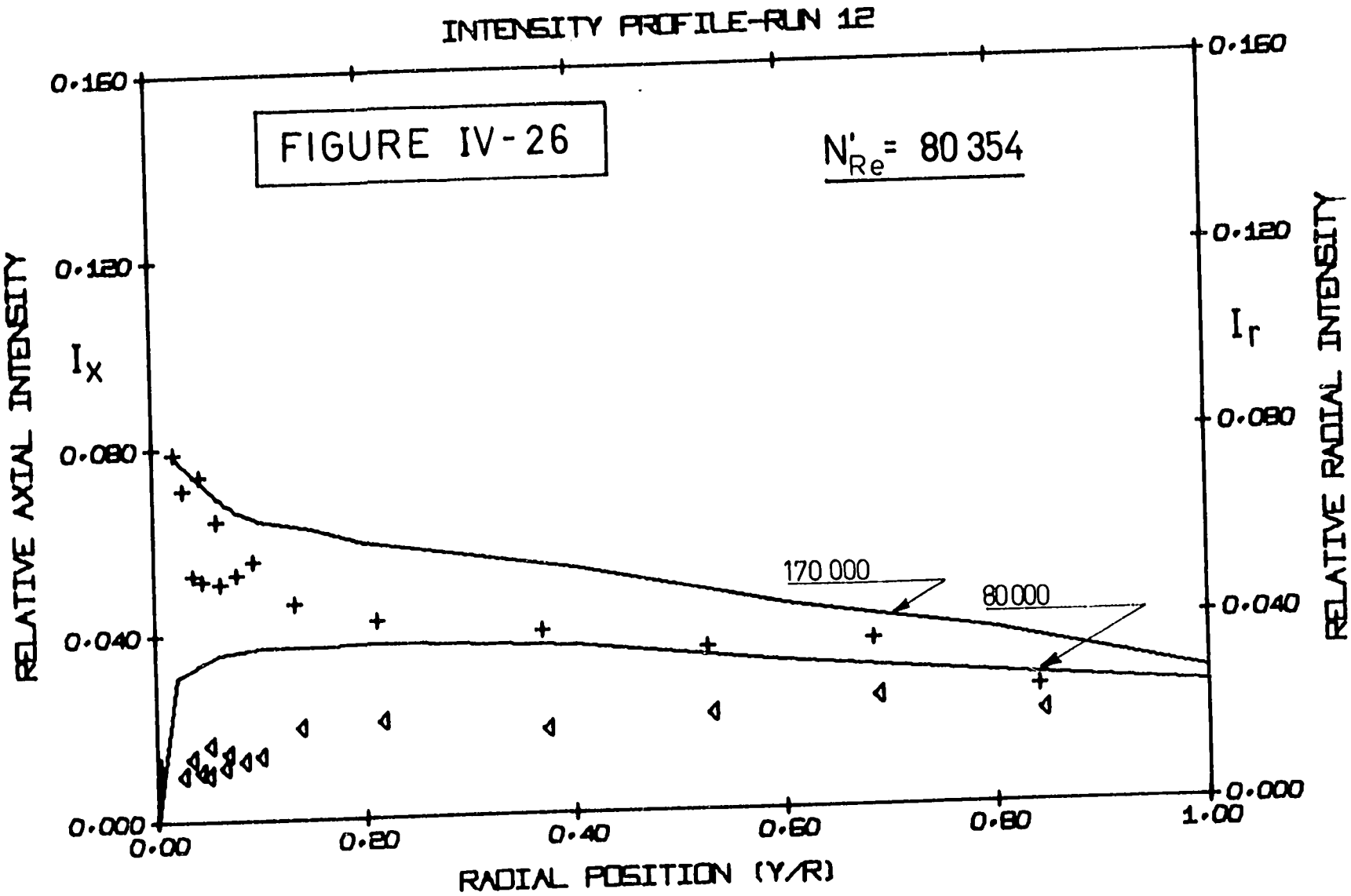
INTENSITY PROFILE-RUN 12
FIGURE IV-26
N'_{Re} = 80 354
RELATIVE AXIAL INTENSITY
I_x
RELATIVE RADIAL INTENSITY
I_r
170 000
80 000
0.160
0.120
0.080
0.040
0.000
0.00
0.20
0.40
0.60
0.80
1.00
RADIAL POSITION (Y/R)

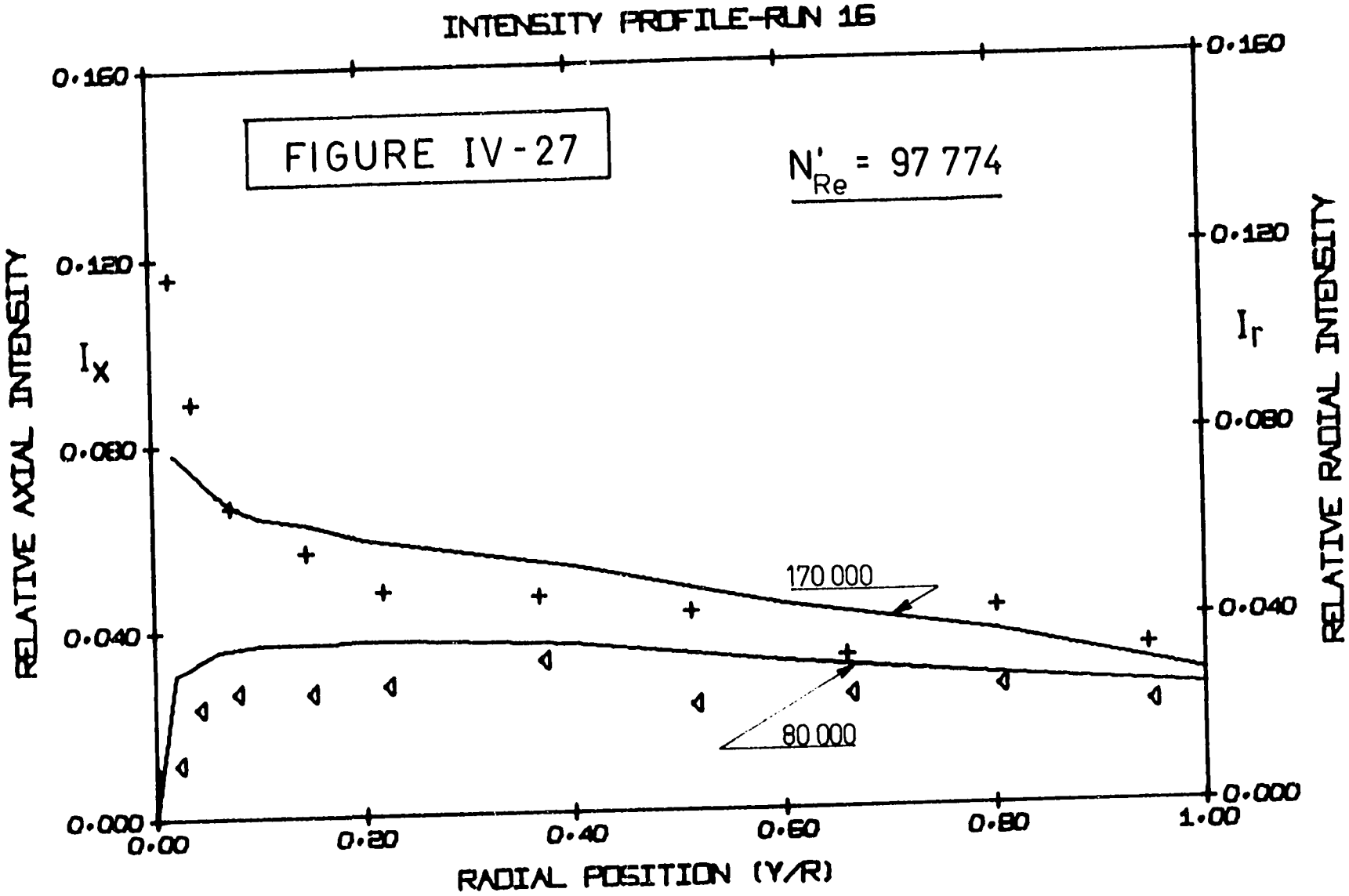
INTENSITY PROFILE-RUN 16
FIGURE IV-27
N'_{Re} = 97 774
RELATIVE AXIAL INTENSITY
I_x
RELATIVE RADIAL INTENSITY
I_r
170 000
80 000
0.160
0.120
0.080
0.040
0.000
0.00
0.20
0.40
0.60
0.80
1.00
RADIAL POSITION (Y/R)

The intensity data made dimensionless with friction velocity U^* are plotted as a function of Y^+ in Figure IV-28. The effect of dividing by U^* is to shift the intensities of the drag reducers upward relative to the water curves. In the lower portion of the figure the radial intensities still tend to be lower than the Newtonian intensities, particularly in the wall region. The general trend is that the polymer intensities are increasing more slowly with radial position, in accord with the thickening of the sublayers. Ultimately, they attain about the same value as for Newtonian fluids. In terms of the bursting arguments the radial intensities indicate that the large wall eddies are simply rescaled in size. It is apparent, however, since the frequency of occurrence can be reduced, as shown in studies by Fortuna and Hanratty (15) as well as Meek and Baer (24), that the process of lowering the radial intensities is more complicated than scaling just the size.

In contrast to the radial intensities the axial intensities in Figure IV-28 relative to U^* are all significantly larger than the Newtonian values in the wall region and approach a single curve in the core region. The shape of these curves is identical to Rudd's (36) for a similar amount of drag reduction. However, these data are not ordered with respect to amount of drag reduction on this type of plot. Reference to Table IV-2 shows that runs 5, 6, 10 in the 1" tube and 16 in the 2.75" tube are all at approximately the same U^* (the value of U^* for run 12 is two times larger).

In Figures IV-17 and IV-18, it is seen that these runs have increasing intercepts owing to different levels of elasticity

FIGURE IV-28

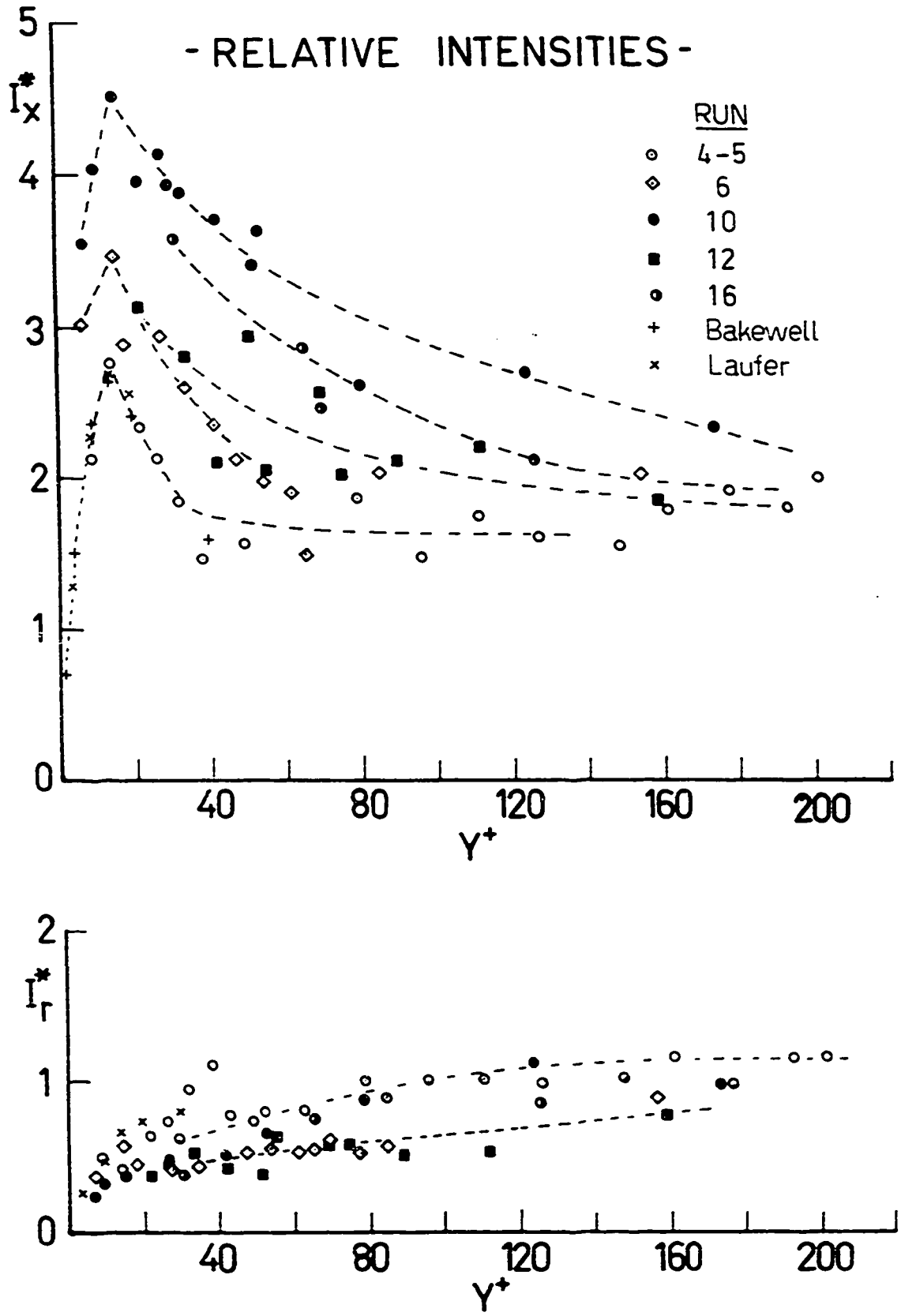
- RELATIVE INTENSITIES -
I_x^*
RUN
4-5
6
10
12
16
Bakewell
Laufer
0
1
2
3
4
5
40
80
120
160
200
Y^+
I_r^*
0
1
2
40
80
120
160
200
Y^+

of the fluid. The increased intensities are in the order of increasing elasticity or equivalently increase in the velocity profile intercept, B, at fixed U^*. It is obvious that the level of intensity, at a fixed U^*, is very sensitive to the elasticity of the system.

Consideration of the velocity intercept for run 12, which has the highest intercept of all the runs, would indicate the intensities for this run should be extremely high. This is not the case, however, as these intensities are lower than for runs 10 and 16 and about the same as those of run 6. In the core these data are consistent with the other runs.

Dimensional considerations suggest (see Chapter II) that the increase in intensities in the wall region should be ordered with respect to the parameter $\theta^+ = \frac{\theta U^{*2}}{\nu}$. Rudd (37) as indicated earlier has formulated an explicit expression for the dependence of the flow parameters on θ^+. Figure IV-29 is a plot of the rescaled intensities and distances as suggested by Rudd. The parameter D, defined in Equation IV-1, has been determined directly by substituting values of B from the velocity profiles. Notice if equation IV-2 were used to find relaxation times, the times so determined would be slightly different than those shown in Appendix A. The axial intensities for the runs with equal U^* are collapsed to single curve which coincides with the curve for water. Rudd has based his conclusions on a similar plot for only one intensity profile. The intensities for run 12, which is at different U^*, are not scaled properly. In fact the spread of intensities between run 12 and the master curve is about the same as the maximum spread in the previous

FIGURE IV-29

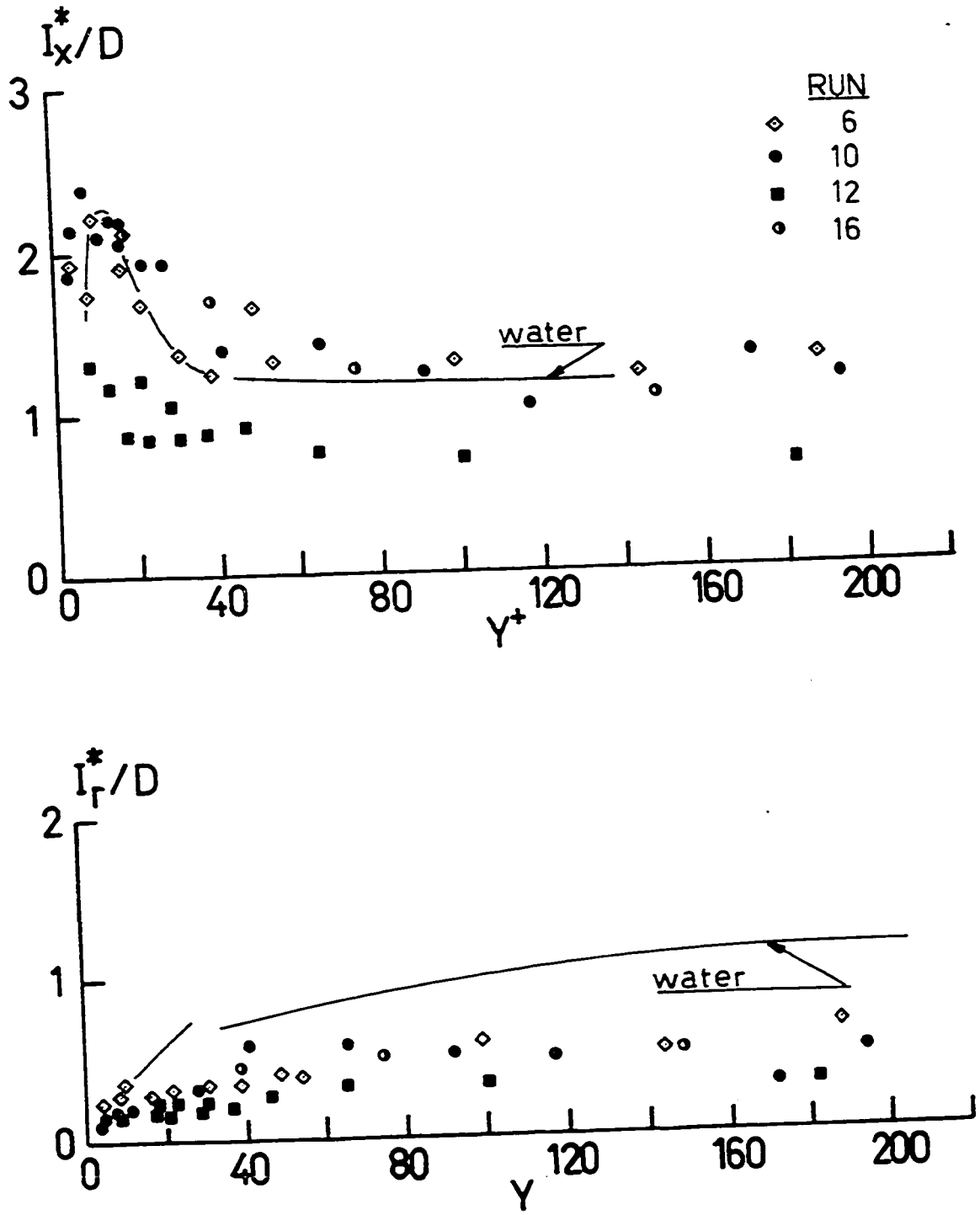

- RELATIVE INTENSITIES -

figure.

The radial intensities do not superimpose on the water curve, but are much lower at all radial positions. The polymer intensities follow a single curve but there is no obvious improvement over the plot of the same data in Figure IV-28.

CONCLUSION AND RECOMMENDATIONS

An extensive series of measurements of instantaneous velocity streak photographs have been obtained in Newtonian and drag reducing fluids. Based on a comparison with available Newtonian data of velocity profiles and axial and radial intensities, the quantitative usefulness of the technique is verified. Since the streak photograph technique does not suffer from the serious limitations of probe devices in drag reducers it is implicit that the measurements in the drag reducing fluids are also quantitatively correct.

Histograms of instantaneous axial velocity confirm the presence of binodal distributions in the boundary layer. Histograms of radial velocity are binodal for water but there is no evidence of two peaks for the polymer solutions. By ordering the set of instantaneous velocities according to the sign of radial component it is found that on the average the fluctuating velocities toward the center of tube are large than those toward the wall. This observation agrees with the visual observations of "bursting" described by Brodkey amongst others. For a given radial position the largest fluctuations in radial histograms for polymer solutions are less than those for Newtonian fluids at similar conditions.

For drag reducing fluids Bogue's correction function must be applied to the data in order to obtain a consistent representation of velocity profiles. Failure to use the correction function can result in large uncertainties in determining the intercept $B(\delta^+)$ of the velocity profiles.

The correct form of the function $B(\theta^+)$ determined by Seyer and Metzner is correct for θ^+ less than approximately 12. At large θ^+, where a drag reduction asymptote is predicted the function is not unique. The data in this work show that lower friction factors can be observed than Seyer and Metzner's.

Turbulence intermittency factors, determined from velocity profiles for a 0.1% solution in a one-inch pipe show the first turbulence appears at a generalized Reynolds number of 2100. Extrapolation of the data show that the flow is not fully turbulent until Reynolds numbers in the vicinity of 10^6 are attained. Consideration of earlier data and data obtained in a 2.75" pipe show the intermittency is highly sensitive to level of elasticity as well as the diameter. These measurements show the need for further consideration of the so-called asymptote as well as the limits of transition.

If the root mean square of the axial and radial velocity fluctuations of the polymeric solutions are made dimensionless with the maximum velocity, both are found to be lower than those for water at all radial positions; the amount of lowering being larger as the level of elasticity of the solutions increases. On the other hand when compared to friction velocity the axial fluctuations are larger while the radial remain smaller than those for Newtonian fluids. Scaling of the intensities according to Rudd does not superimpose the curves unless only data obtained at the same friction velocity are considered.

Further work is needed to determine the proper scaling factors for turbulence in these systems.

BIBLIOGRAPHY

1. Astarita, G., and Nicodemo, L., "Behavior of Velocity Probes in Viscoelastic Dilute Polymer Solutions", I.&E.C. Fund., 8, 582, (1969).

2. Astarita, G., and Nicodemo, L., "Velocity Distributions and Normal Stresses in Viscoelastic Turbulent Pipe Flow", A.I.Ch.E.J., 12, 478, (1966).

3. Bakewell, H.P., and Lumley, J.L., "Viscous Sublayer and Adjacent Wall Region in Turbulent Pipe Flow", The Physics of Fluids, 10, No. 9, 1880, (1967).

4. Brodkey, R.S., Cohen, M.F., Knox, J.S., McKee, G.L., McKelvey, K.N., Rao, M.A., Zakanycz, S., and Yieh, H.C., "Turbulence Measurements in Shear Flow Liquids Systems", paper presented at Proceedings of Symposium on Turbulence Measurements in Liquids, Sept. 1969; "Turbulence Measurements in Liquids", edited by Patterson, G.K. and Zakin, J.L., U. of Missouri-Rolla, 1971.

5. Boque, D.C., and Metzner, A.B., "Velocity Profiles in Turbulent Pipe Flow", I.&E.C. Fund. 2, No. 2, 143, (1963).

6. Catania, P.J., "Turbulent Entry Region of Viscoelastic Fluids", M.Sc. Thesis, University of Alberta, 1969; Catania, P.J., and Seyer, F.A., "Laminar and Turbulent Entry Flow of Polymer Solutions", to be presented at the 21st Can. Chem. Eng. Conference, Montreal, Canada, October, 1971.

7. Corino, E.R., and Brodkey, R.S., "A Visual Investigation of the Wall Region in Turbulent Flow", J. Fluid Mech., 37, Part I, 1, (1969).

8. Denn, M.M., and Marrucci, G., "Stretching of Viscoelastic Liquids", A.I.Ch.E.J., 17, 101, (1971).

9. Denn, M.M., and Porteous, K.C., "Elastic Effects in Flow of Viscoelastic Liquids", A.I.Ch.E.J., in press, (1971).

10. Dodge, D.W., and Metzner, A.B., "Turbulent Flow of Non-Newtonian Systems", A.I.Ch.E.J., 5, 189, (1959).

11. Elata, C., Lehrer, J., and Kahanovitz, A., "Turbulent Shear Flow of Polymer Solutions", Israel Journal Technol., 4, 87, (1966).

12. Ernst, W.D., "Investigation of the Turbulent Shear Flow of Dilute Aqueous CMC Solutions", A.I.Ch.E.J., 12, 581, (1966).

13. Fabula, A.G., "An Experimental Study of Grid Turbulence in Dilute High-Polymer Solutions", Sixth Symposium on Naval Hydrodynamics, Office of Naval Research, Dept. of the Navy, Washington, D.C., 1966.

14. Fage, A., and Townend, H.C.H., "An Examination of Turbulent Flow with an Ultramicroscope", Proc. Royal Soc., Ser. A, 135, (1932).

15. Fortuna, G., and Hanratty, T.J., "The Influence of Drag-Reducing Polymers on Turbulence in the Viscous Sub-Layer", January, 1971 presented at

16. Fowles, P.E., "The Velocity and Turbulence Distribution in the Laminar Sublayer", Sc.D. Thesis, Chem. Eng. Dept., M.I.T., (1966).

17. Gordon, R.J., "On the Explanation and Correlation of Turbulent Drag Reduction in Dilute Macromolecular Solutions", J. of Appl. Polymer Sci., 14, 2097, (1970).

18. Hinze, J.O., "Turbulence", ed. McGraw-Hill, New York, 477, (1959).

19. Klebanoff, P.S., "Characteristic of Turbulence in a Boundary Layer with Zero Pressure Gradient", NACA, Report 1247, (1955).

20. Kline, S.J., Reynolds, W.C., Schraub, F.A., and Runstadler, P.W., "The Structure of Turbulent Boundary Layers", J. Fluid Mech., 30, Part 4, 741, (1967).

21. Laufer, J., "The Structure of Turbulence in Fully Developed Pipe Flow", NACA Tr 1174, (1954).

22. Lindgren,R.E., and Chao, J.L., Phys. Fluids, 10, 667, (1967)

23. Marucci, G., and Astarita, G., "Turbulent Heat Transfer in Visco-elastic Fluids", Ind. Eng. Chem. Fund., 6, 470, (1967).

24. Meek, R.L., and Baer, A.D., "The Periodic Viscous Sublayer in Turbulent Flow", A.I.Ch.E.J., 16, 841, (1970).

25. Metzner, A.B., and Astarita, G., "External Flows of Viscoelastic Materials: Fluid Properties Restrictions on the Use of Velocity-Sensitive Probes", A.I.Ch.E.J., 13, 550, (1967).

26. Meyer, W.A., "A Correlation of the Frictional Characteristics for Turbulent Flow of Dilute Viscoelastic Non-Newtonia Fluids in Pipes", A.I.Ch.E.J., 12, 523, (1966).

27. Millikan, C.B., "A Critical Discussion of Turbulent Flows in Channels and Circular Pipes", Proc. 5th Intern. Congr. Appl. Mech., p. 386, John Wiley, N.Y., (1939).

28. Nedderman, R.M., "The Use of Stereoscopic Photography for the Measurements of Velocities in Liquids", Chem. Eng. Sci., 16, 113, (1961).

29. Nicodemo, L., Acierno, D., and Astarita, G., "Velocity Profiles in Turbulent Pipe Flow of Drag-Reducing Liquids", Chem. Eng. Sci., 24, 1241, (1969).

30. Oliver, D.R., "The Expansion/Contraction Behavior of Laminar Liquid Jets", Can. J. Chem. Eng. 44, 100, (1966).

31. Patel, V.C., and Head, M.R., "Some Observations on Skin Friction and Velocity Profiles in Fully Developed Pipe and Channels Flow", J. Fluid Mech. 38, 181, (1969).

32. Patterson, G.K., Zakin, J.L., Rodriquez, J.M., "Drag Reduction, Polymer Solutions, Soap Solutions and Solid Particle Suspensions in Pipe Flow", A.I.Ch.E.J., 14, 434, (1968).

33. Popovich, A.T.,"Statistical Analysis of Fluid Flow Fluctuations in the Viscous Layer Near a Solid Wall", I.&E.C. Fund., 8, 609, (1969).

34. Popovich, A.T., and Hummel, R.L., "Experimental Study of the Viscous Sublayer in Turbulent Flow", A.I.Ch.E.J., 13, No. 5, 854, (1967).

35. Rotta, J., "Experimenteller Beitrag zur Entstehung turbulenter Stromung im Rohr", Ing. Ach. 24, 258 (1956).
- "Boundary Layer Theory", by Schlichting, H., 4th ed., McGraw-Hill, N.Y., (1960).

36. Rudd, M.J., "Measurements Made on a Drag Reducing Solution with a Laser Velocimeter", Nature, 224, 587, (1969).

37. Rudd, M.J., "The Laser Doppler Meter and Polymer Drag Reduction" paper presented at the 67th National Meetings and Biennial Materials Sciences and Eng. Division Conference, A.I.Ch.E., Atlanta, Feb. 1970.

38. Sandborn, V.A., "Study of the Momentum Distribution of Turbulent Boundary Layers in Adverse Pressure Gradients", NACA, TN 3266, (1955).

39. Savins, J.G., "Contrasts in Solution Drag Reduction Characteristics of Polymers Solutions and Micella Systems"; Viscous Drag Reduction by C.S. Wells, Plenum Press, N.Y., 1969.

40. Serth, R.W., and Kiser, K.M., "The Effect of Turbulence on Hot-Film Anemometer Response in Viscoelastic Fluids", A.I.Ch.E.J., 16, 163, (1970).

41. Seyer, F.A., "Turbulence Phenomena in Drag Reducing Systems" Chemical Engineering Department, University of Delaware, 1968.

42. Seyer, F.A., "Friction Reduction in Turbulent Flow of Polymer Solution", J.Fluid Mech., 40, 807, (1970).

43. Seyer, F.A., and Metzner, A.B., "Turbulence Phenomena in Drag Reducing System", A.I.Ch.E.J., 15, 426, (1969).

44. Spangler, J.G., "Studies of Viscous Drag Reduction with Polymers Including Turbulence Measurements and Roughness Effects"; Viscous Drag Reduction by C.S. Wells, Plenum Press, N.Y., (1960).

45. Townsend, A.A., "The Structure of Turbulent Shear Flow", Cambridge University Press, (1956).

46. Virk, P.S., Merrill, E.W., Mickley, H.S., Smith, K.A., Mollo-Christensen, E.C., "The Toms' Phenomena: Turbulent Pipe Flow of Dilute Polymers Solutions", J. Fluid Mech., 30, 305, (1967).

47. Virk, P.S., Mickley, H.S., Smith, K.A., "The Ultimate Asymptote and Mean Flow Structure in Toms' Phenomenon", Trans, of the ASME, Journal of Applied Mechanics, ___, 468, (1970).

48. Wells, C.S., and Spangler, J.G., "Injection of a Drag-Reducing Fluid into Turbulent Pipe Flow of a Newtonian Fluid", The Physics of Fluids, 10, 1890, (1967).

49. Wells, C.S., "Viscous Drag Reduction", Plenum Press, N.Y., 1969.

APPENDIX A

RHEOLOGICAL BEHAVIOR OF THE SOLUTIONS

i) 0.01% Solution

A sample of solution was drawn from the experimental apparatus when pressure drop measurements, recorded in the 1" and 2.75" pipes, corresponded to the predetermined curves for 0.01% solution as presented in Figure IV-1. Viscometric measurements were done with a Weissenberg Rheogoniometer precalibrated with a standard oil. Curves for the standard oil and polymer solutions are presented in Figure A-1. The straight line obtained for the standard oil is representative of Newtonian behavior with a slope of unity and a viscosity of 8.62 cps. The specified viscosity at the same temperature is 8.63 cps.

The curve of the 0.01% solution indicated a slightly pseudoplastic behavior in the range of shear rates obtained with the Rheogoniometer. The flow behavior index varied from 0.922 to 0.930 and the apparent viscosity from 1.25 cps to 1.50 cps at the lowest shear rate. Although the Rheogoniometer data are at much lower shear rates than those in the pipe experiments, they join smoothly with Seyer's data (41) at the shear stresses of interest. Thus the kinematic viscosity is assumed to be 1.2×10^{-5} ft^2/sec for τ_w ranging from 0.06 to 0.25 lb/ft^2, which is the value used by Seyer. Table A-1 represents the viscometric data and the results obtained from the Rheogoniometer for the standard oil and 0.01% solution.

FIGURE A-1

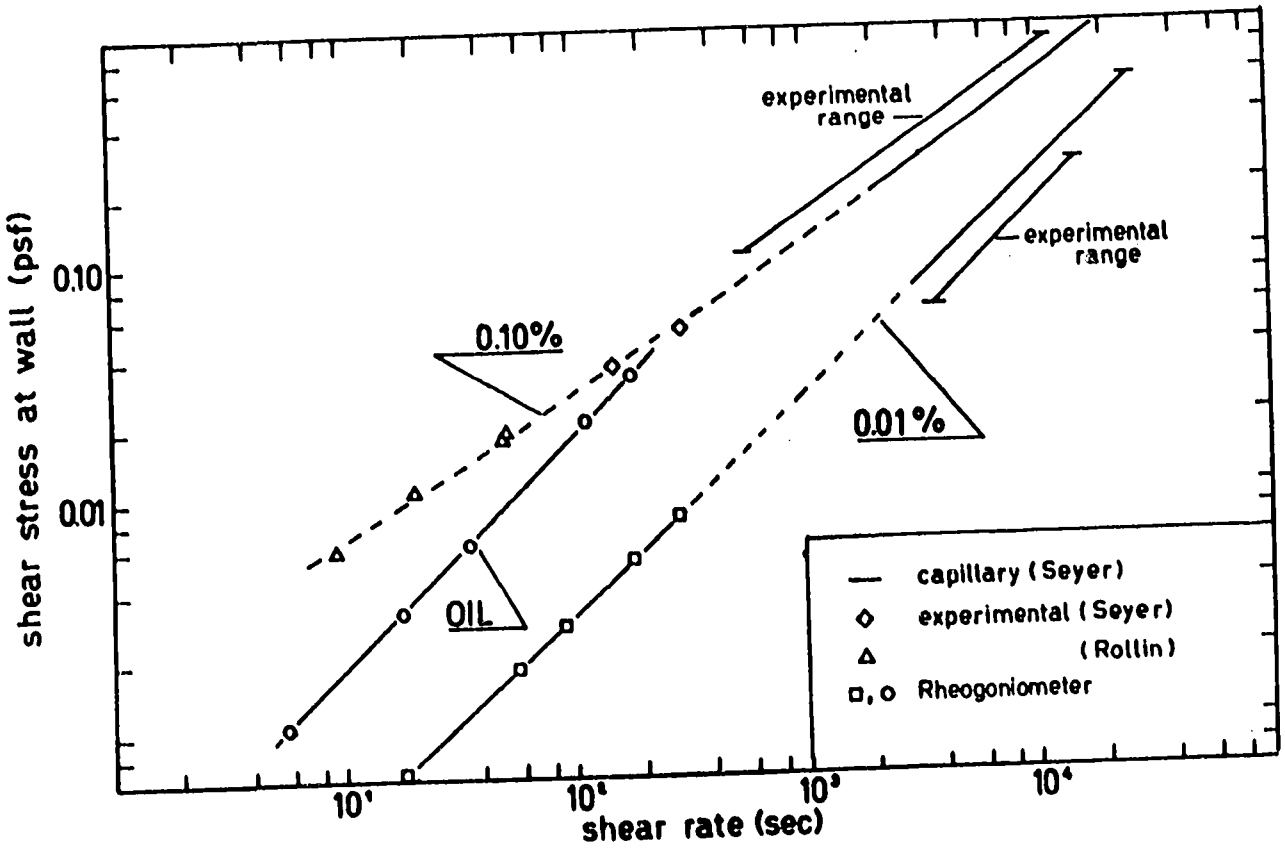

FLOW CURVES FOR POLYMERIC SOLUTIONS

TABLE A-I

VISCOMETRIC MEASUREMENTS FOR OIL AND POLYMERIC SOLUTIONS

Standard Oil (9 centipoise) at 22.5°C

RUN	DISPLACEMENT volts	ROTATION rpm	SHEAR RATE sec^{-1}	SHEAR STRESS $dynes/cm^2$	SHEAR STRESS psf
1	8.85	5.68	35.80	3.04	0.00637
2	282.00	17.09	113.20	9.68	0.02030
3	448.00	28.40	179.00	15.38	0.03220
4	44.50	2.84	17.90	1.53	0.00321
5	14.00	0.90	5.68	0.48	0.00101

Separan AP-30 0.01% at 22.5°C

1	9.00	2.84	17.90	0.31	0.00065
2	25.00	9.00	56.80	0.857	0.00179
3	72.00	28.40	179.00	2.470	0.00515
4	111.00	45.20	285.00	3.800	0.00793
5	38.60	14.30	90.00	1.300	0.00271
6	71.00	28.40	179.00	2.440	0.00509

RHEOGONIOMETER PARAMETERS

α - angle of the cone	0.952°
d - diameter of the cone	10.00 cm
K_t - torsion bar constant	8.916 dynes-cm/microns
Δt - displacement	volts
β - transducer calibration	1.009 micron/volt
W - rotational speed	rpm

FORMULAE

SHEAR STRESS $\tau = (3.82\ \beta\ \Delta_t\ K_t)/d^3 = 0.0343\ \Delta_t\ dynes/cm^2$

SHEAR RATE $8\langle\bar{u}_x\rangle/D = (360\ W)/(60\ \alpha) = 3.61\ W\ sec^{-1}$

ii) 0.10% Solution

The experimental points, calculated from the laminar friction data, are compared to Seyer's (41) viscometric data for the 0.10% solutions on Figure A-1. Calculated values are tabulated in Table A-II. The procedural similarity in the preparation of the solutions and the excellent agreement obtained with Seyer's data for the same concentration show the shear rate-shear stress behavior of the 0.10% solution is the same. Therefore for calculational purposes the same relation assumed by Seyer will be used for $6 \times 10^2 < \frac{8\bar{u}_x>}{D} < 1.2 \times 10^4$.

$$\ln \tau_w = -6.540 + 0.598 \ln \frac{8<\bar{u}_x>}{D} + 0.00599 \left(\ln \frac{8<\bar{u}_x>}{D}\right)^2$$

where τ_w is in psf

$\frac{8<\bar{u}_x>}{D}$ is in sec^{-1}.

TABLE A-II

EXPERIMENTAL VISCOMETRIC DATA FOR 0.10% SOLUTION

Flow (US gal/min)	5.0	11.0	26.4	27.5
Manometer Reading (inches Hg)	1.31	2.09	3.42	3.68
Length Between Pressure Taps (ft)	17.5	17.5	17.5	17.5
Diameter of Pipe (ft)	0.230	0.230	0.230	0.230
Temperature (°F)	74.0	74.0	74.0	74.0
Bulk Velocity (ft/sec)	0.267	0.591	1.419	1.478
Pressure Drop (psf)	2.073	3.308	5.413	5.824
Shear Stress at Wall (psf)	0.0060	0.0109	0.0178	0.0191
Shear Rate $(8<\bar{u}_x>/D)(sec^{-1})$	9.32	20.56	49.36	51.43

iii) Estimate of the Elasticity Level and Calculations for Prediction of 2.75" Friction Factor from 1" Data

Using Equations II-16, II-12 and I-4, four of the experimental friction points tabulated in Appendix I for the 0.01% solution were used to estimate (by a trial and error solution of Equation II-16) values of B and consequently relaxation time in the range of the experimental photographic runs. These calculations are tabulated in Table A-III. Figure A-2 shows the relaxation time as a function of τ_w along with Seyer's (41) and Oliver's (30) data for their respective 0.01% Separan solutions. As suggested, from the lower friction measurements, the level of elasticity of the present solutions is higher than Seyer's solutions. The dashed line is taken to represent the relaxation time of the 0.01% solution in this work and for purposes of calculation, can be represented empirically by

$$\ln \theta = 0.000388 - 0.4930 \ln \tau_w$$

where τ_w is expressed in psf and θ in sec^{-1}.

TABLE A-III

LEVEL OF ELASTICITY FOR 0.01% SOLUTIONS

Reynolds number	132980	93369	50000	30000
Friction factor	0.00140	0.00177	0.00270	0.00382
$B(\theta^+)$	23.96	20.30	15.00	11.50
θ^+	11.70	9.25	6.00	4.00
Shear stress at wall (psf)	0.496	0.309	0.135	0.069
Relaxation time $\theta \times 10^4$ sec^{-1}	5.48	6.93	10.29	13.47

FIGURE A-2

— RELAXATION TIME —

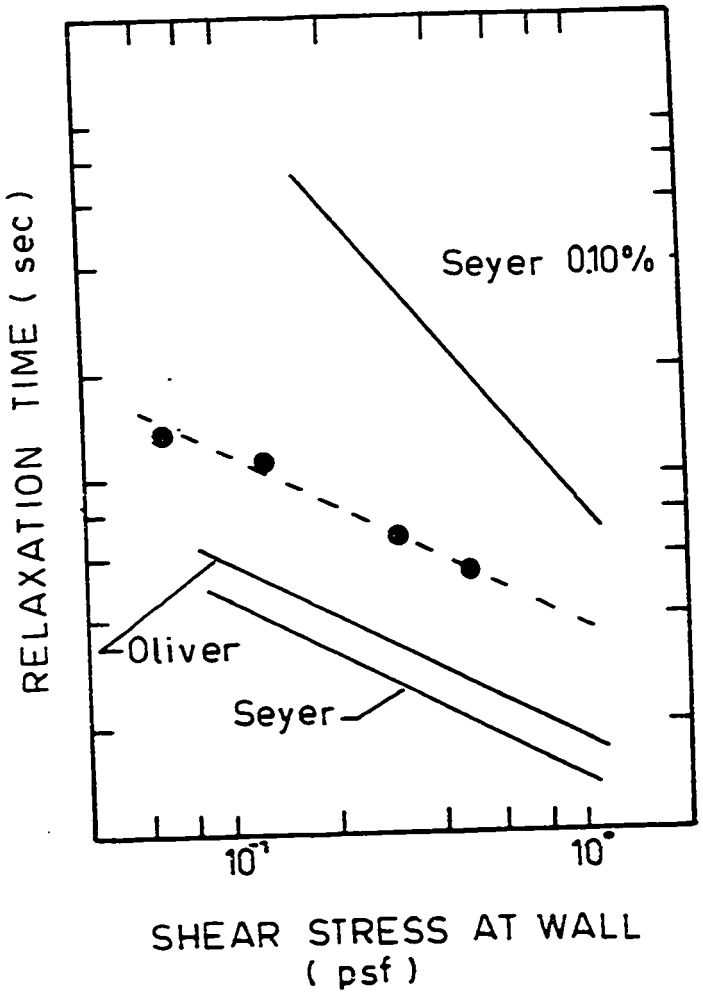

Table A-IV represents the predicted friction factors for the 1" and 2.75" pipes using the relaxation time estimated in Figure A-2. The predicted friction factors are plotted in Figure IV-1.

TABLE A-IV

PREDICTED DRAG REDUCTION

	1" Pipe		2.75" Pipe	
Reynolds number	friction factor	friction velocity (ft/sec)	friction factor	friction velocity (ft/sec)
N_{Re}	f	U^*	f	U^*
5,000	0.00873	0.0475	0.00952	0.0180
10,000	0.00628	0.0807	0.00748	0.0320
20,000	0.00438	0.1340	0.00575	0.0562
50,000	0.00264	0.2610	0.00382	0.1140
100,000	0.00166	0.4150	0.00272	0.1930
200,000	0.00107	0.6680	0.00185	0.3180

iv) B Function Obtained from Velocity Profiles

Table A-V represents the intercept values of the corrected semi-logarithmic velocity profiles in Figure IV-17. These values of B for the 0.01% solutions are plotted versus the friction velocity in Figure IV-18.

TABLE A-V

VALUES OF B FUNCTION

Run Number	U^* friction velocity (ft/sec)	$B(\theta^+)$
6	0.1890	11.0
16	0.1832	12.5
10	0.1830	14.7
12b	0.3606	19.2
12a	0.3462	$\approx$ 21.0

APPENDIX B

CALIBRATION

i) Calibration of the Magnetic Flowmeter

The bulk flow rate was measured by a 2" Foxboro, Model 696, magnetic flowmeter connected to a Hewlett Packard strip chart recorder. From a previous study (6), calibration curves for water were obtained from a weighing procedure for two sensitivities in order to cover a range of flow rates from 0-32 and 0-210 USgal/min. Figure B-1 shows the high and low sensitivity curves of flow rate versus voltage obtained from the previous study. The data points presented on the figure serve as check points. These data were taken during the course of this work and verify the calibration curves.

ii) Check of Velocity Profiles

For every photographic run, a check of the velocity profile against the flowmeter reading was obtained by integrating the velocity profile. The percent difference between the bulk velocities obtained from the integrated profiles and the recorded bulk velocities are shown on Table B-I. A $\pm$ 2% average difference can be found (except for run 12 which was -4%) confirming good agreement for the measured profiles.

FIGURE B - 1

FLOWMETER CALIBRATION

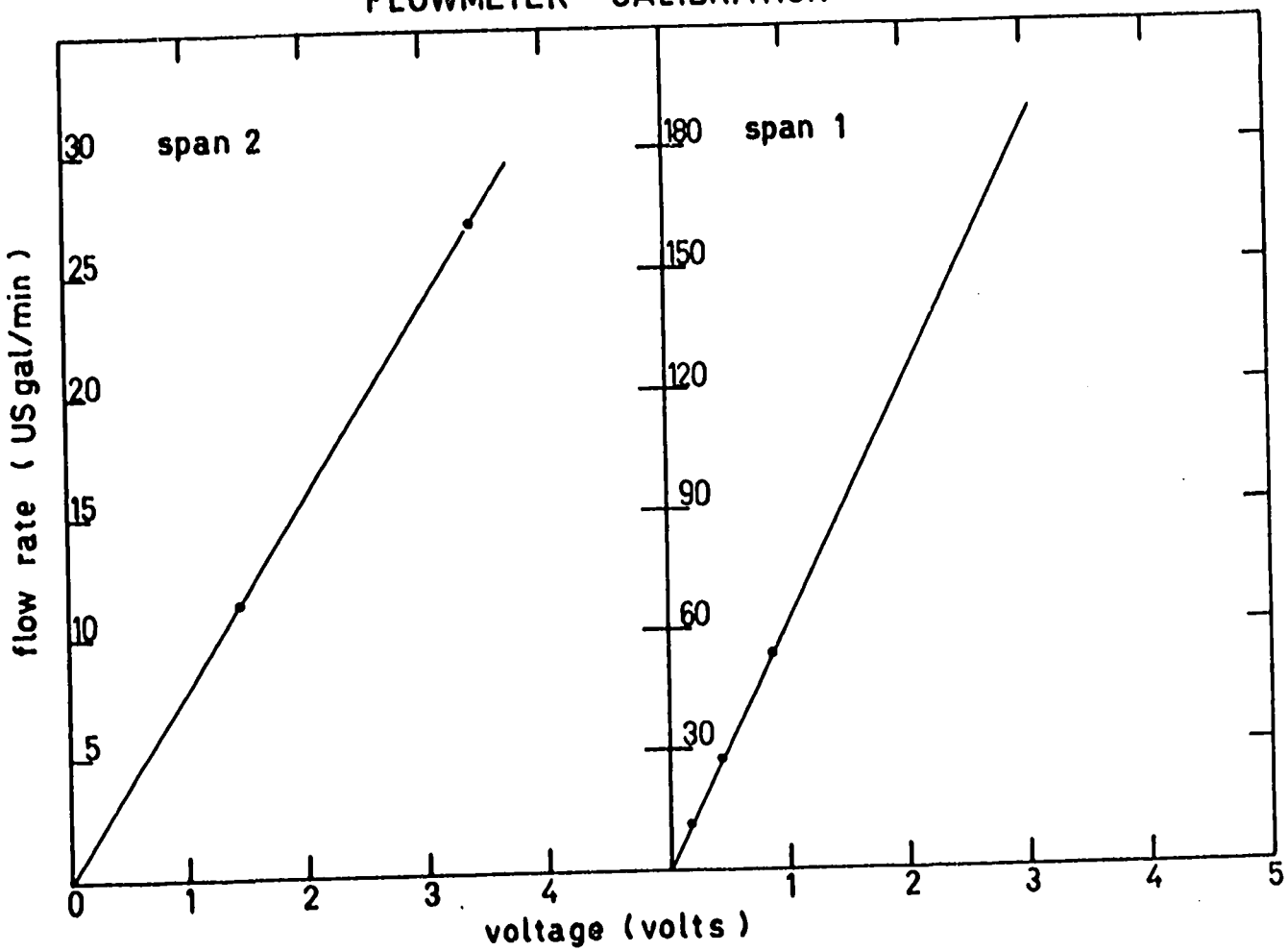

TABLE B-I

COMPARISON OF RECORDED BULK VELOCITY WITH INTEGRATED BULK VELOCITY

RUN NUMBER	BULK VELOCITY (ft/sec)		PERCENT DIFFERENCE
	Recorded	Integrated	
4	4.825	4.802	+0.48
6	4.428	4.428	-1.76
9	4.975	5.084	-2.15
10	4.980	5.080	-1.97
11	13.26	13.672	-2.49
12	11.62	12.128	-4.18
13	22.02	21.616	+1.87
14	33.40	33.64	+0.72
15	4.996	5.142	+2.79
16	5.068	5.09	+0.43
17	8.77	8.668	+1.08

iii) Axis of the Digitizer

As already mentioned, the full scale movement of the digitizer cross hair for both axes of the digitizer was 10 volts. In order to transform the digitizer readings (in mvolts) into length scales, calibration functions for both axes were obtained, mainly in the limits of the projected frames by taking readings of a 10 cm ruler.

Figure B-2 shows the voltage corresponding to 10 cm movement in both the X and Y directions for positions spanning the digitizer screen. Calibration points in the X-direction have been determined for various Y positions and similarly Y-direction readings have been taken for various X-positions. The data show the response is constant over the entire surface of the screen. Before analyzing a series of photographs these data were used as a check to ascertain that the digitizer electronics were stable and operating properly.

iv) Projected Axial Magnification

As mentioned in Chapter III, several pictures of a ruler divided into 1/10 cm increments were taken and projected on the digitizer screen where the projected length was measured. Because difficulties were encountered in disconnecting the optical box for every run, in order to take a picture of the ruler inside the pipe, the pictures were taken with the ruler outside the pipe. To assure the validity of this procedure, the projected axial magnification was obtained from two different rulers, one inside the pipe, the other outside. As shown in Table B-II for run 15 as an example, the percentage difference in magnification for the photographs of rulers inside and outside the pipe demonstrates the correctness of the procedure.

FIGURE B-2

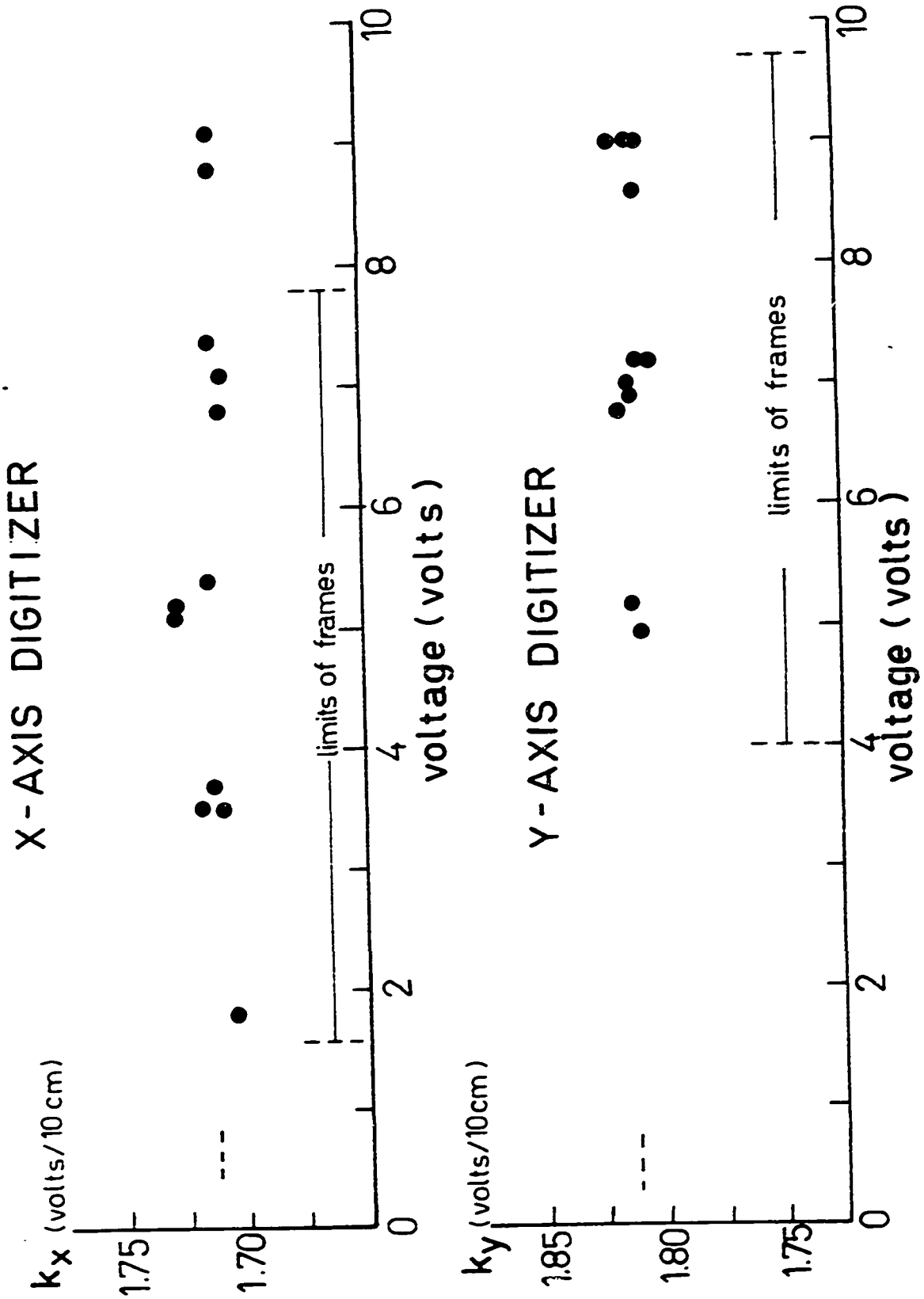
X-AXIS DIGITIZER
k_x (volts/10 cm)
1.75
1.70
0
2
4
6
8
10
limits of frames
voltage (volts)
Y-AXIS DIGITIZER
k_y (volts/10cm)
1.85
1.80
1.75
0
2
4
6
8
10
limits of frames
voltage (volts)

Very careful attention was given to the focus of the ruler, particularly with the 1.9 lens assembly which had a relatively large depth of focus. Table B-III shows results for run 15 where magnifications were obtained for different focal distances (the ruler still in focus). For a maximum deviation of 30 microns from the apparent point of focus, the magnification could be off by 1%. This indicates little variability in magnification owing to focus of the camera.

TABLE B-II

AXIAL MAGNIFICATION DATA FOR RUN 15

Projected axial magnification

ruler inside	ruler outside
31.2	31.0
31.7	31.5
31.3	31.5
31.5	31.7
31.5	31.7
31.2	31.5
31.7	31.5
31.9	31.7
31.8	31.8
31.1	--
31.49 cm/ cm	31.54 cm/ cm

Percent difference is 0.159%

TABLE B-III

AXIAL MAGNIFICATION WITH CHANGE OF FOCUS

For the camera raised higher than the focal point for run 15.

focal point	10 microns	20 microns	30 microns
31.50	31.30	31.50	31.12
31.50	31.54	31.30	31.34
31.50		31.46	31.24

v) Radial Magnification

As in the case of defining the axial magnification, projected radial lengths were measured to determine the radial magnification. As explained in Chapter III, Section III-6, photographs of the tip of a needle were taken at known radial positions. Figures B-3 and B-4 show, as an example for run 6, the curves obtained for high and low magnification of actual distance from the wall versus the distance measured on the digitizer screen. It can be noted that the curve for high magnification crosses the origin and that pipe curvature makes the magnification vary. A third order Lagrangian interpolating polynomial was used in the computer program to represent these curves.

Data obtained for calibrations for each of these runs in this work have been omitted from this thesis because they are of no significance once the projecting apparatus has been moved. The axial and radial magnifications can be determined directly from the photographs which have been filed.

FIGURE B-3

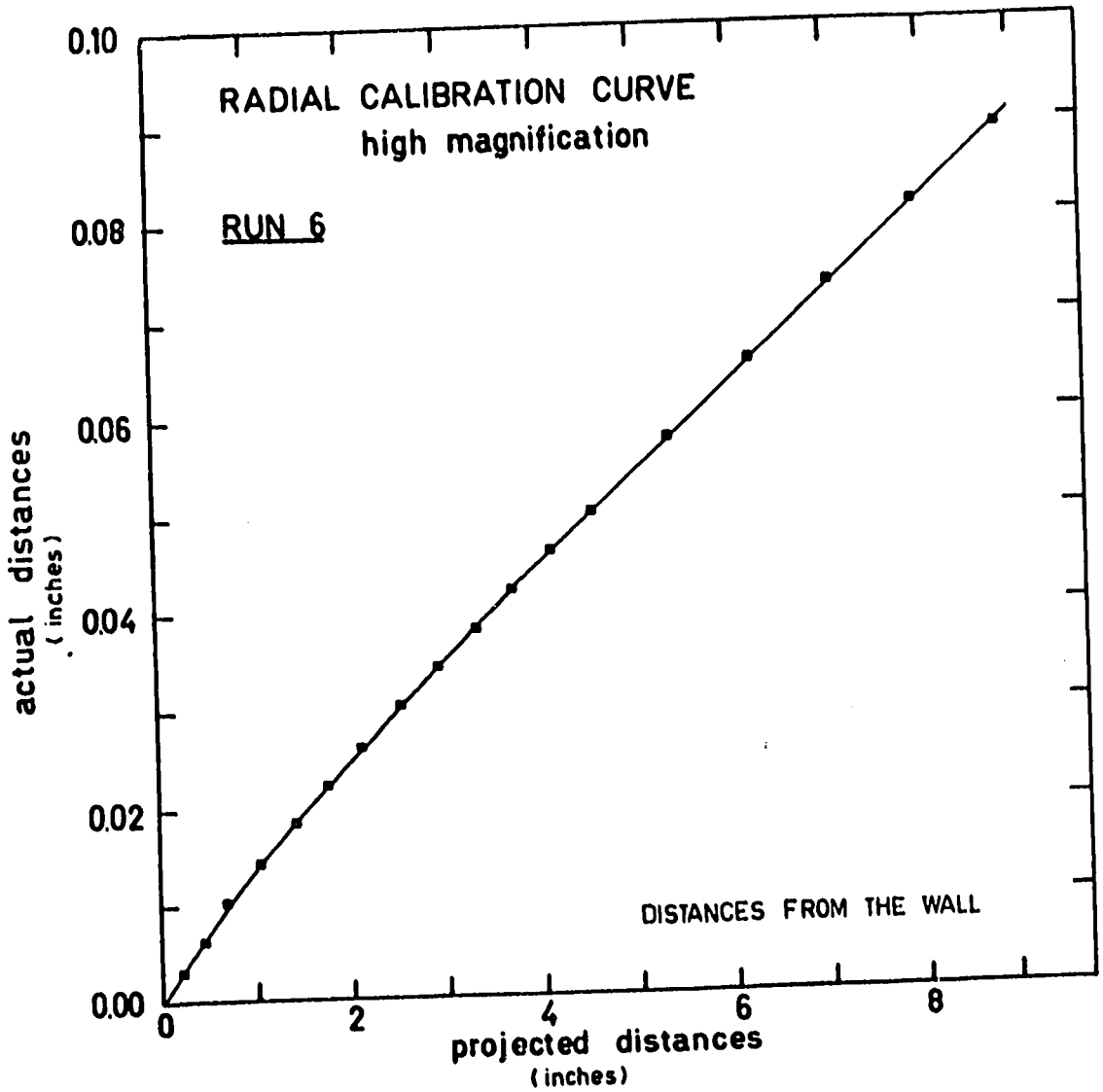
RADIAL CALIBRATION CURVE
high magnification
RUN 6
DISTANCES FROM THE WALL
actual distances
(inches)
0.10
0.08
0.06
0.04
0.02
0.00
0
2
4
6
8
projected distances
(inches)

FIGURE B-4

RADIAL CALIBRATION CURVE

low magnification

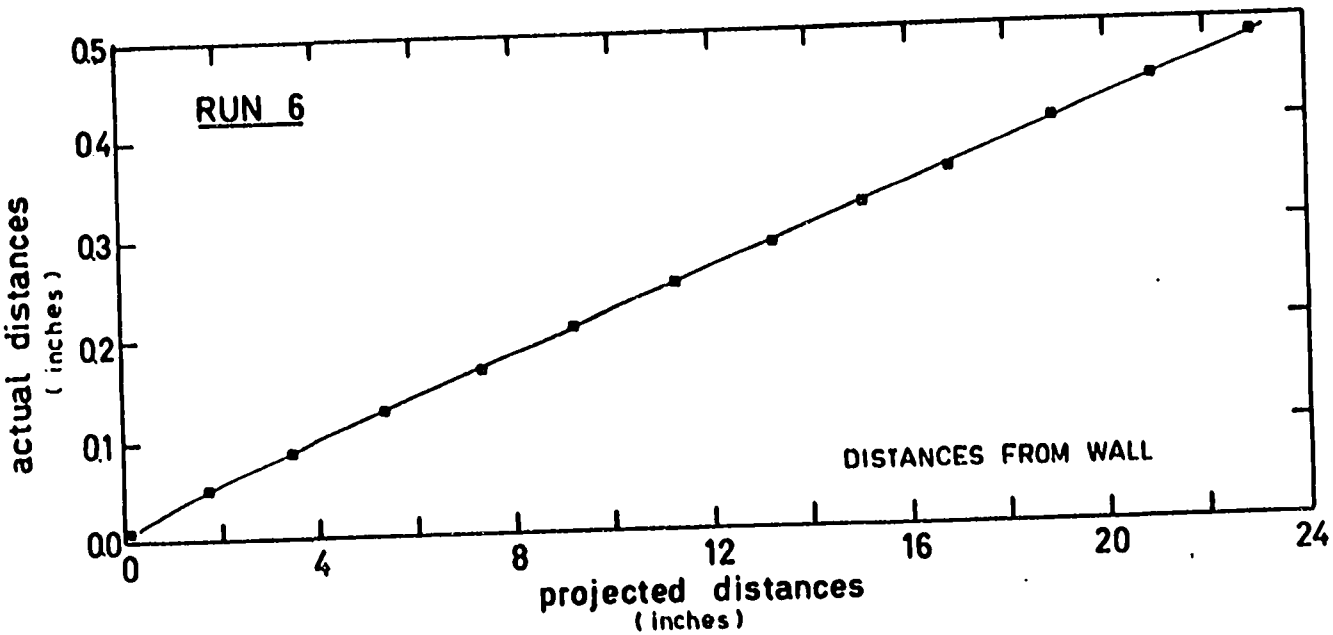

APPENDIX C

ANALYSIS OF ERRORS

i) Confidence Interval for Time Average Velocities and Variances

The mean values and variances of the axial and radial velocities were obtained from measurements of instantaneous velocities. Because the population from which the sample was drawn has unknown mean (μ) and unknown variance (σ^2), the 100(1 - α)% confidence interval for the mean value in which μ is contained, if 30 or more observations are taken, is

$$\bar{u} \pm Z_{\frac{\alpha}{2}} \left(\frac{S_m}{\sqrt{n}}\right) \qquad \text{C-1}$$

and the 100(1 - α)% confidence interval for σ^2 is

$$\frac{(n-1)S_m^2}{X^2_{n-1,\alpha/2}} \leq \sigma^2 \leq \frac{(n-1)S_m^2}{X^2_{n-1,1-\alpha/2}} \qquad \text{C-2}$$

where S_m is the variance of a sample of n observations from a normal distribution $N(\mu,\sigma^2)$*.

As already mentioned and tabulated in Appendix H most of the mean velocities and variances were obtained from a large sample (larger than 80). In order to show the confidence limit associated with the data of this work an example is done for the case where the number of observations was small. This gives the largest confidence interval.

---

*"Introductory Engineering Statistics", by Guttman, I. and Wilks, S.S., John Wiley, N.Y., 1965.

For run 6 at a radial position near the wall 27 observations were recorded and the sample mean velocity and variance (in the axial direction) obtained were

$$\overline{u}_x = 1.958 \text{ ft/sec}$$

$$S_m = 0.568 \text{ ft/sec}$$

Thus the 95% confidence interval for the mean velocity is

$$\pm 0.318\ S_m$$

and for the variance

$$0.818\ S_m \leq \sigma \leq 1.373\ S_m$$

Thus the time averaged velocities are generally estimated to within less than 5% at 95% confidence. The confidence interval for variance is somewhat larger.

ii) Experimental Errors in Reading the Streaks

The mechanical errors, e, involved in reading the streaks from the digitizer table can be expressed as

$$X_m = X_t + e \qquad \text{C-3}$$

where X_m is the measured length of a streak

X_t is the true length of a streak.

If no intrinsic error is assumed and the mechanical errors are normally distributed, then the net effect on the measured mean value is zero and

$$\overline{X}_t = \overline{X}_m \qquad \text{C-4}$$

In the case of the sample variance, the mechanical errors are additive. The measured sample variance can be expressed as

$$S_m^2 = \frac{1}{n-1} \sum_1^n (X_m - \overline{X})_i^2 \qquad \text{C-5}$$

Substituting Equation C-3 in the last equation and manipulating the terms the following expression is obtained

$$S_m^2 = \frac{1}{n-1} \sum_1^n e_i^2 + \frac{1}{n-1} \sum_1^n (X_t - \overline{X})_i^2 + \frac{1}{n-1} \sum_1^n 2e_i(X_t - \overline{X})_i \qquad \text{C-6}$$

The first term in this equation can be estimated from repeated readings of a known length with digitizer apparatus. The last term of Equation C-6 represents the covariance between the error and $(X_t - \overline{X})$ and is zero because random mechanical errors cannot be correlated with turbulent fluctuation $(X_t - \overline{X})$.

Thus Equation C-6 can be expressed as

$$S_m^2 = S_e^2 + S_T^2 \qquad \text{C-7}$$

or rearranging the equation

$$\frac{S_T}{S_m} = \sqrt{1 - \frac{S_e^2}{S_m^2}} \qquad \text{C-8}$$

To estimate S_e, Figure C-1 gives the variance obtained from reading a given streak many times with the digitizer as a function of the length of the streak. These readings show scatter or variance because of the digitizer electronics error involved, because of the blurry ends of the streaks, and human error in positioning the cross hair. The error

FIGURE C-1

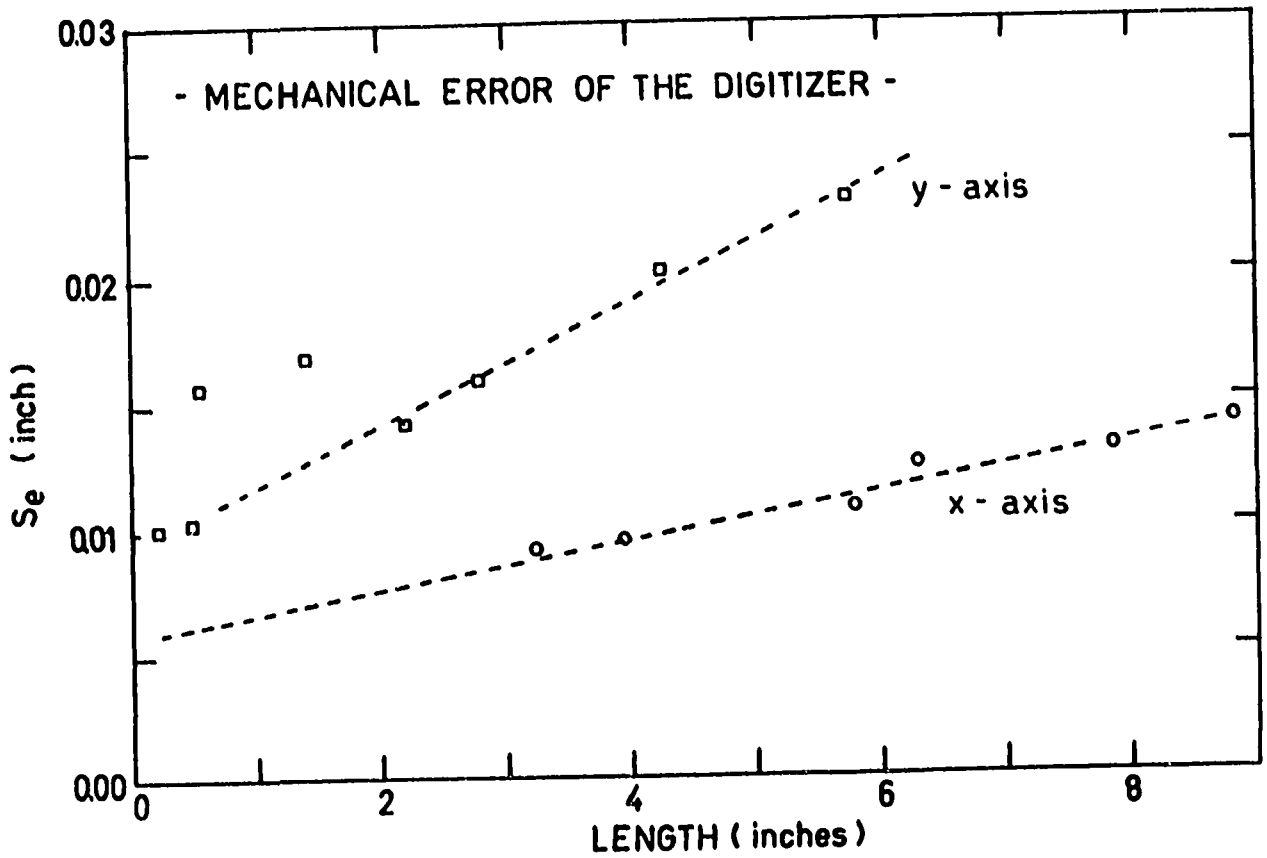
- MECHANICAL ERROR OF THE DIGITIZER -
y - axis
x - axis
0.03
0.02
0.01
0.00
Se (inch)
0
2
4
6
8
LENGTH (inches)

increases slightly with length because the longer streaks have a larger tail or blurried region and it is therefore more difficult to locate the beginning or end of the streak.

As an example, run 14 was chosen because of the measured low intensities. The calculated sample variances obtained at y = 0.0119 are

$$S_{mx} = 2.76 \text{ ft/sec}$$

$$S_{mr} = 0.239 \text{ ft/sec} \quad \text{for } n = 87$$

as found in Appendix H.

At this position the corresponding average actual lengths measured were

$$\Delta x = 0.100'' \quad \text{and} \quad \Delta r = 0.000''$$

Taking the axial magnification (31.4) and using the radial calibration curve both lengths can be transferred into projected lengths on the digitizer screen

$$\Delta x = 3.05'' \quad \text{and} \quad \Delta r = 0.00''$$

Using Figure C-1, S_e can be found as

$$S_{ex} = 0.0084'' \quad \text{and } S_{er} = 0.010''$$

Or in terms of velocities, using the time scales in Table C-I

$$S_{ex} = 0.0398 \text{ ft/sec}, \; Ser = 0.1485 \text{ ft/sec}$$

Plugging into Equation C-8

$$S_{tx} = S_{mx}$$

$$S_{tr} = 0.785 \; S_{mr}$$

This calculation shows that errors in the calculated axial intensity owing to measuring errors are entirely negligible. For the radial intensity however, the calculated value can be as much as 21.5% higher than the true value owing to the mechanical error. This is the extreme case and generally for other runs or other radial positions the percent error will be much smaller.

iii) Location of Wall and Tracers

From Figure III-6b it can be observed that the wall location is masked by a shadow region. Along with uncertainty because of wall curvature it was estimated from a projected photograph that the wall could be located to within ± 0.0010". The smallest reading recorded for the radial position near the wall is for run 6 and is 0.0040". This radial position can then be 25% in error, but represents the worst case encountered. Furthermore the error of ± 0.001" in the locating the wall is of the same order as the length corresponding to non-zero average radial velocities reported in Appendix H.

iv) Error in Intensity

a) air bubbles

As already discussed in Seyer's thesis (41), the influence of the air bubbles on the intensity measurements will be negligible if their size is smaller than the scale of the energy containing eddies (approximately 0.006"). Because in this work the average diameter of the bubbles was found to be 0.002", no influence is expected.

b) uncertainty in radial position

The fact that velocities were taken over a band of positions

rather than at a single radial position causes the calculated intensities to be too high. This occurs because of the mean velocity gradient and so velocities of streaks at the bottom of the band (nearest to wall) are on the average slightly smaller than velocities of streaks near the top. Thus there is a fluctuation in velocity owing to variations in the radial position of the streaks. The magnitude of the error depends on the velocity gradient as well as the width of the band.

In reading the photographs the radial positions of interest were determined by lines drawn on a clear plastic sheet which was placed on the digitizer screen. The situation is illustrated by Figure III-7 where the limits of the band correspond to lines on the plastic sheet. For positions near the wall the spacing of the lines on the sheet was approximately .25" and was about 1" for positions near the centre. Fore the high magnification portion of run 6 the .25" band on the plastic sheet corresponds to a band .0024 inches wide in the one inch pipe.

A conservative estimate of the error in the calculated intensity can be obtained by assuming the streaks are located either at the center or top or bottom of the band. In fact there will be a distribution of positions which peaks sharply at the center of the band. In the following sketch the positions $y + \Delta y$ and $y - \Delta y$ represent the limits of the band for a radial position y. Suppose that

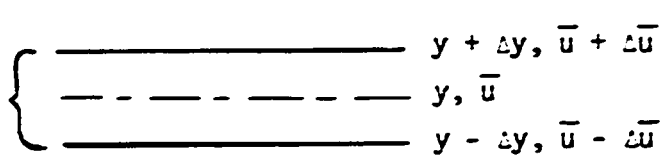

n streaks are observed in the band. Roughly n/2 streaks will have a velocity characteristic of position y, while n/4 streaks will have

velocities reflecting the top position and n/4 reflecting bottom. Thus the variance owing to velocity gradient will be

$$S_u^2 = \frac{1}{n-1} \left\{ \sum_i^n (\bar{u} - u)_i^2 \right\}$$

$$= \frac{1}{n-1} \left\{ \sum_{i=1}^{n/2} (\bar{u} - \bar{u})^2 + \sum_{n/2}^{3/4n} (\bar{u} - (\bar{u} + \Delta\bar{u}))_i^2 \right.$$

$$\left. + \sum_{3/4n}^{n} (\bar{u} + (\bar{u} - \Delta\bar{u}))_i^2 \right\}$$

$$= \frac{1}{2} (\Delta\bar{u})^2 \qquad \text{C-9}$$

If S_m and S_t are the measured and true variances then

$$S_m^2 = S_t^2 + S_u^2$$

or

$$\frac{S_t}{S_m} = \sqrt{1 - \left(\frac{S_u}{S_m}\right)^2} \qquad \text{C-10}$$

This equation shows the influence of the velocity gradient on the true intensity.

As an example we will consider the first 3 data points in Table H-I-3 for Run 6. Consideration of the velocity profiles shows this case will have the largest error owing to the above considerations. In the following table the appropriate data for use of equation C-10 is tabulated. The $\Delta\bar{u}$

No.	y inch	$\Delta\bar{u}$ ft/sec	S_m ft/sec	S_t/S_m
1	.0040	.18	.567	.95
2	.0073	.13	.508	.97
3	.0102	.04	.535	.97

for a band width of .0024 inches have been determined directly from the slopes of a plot of the velocity profile at the indicated radial positions. The measured intensity is obtained directly from Table H-I-3 by multiplying I_x by the maximum velocity.

It is evident from the tabulated values of S_t/S_m there is little difference between the measured and true intensities. For the radial position nearest to the wall, where the velocity gradient is largest, the error would be approximately 5%. In view of the conservative nature of this calculation it is concluded that for all runs in this work error in intensity because of velocity gradient is negligible.

v) Time Scale Relative to the Dissipative Frequencies

Table C-I compares the time scales used for each photographic run and the estimated frequency of maximum energy dissipation for organic solvents as found by Patterson and Zakin (32) for 1 and 2" pipes. It can be observed that for all the runs, except run 14, the time scale used are lower than the dissipative frequencies. A true indication of the turbulence intensity, (containing the contribution from all significant frequencies) was therefore obtained.

TABLE C-1

TIME SCALE VERSUS DISSIPATIVE FREQUENCIES

RUN NUMBER	BULK VELOCITY ft/sec	N_{max} sec^{-1}	TIME SCALE sec^{-1}
4	4.8	250	596.6
5	3.1	130	596.6
6	4.4	220	596.6
7	5.0	260	596.6
9	5.0	260	1194
10	5.0	260	1197
11	13.2	1000	1787.5
12	11.6	800	1787.5
13	22.0	1900	1787.5
14	33.4	$\simeq$4000	1787.5
15	5.0	260	895
16	5.0	260	895
17	8.8	600	895

APPENDIX D

SAMPLE CALCULATIONS

i) Velocities

The sample calculation will be made for water run 11 at a radial position y = 0.0906 inch from data tabulated in Appendix H.

Conditions of Operation

Temperature	70°F
Flow	32.4 gal/min
Manometer Reading	6.1 in of Hg
Length between taps	11.0 ft
Diameter of tube	1.0 in
Rotation of disk	3575 rpm
Number of slits	60 slit-spoke/rev

Readings from the Digitizer of Streak Relative to Pipe Wall

Referring to Figure III-7 the following points correspond to the reading of the streak and spoke and the wall. The points are in volts and relative to the digitizer axis as zero.

Y_1 = 6.287 volts X_1 = 5.401 volts

Y_2 = 6.221 volts X_2 = 3.363 volts

Y_3 = 8.077 volts X_3 = 7.552 volts

Y_4 = 8.052 volts X_4 = 4.972 volts

With calibration constants as shown in Figure B-2

k_x = 0.1718 volt/cm k_y = 0.1811 volt/cm

these readings can be transformed into lengths on the projection screen.

Y_1 = 13.668 inches X_1 = 12.377 inches

Y_2 = 13.524 inches X_2 = 7.707 inches

Y_3 = 17.559 inches X_3 = 17.306 inches

Y_4 = 17.505 inches X_4 = 11.394 inches

With these numbers, from the geometry of the figure the axial component of the streak, Δx, parallel to the wall is found to be

$$\Delta x = 4.72 \text{ inches}$$

The measured axial magnification is 53.18 and therefore the true length of the streak is 4.72/53.18 = .0887 inch.

From the rotational speed of the chopping wheel and number of slit-spoke of the wheel the time scale can be found

$$T = (60 \text{ sec/min})/(30 \text{ division/rev})(3575 \text{ rpm}) = 0.00056 \text{ sec}$$

and the instantaneous velocity is

$$u_x = \Delta x/T(53.18) = 13.184 \text{ ft/sec}$$

Similarly, the radial instantaneous velocity was found to be (using the radial calibration curve, as shown for run 6 as an example, in Figures B-III, B-IV)

$$u_r = -0.330 \text{ ft/sec}$$

From the computer the average of all these readings gives for the mean velocities

$$\bar{u}_x = 13.400 \text{ ft/sec} \quad \text{and} \quad \bar{u}_r = +0.219 \text{ ft/sec}$$

and the variances S_x = 1.022 ft/sec and S_r = 0.47 ft/sec.

ii) Flow Calculations for Water

The pressure drop between two pressure taps can be calculated from the manometer reading

$$\Delta P = \frac{(6.1)(62.3)(12.55)}{(12)(32.2)} = 397.5 \text{ psf}$$

The Reynolds number

$$N_{Re} = \langle \bar{u}_x \rangle D/\nu$$

$$N_{Re} = Q\ D\ (8.337)/(\rho A \nu) = 104299$$

The shear stress at the wall

$$\tau_w = D\Delta P/4L = 0.753 \text{ psf}$$

The friction factor

$$f = 2\tau_w/(\rho \langle \bar{u}_x \rangle^2) = 0.00442$$

The friction velocity

$$U^* = \sqrt{\tau_w g_c/\rho} = 0.624 \text{ ft/sec}$$

The dimensionless distance from the wall

$$Y^+ = y\ U^*/\nu = 444.5$$

The dimensionless velocity

$$U^+ = \bar{u}_x/U^* = 2.148$$

iii) Calculations of K', n' and N'_{Re}

A sample calculation is made for run 13 as an example for Separan AP-30 0.10% and these data can be found in Appendix H.

Flow	54.00 USgal/min
Manometer reading	7.95 inches of Hg
Length between taps	22.00 ft

From these

$$\Delta P = 519.38 \text{ psf}$$

$$\tau_w = 0.491 \text{ psf}$$

The constants of viscometric equation are (see Appendix A)

$$A = -6.540 \qquad B = 0.5989 \qquad C = 0.00599$$

so that

$$\ln 8\langle\bar{u}_x\rangle/D = \frac{-0.5989 + \sqrt{(0.5989)^2 - 4(0.0060)(-6.540 - \ln 0.491)}}{2(0.00599)}$$

$$\ln 8\langle\bar{u}_x\rangle/D = 8.95$$

$$8\langle\bar{u}_x\rangle/D = 7.71 \times 10^3 \text{ sec}^{-1}$$

$$n' = 0.5989 + 2(0.00599)(8.95) = 0.705$$

$$K' = 0.491/(7.71 \times 10^3)^{0.705} = 8.93 \times 10^{-4}$$

iv) Determination of θ from Friction Data

The relaxation time found from friction data in the 1" pipe is tabulated in Table A-3. From Appendix I the friction factor is

$$f = 0.00177$$

and $N_{Re} = 93369$

Putting the constants in Equation III-16 the following expression is obtained

$$\frac{1}{\sqrt{f}} = 1.74(1 - \xi_1)^2 \ln (N_{Re}\sqrt{f}) + 0.707(1 - \xi_1)^2[B(\theta^+) - 2.56)] - \frac{3.0}{\sqrt{f}}$$

From the data

$\sqrt{f} = 0.0421$ $\qquad$ $1/\sqrt{f} = 23.753$

$N_{Re}\sqrt{f} = 3931$ $\qquad$ $\ln(N_{Re}\sqrt{f}) = 8.2764$

For the first trial assuming $\xi_1 = 0$, we have, solving the above equation for B,

$$B(\theta^+) = (23.753 - 14.401 + 1.810 + 2.121)/0.707 = 18.79$$

Thus using Equation II-12, the first estimate of ξ_1 is

$$Y_1^+ - 2.46 \ln Y_1^+ = 18.79$$

and $\quad Y_1^+ = 26.9$ and $\xi_1 = 0.0194$

For the second trial $\xi_1 = 0.0194$ is used as an approximation and

$$B(\theta^+) = 20.25$$

$$Y_1^+ = 28$$

$$\xi_1 = 0.0202$$

The final $B(\theta^+)$ which satisfies the above equation is $B(\theta^+) = 20.30$. From the Seyer's B function (see Figure II-3) $\theta^+ = 9.25$ and from the experimental values of

$$U^* = 0.4002 \text{ ft/sec}$$

$$\tau_w = 0.3096 \text{ psf}$$

$$\theta = \theta^+ \nu/U^{*2} = 6.93 \times 10^{-4} \text{ sec}$$

APPENDIX E

TURBULENT SHEAR STRESS AND KINETIC ENERGY DATA

In order to provide additional support for the turbulence measurements, it is possible to estimate the covariance of the instantaneous velocities as well as the axial kinetic energy of the turbulence

$$S_{xr} = \frac{1}{n-1} \sum_{1}^{n} [(u_x - \bar{u}_x)(u_r - \bar{u}_r)]_i \qquad \text{E-1}$$

which is proportional to the Reynolds shearing stress. Similarly for the kinetic energy in axial direction

$$S_{xx} = \frac{1}{n-1} \sum_{1}^{n} [(u_x - \bar{u}_x)^2]_i \qquad \text{E-2}$$

Sample calculations were done for two radial positions for water run 11 in the 1" pipe because of the large number of observations available. From Appendix K in Book II the instantaneous velocities can be found for positions y = 0.462 inch and y = 0.387, and the mean velocities can be found in Appendix H.

Table E-I represents the calculated Reynold stress and the kinetic energy. These terms are plotted on Figure E-1 and compared to Laufer's data.

TABLE E-I

TURBULENCE PROPERTIES

Radial position -y (inch)	0.462	0.387
Number of observations	210	192
$\overline{u_x u_r}$	-0.0483	0.0098
$\overline{u_x u_x}$	0.6859	0.7075
$\overline{u_x u_r}/U^{*2}$	-0.1242	0.0252
$\overline{u_x u_x}/U^{*2}$	1.763	1.819

Three of the four points are in excellent agreement with the expected values. The low point for shear stress is in fact in reasonable agreement in view of the extreme difficulty in estimating a covariance. Reference to statistical tables shows that with these points the 95% confidence interval about the lower point includes the known curve of shear stress.

FIGURE E-1

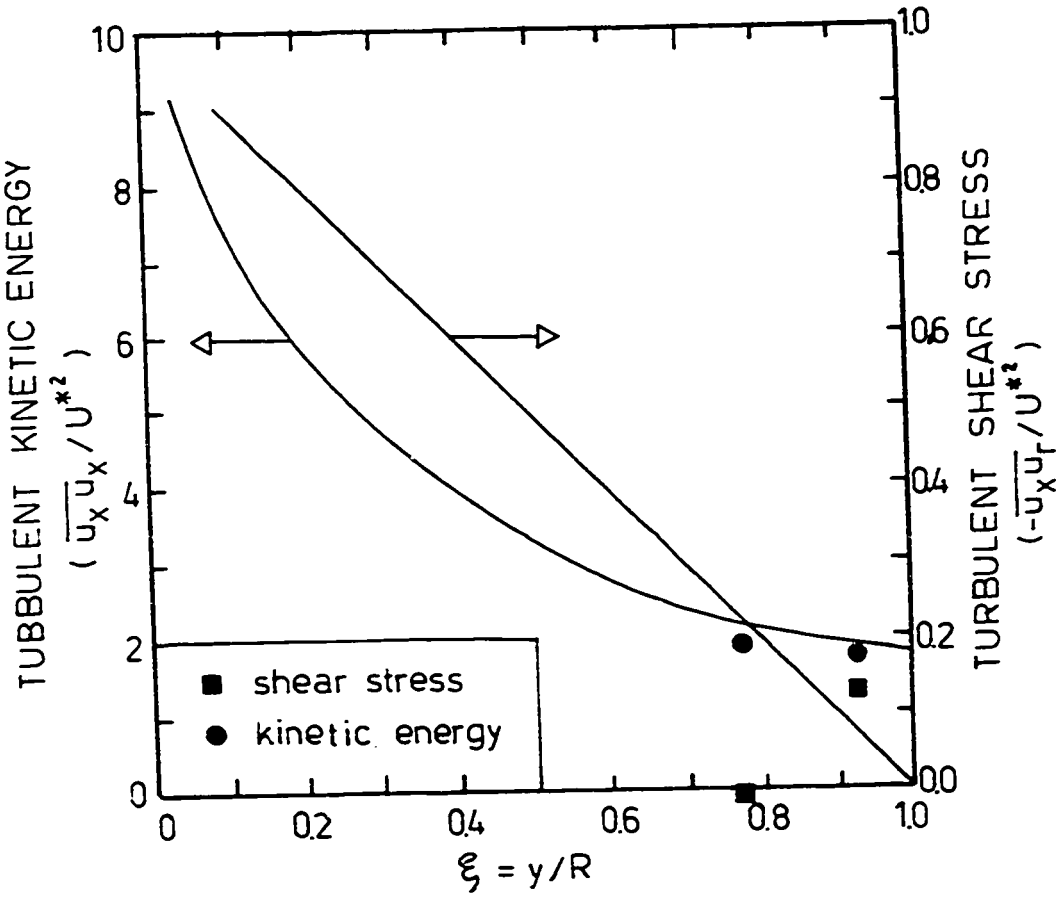

REYNOLDS STRESS AND KINETIC ENERGY

APPENDIX F

R_0 CORRELATION FACTOR

The R_0 correlation factor given in Table F-I and defined in Equation II-2 was calculated for all the radial positions of all the runs in this work and also for some of Seyer's data (41). R_0 is simply the ratio of number of positive radial velocities to the number of negative radial velocities. To calculate R_0 raw data, that is each instantaneous radial velocity in Appendix L, has been adjusted slightly by requiring that the mean radial velocity be exactly zero. Alternatively the non-zero mean radial velocity has been subtracted from each instantaneous velocity. This effectively removes bias in the data owing to small error in locating the wall. This has the effect of changing the relative number of negative and positive fluctuations; but only insignificantly.

TABLE F-I

Run No.	n	$\xi=y/R$	R_o
4	30	0.0302	1.14
	74	0.0476	0.92
	63	0.0617	1.36
	61	0.0790	1.48
	77	0.0949	1.43
	79	0.1092	1.30
	75	0.1250	1.50
	72	0.1450	1.49
	67	0.1575	1.16
	70	0.1735	1.00
	62	0.1890	0.83
	47	0.2050	1.86
	50	0.2205	1.38
	63	0.2390	1.10
5	15	0.0141	0.67
	22	0.0203	1.75
	26	0.0316	1.60
	37	0.0375	0.54
	37	0.0473	0.95
	32	0.0559	0.883
	11	0.0638	

Run No.	n	$\xi=y/R$	R_o
6	27	0.0079	1.25
	39	0.0146	1.79
	33	0.0178	2.67
	53	0.0204	2.12
	64	0.0311	3.27
	51	0.0389	1.83
	79	0.0467	2.16
	60	0.0540	1.40
	67	0.0614	1.79
	67	0.0689	1.23
	47	0.0743	1.24
	32	0.0783	1.29
	29	0.0873	2.22
	78	0.0966	1.23
	79	0.1756	1.19
	37	0.02543	1.64
	34	0.333	1.43
	23	0.412	2.29

(Table F-I - Continued)

Run No.	n	$\xi=y/R$	R_o
9	22	0.012	2.66
	31	0.021	1.58
	34	0.029	0.70
	49	0.034	0.75
	68	0.044	0.79
	37	0.052	0.76
	44	0.059	1.44
	51	0.067	2.00
	52	0.075	1.26
	43	0.084	1.05
	59	0.093	1.36
	75	0.132	1.42
	73	0.111	1.43
	73	0.149	0.59
	51	0.169	1.22
	27	0.034	0.50
	55	0.058	0.83
	83	0.073	1.13
	97	0.112	0.94
	95	0.190	0.86
	70	0.308	0.71
	56	0.464	1.00
	39	0.621	0.44
	21	0.855	1.63

Run No.	n	$\xi=y/R$	R_o
10	43	0.016	2.91
	62	0.022	1.14
	48	0.032	3.00
	58	C.040	2.62
	79	0.048	1.39
	79	0.062	1.92
	79	0.078	1.83
	79	0.094	2.16
	79	0.124	2.16
	79	0.050	1.92
	79	0.086	1.25
	79	0.130	1.34
	79	0.206	1.08
	79	0.286	1.55
	79	0.366	1.82
	79	0.460	1.72
	79	0.534	1.82
	55	0.602	0.72
	55	0.682	1.03
	52	0.832	2.25

(Table F-I - Continued)

Run No.	n	$\xi=y/R$	R_o
11	18	0.032	0.64
	20	0.049	1.86
	64	0.064	1.21
	79	0.104	1.14
	69	0.145	1.03
	79	0.181	1.85
	79	0.224	2.00
	79	0.384	1.17
	79	0.460	1.26
	79	0.614	0.49
	79	0.774	1.08
	79	0.924	2.04
	94	0.181	1.19
	123	0.698	2.32
	110	0.843	1.62
	99	0.384	1.25
	193	0.774	0.77
	221	0.924	1.11

Run No.	n	$\xi=y/R$	R_o
12	15	0.019	2.00
	18	0.028	3.50
	28	0.037	4.60
	55	0.044	3.23
	90	0.040	2.85
	107	0.078	2.34
	13	0.046	1.17
	28	0.062	1.00
	76	0.094	1.11
	100	0.130	1.18
	100	0.212	1.56
	107	0.366	1.68
	97	0.524	0.90
	75	0.684	0.97
	85	0.842	1.18

(Table F-I - Continued)

Run No.	n	$\xi=y/R$	R_o
13	72	0.019	3.00
	57	0.028	5.35
	63	0.036	6.88
	64	0.052	8.14
	63	0.666	11.60
	59	0.082	10.80
	16	0.012	4.33
	46	0.048	1.88
	103	0.090	4.15
	103	0.130	5.06
	95	0.212	4.00
	95	0.290	6.31
	95	0.368	7.64
	87	0.600	0.67
	87	0.760	16.40

Run No.	n	$\xi=y/R$	R_o
14	99	0.024	7.25
	102	0.064	6.29
	98	0.098	3.66
	103	0.142	3.90
	106	0.258	9.60
	102	0.422	9.20
	112	0.498	3.00
	100	0.576	7.33
	98	0.734	11.25
	100	0.948	0.22

(Table F-I - Continued)

Run No.	n	$\xi=y/R$	R_0
15	11	0.008	0.83
	59	0.022	0.69
	78	0.040	0.90
	95	0.056	0.90
	95	0.069	0.98
	95	0.111	0.94
	95	0.149	0.98
	95	0.226	1.16
	95	0.298	1.32
	45	0.441	0.96
	95	0.510	1.02
	42	0.583	0.83
	58	0.728	0.93
	26	0.873	0.63
	40	1.000	1.00

Run No.	n	$\xi=y/R$	R_0
16	89	0.018	1.87
	95	0.039	1.07
	95	0.075	1.57
	95	0.146	1.38
	95	0.218	1.44
	95	0.367	1.57
	95	0.511	1.97
	75	0.657	0.66
	70	0.808	2.04
	90	0.945	2.75
17	22	0.015	1.75
	60	0.037	2.53
	91	0.074	1.94
	95	0.114	4.59
	87	0.148	2.95
	95	0.219	2.52
	79	0.291	3.39
	84	0.436	2.82
	30	0.580	0.58
	33	0.728	2.00
	35	0.871	2.50
	35	0.944	2.50

(Table F-I - Continued)

DATA FROM SEYER'S WORK (41)

Run No.	n	$\xi=y/R$	R_o
1	32		1.67
	35		1.00
	49		1.72
	46		1.42
	61	0.702	0.90
	29	1.014	0.45
2	36		1.25
	55		1.61
	56		1.55
	77	0.682	1.08
	50	0.988	0.82
3	93		1.06
	99		1.15
	98		1.65
	58	0.606	0.66
	40	0.941	1.22

Run No.	n	$\xi=y/R$	R_o
4	59	0.074	1.03
	59	0.146	1.35
	68	0.290	0.79
	76	0.612	1.11
	47	0.929	1.35
5	113	0.073	1.69
	57	0.658	1.28
6	65	0.084	0.76
	64	0.154	1.20
	71	0.300	0.97
	69	0.618	1.38
	46	0.938	0.70
7	65	0.083	1.32
	64	0.155	1.20
	71	0.300	1.03
	69	0.618	1.38
	46	0.938	0.71

APPENDIX G

MIGRATION OF AIR BUBBLES

As already indicated in Chapter III, Section III-1 , the tiny air bubbles (average diameter of 0.002") used as tracers were uniformly distributed in the calming section. On the other hand it was noticed (as suggested crudely by Figure III-5a, for example) that most bubbles were at a radial position of $\xi \approx 0.11$. Figure G-1 presents for photographic runs (4,9,16,12,13) the number of observed air bubbles as a function of their radial position. It can be noticed that for most of the runs a peak is located at the radial position already mentioned. For water runs (4.9) the peak is sharp and represent approximately 25% of all bubbles observed during the photographic run. For the case of the photographic runs with Separan AP-30 solutions, the air bubble distribution is more uniform in the core region of the pipe.

Even though there is an apparent migration of bubbles to the radial position of 0.1, the concentration in volume % is still extremely small and no influence on the turbulence is expected. The curves show one of the limitations of the technique for velocities near the wall is the small number of bubbles that occur there and therefore a large number of photographs is needed to get a reasonable number of instantaneous velocities.

FIGURE G-1

DISTRIBUTION OF AIR BUBBLES IN PIPE

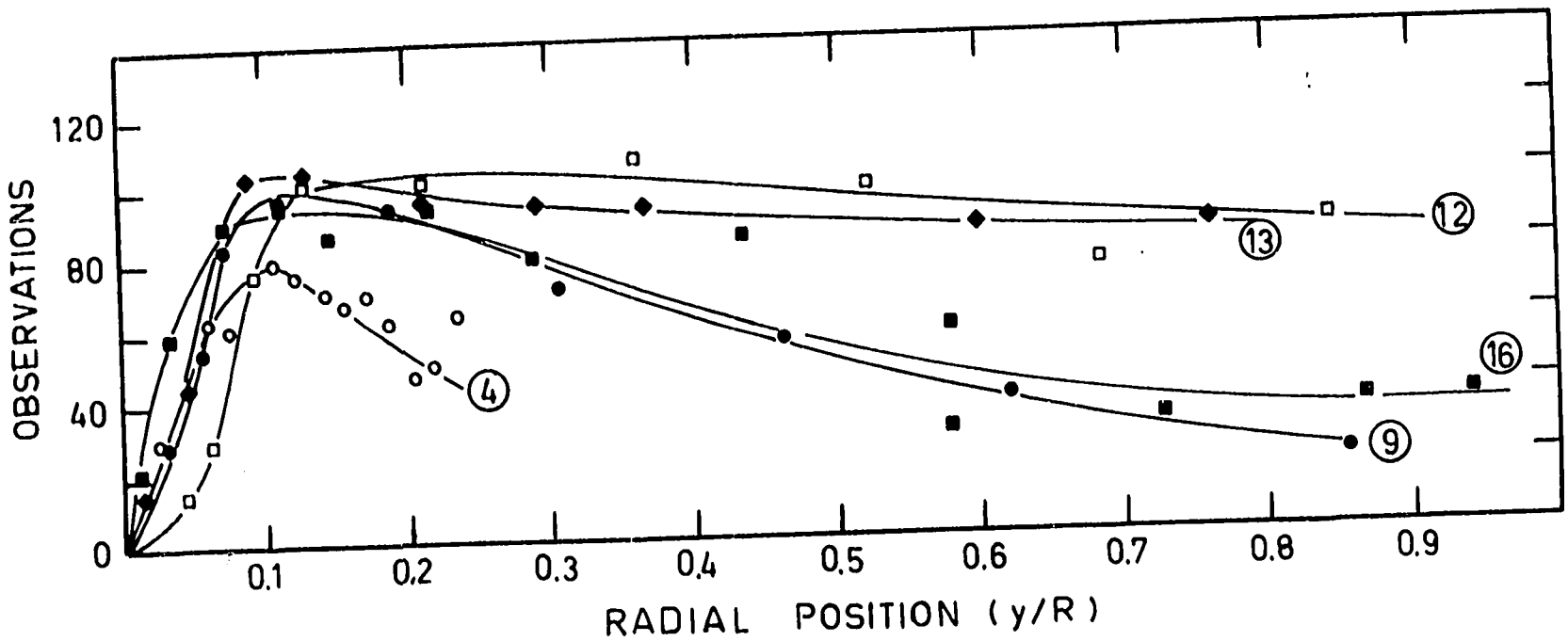

APPENDIX H

SUMMARY OF ALL RUNS

In this appendix all of the data have been tabulated in Table H-I in a format to summarize the velocity and intensity profiles at all the radial positions for each photographic run. The primary data concerning the velocity measurements can be found in Appendix L (in Book II) and the flow conditions are tabulated in Table IV-I. The axial and radial turbulent intensities tabulated are made dimensionless to the maximum velocity.

TABLE H-I-1

RUN 4

water

Q	= 11.8 USgal/min	τ_w	= 0.130 psf
T	= 77.5°F	U^*	= 0.259 ft/sec
N'_{Re}	= 38123	$\langle\bar{u}_x\rangle$	= 4.80 ft/sec
f	= 0.0057	$\langle\bar{u}_x\rangle_{max}$	= 5.80 ft/sec

	n	y inch	$\bar{u}_x$ ft/sec	$\bar{u}_r$ ft/sec	Y^+	U^+	I_x	I_r
1	30	0.0148	3.344	+0.011	30.29	12.93	0.130	0.028
2	74	0.0239	3.790	-0.021	48.92	14.65	0.072	0.034
3	63	0.0309	4.021	+0.037	63.20	15.54	0.104	0.037
4	61	0.0385	4.225	+0.027	78.78	16.33	0.085	0.045
5	77	0.0467	4.312	+0.045	95.69	16.64	0.068	0.046
6	79	0.0540	4.376	+0.034	111.08	16.91	0.080	0.046
7	75	0.0620	4.463	+0.066	127.14	17.25	0.074	0.045
8	72	0.0720	4.735	+0.083	148.04	18.30	0.072	0.054
9	67	0.0786	4.791	+0.063	161.18	18.52	0.081	0.053
10	70	0.0865	4.591	+0.021	177.19	17.74	0.089	0.045
11	62	0.0945	5.134	+0.056	193.63	19.84	0.084	0.053
12	47	0.1025	4.990	+0.057	209.89	19.29	0.093	0.054
13	50	0.1096	4.809	+0.004	224.42	18.59	0.071	0.036
14	63	0.1183	5.036	-0.012	242.37	19.46	0.089	0.043

TABLE H-I-2

RUN 5

water

Q	= 7.50 USgal/min	τ_w	= 0.0592 psf
T	= 69.0°F	U^*	= 0.1749 ft/sec
N'_{Re}	= 23785	$\langle\bar{u}_x\rangle$	≈ 3.070 ft/sec
f	= 0.00642	$\langle\bar{u}_x\rangle_{max}$	≈ 3.800 ft/sec

	n	y inch	$\bar{u}_x$ ft/sec	$\bar{u}_r$ ft/sec	Y^+	U^+	I_x	I_r
1	15	0.0071	1.595	-0.007	9.59	9.12	0.099	0.022
2	22	0.0103	1.805	+0.026	13.92	10.32	0.127	0.019
3	26	0.0158	2.236	+0.041	21.44	12.78	0.108	0.029
4	37	0.0194	2.361	-0.035	26.27	13.49	0.098	0.033
5	37	0.0236	2.445	+0.009	32.07	13.98	0.085	0.043
6	32	0.0280	2.559	+0.006	37.96	14.63	0.067	0.052
7	11	0.0319	2.565	-0.012	43.29	14.66	0.103	0.035

TABLE H-I-3

RUN 6

Solution of SEPARAN AP-30 at a conc. of 0.01%

Q	= 10.65 USgal/min	τ_w	= 0.0690 psf
T	= 99.0°F	U^*	= 0.189 ft/sec
N'_{Re}	= 35931	$\langle\bar{u}_x\rangle$	= 4.38 ft/sec
f	= 0.0038	$\langle\bar{u}_x\rangle_{max}$	= 5.35 ft/sec

	n	y inch	$\bar{u}_x$ ft/sec	$\bar{u}_r$ ft/sec	Y^+	U^+	I_x	I_r
1	27	0.0040	1.958	0.024	6.93	10.35	0.106	0.013
2	39	0.0073	2.540	0.033	12.8	13.42	0.095	0.016
3	53	0.0102	3.022	0.048	17.9	15.97	0.100	0.016
4	64	0.0156	3.290	0.065	27.4	17.39	0.104	0.015
5	51	0.0194	3.527	0.028	34.1	18.62	0.092	0.016
6	79	0.0233	3.609	0.034	40.9	19.05	0.083	0.014
7	60	0.0270	3.878	0.026	47.3	20.45	0.075	0.019
8	67	0.0307	3.888	0.049	53.8	20.52	0.070	0.020
9	67	0.0345	3.962	0.027	60.5	20.93	0.067	0.019
10	47	0.0372	4.101	0.018	65.3	21.64	0.053	0.020
11	32	0.0392	4.166	0.061	68.8	22.00	0.088	0.026
12	29	0.0437	4.162	0.023	76.7	22.00	0.091	0.022
13	33	0.0089	2.310	0.062	15.6	12.21	0.122	0.020
14	78	0.0483	4.112	0.001	84.7	21.70	0.072	0.019
15	79	0.0878	4.290	0.023	154	22.62	0.072	0.032
16	37	0.1272	4.538	0.093	223	23.92	0.067	0.028
17	34	0.1666	4.834	0.019	292	25.50	0.070	0.036
18	23	0.2060	4.695	0.056	362	24.78	0.062	0.028
19	7	0.2450	5.110	0.043			0.025	0.024
20	8	0.2850	5.070	0.109			0.052	0.027

TABLE H-I-4

RUN 7

Solution of SEPARAN AP-30 at a conc. of 0.10%

Q	= 12.1 USgal/min	τ_w	=0.075 psf
T	= 87°F	U^*	=0.197 ft/sec
N'_{Re}	= 5192	$\langle\bar{u}_x\rangle$	=4.98 ft/sec
f	= 0.00320	$\langle\bar{u}_x\rangle_{max}$	=7.74 ft/sec

	n	y inch	$\bar{u}_x$ ft/sec	$\bar{u}_r$ ft/sec	Y^+	U^+	I_x	I_r
1	40	0.1648	5.553	+0.025	300	28.15	0.235	0.024
2	40	0.2435	6.506	+0.019	447	32.99	0.188	0.032
3	40	0.3222	6.940	0.000	588	35.19	0.195	0.055
4	40	0.3616	7.361	-0.001	659	37.33	0.291	0.067
5	40	0.4404	7.650	0.025	816	38.80	0.220	0.046

TABLE H-I-5

RUN 9

water

Q = 12.15 USgal/min

T = 76.0°F

N'_{Re} = 42229

f = 0.0055

τ_w = 0.1319 psf

U^* = 0.2612 ft/sec

$\langle \bar{u}_x \rangle$ = 4.975 ft/sec

$\langle \bar{u}_x \rangle_{max}$ = 6.227 ft/sec

	n	y inch	$\bar{u}_x$ ft/sec	$\bar{u}_r$ ft/sec	Y^+	U^+	I_x	I_r
1	22	0.0061	2.889	+0.037	13.48	11.06	0.137	0.014
2	31	0.0105	3.642	+0.051	23.30	13.94	0.096	0.024
3	34	0.0145	3.598	-0.016	32.20	13.78	0.071	0.026
4	49	0.0174	3.741	-0.036	38.63	14.32	0.075	0.027
5	68	0.0219	3.946	-0.027	48.51	15.11	0.094	0.034
6	37	0.0259	3.962	-0.002	57.52	15.17	0.069	0.025
7	44	0.0294	4.111	+0.030	65.21	15.72	0.051	0.029
8	51	0.0334	4.055	+0.077	74.06	15.52	0.056	0.029
9	52	0.0376	4.242	+0.007	83.35	16.24	0.064	0.028
10	43	0.0418	4.288	+0.009	92.62	16.42	0.077	0.028
11	59	0.0462	4.426	+0.024	102.44	16.95	0.076	0.033
12	75	0.0658	4.747	+0.025	145.88	18.17	0.065	0.029
13	73	0.0551	4.539	+0.072	122.24	17.38	0.061	0.030
14	73	0.0745	4.732	-0.042	165.08	18.12	0.061	0.026
15	51	0.0846	4.910	+0.023	187.63	18.80	0.068	0.033
16	27	0.0172	3.492	-0.118	38.14	13.37	0.089	0.041
17	55	0.0289	3.838	+0.024	64.08	14.70	0.085	0.042
18	83	0.0367	4.269	+0.001	81.37	16.35	0.080	0.043
19	97	0.0562	4.600	-0.017	124.61	17.61	0.066	0.049
20	95	0.0952	4.796	+0.004	211.09	18.36	0.066	0.044
21	70	0.1537	5.204	-0.025	340.80	19.92	0.070	0.039
22	56	0.2317	5.688	+0.014	513.75	21.78	0.051	0.034
23	39	0.3097	6.035	-0.076	686.70	23.11	0.051	0.035
24	21	0.4267	6.222	+0.092	946.12	23.82	0.031	0.026
* 25	50	0.0652	4.645	+0.028	144.56	17.78	0.0561	0.036

* taken separately to check radial intensity on April 20/71

TABLE H-I-6

RUN 10

Solution of SEPARAN AP-30 at a conc. of 0.01%

Q	= 12.15 USgal/min	τ_w	= 0.0656 psf
T	= 77.0°F	U^*	= 0.1830 ft/sec
N'_{Re}	= 40992	$\langle\bar{u}_x\rangle$	= 5.080 ft/sec
f	= 0.00282	$\langle\bar{u}_x\rangle_{max}$	= 6.12 ft/sec

	n	y inch	$\bar{u}_x$ ft/sec	$\bar{u}_r$ ft/sec	Y^+	U^+	I_x	I_r
1	5	0.0056	1.686	-0.003	7.6	8.62	0.105	0.007
2	43	0.0075	2.161	+0.026	10.2	11.05	0.121	0.010
3	62	0.0115	2.943	+0.015	15.6	15.05	0.135	0.011
4	48	0.0164	3.402	+0.050	22.3	17.40	0.118	0.010
5	58	0.0204	3.580	+0.044	27.7	18.31	0.124	0.013
6	79	0.0242	3.967	+0.008	32.9	20.28	0.115	0.012
7	79	0.0309	4.427	+0.029	42.0	22.64	0.110	0.015
8	79	0.0387	4.724	+0.028	52.5	24.15	0.109	0.019
9	79	0.0468	4.500	+0.038	63.5	23.01	0.140	0.022
10	79	0.0623	4.729	+0.061	84.7	24.18	0.147	0.024
11	79	0.0249	3.933	+0.020	30.2	22.48	0.117	0.021
12	79	0.0426	4.326	+0.005	51.8	24.73	0.101	0.023
13	79	0.0648	4.763	+0.034	78.7	27.23	0.078	0.026
14	79	0.1028	5.009	+0.043	123.9	28.64	0.080	0.033
15	79	0.1428	5.313	+0.024	173.5	30.37	0.070	0.028
16	79	0.1826	5.498	+0.043	221.8	31.43	0.057	0.027
17	79	0.2297	5.637	+0.077	279.1	32.23	0.060	0.032
18	79	0.2672	5.872	+0.038	325	33.57	0.075	0.016
19	55	0.3012	5.903	+0.058	366	33.74	0.066	0.027
20	55	0.3406	5.973	-0.001	414	34.15	0.068	0.032
21	52	0.4160	6.018	+0.062	505	34.40	0.061	0.021

TABLE H-I-7

RUN 11

water

Q	= 32.4 USgal/min	τ_w	= 0.753 psf
T	= 70.0 °F	U*	= 0.624 ft/sec
N'_{Re}	= 104299	$\langle\bar{u}_x\rangle$	= 13.672 ft/sec
f	= 0.00442	$\langle\bar{u}_x\rangle_{max}$	= 16.40 ft/sec

	n	y inch	$\bar{u}_x$ ft/sec	$\bar{u}_r$ ft/sec	Y^+	U^+	I_x	I_r
1	18	0.0159	10.706	-0.147	78.03	17.17	0.077	0.019
2	20	0.0245	10.897	+0.218	120.24	17.47	0.050	0.026
3	64	0.0322	11.331	+0.079	158.03	18.18	0.072	0.029
4	79	0.0521	12.301	+0.068	255.69	19.72	0.063	0.033
5	69	0.0723	12.857	-0.063	354.82	20.62	0.059	0.033
6	79	0.0906	13.400	+0.219	444.53	21.48	0.062	0.028
7	79	0.1121	13.562	+0.255	549.90	21.75	0.067	0.029
8	79	0.1922	14.696	-0.005	943.12	23.56	0.064	0.036
9	79	0.2300	15.112	+0.100	1128.56	24.23	0.048	0.027
10	79	0.3068	16.013	-0.225	1505.86	25.68	0.042	0.036
11	123	0.3490	15.827	+0.214	1712.56	25.38	0.047	0.031
12	79	0.3870	16.116	+0.007	1899.30	25.84	0.044	0.031
13	110	0.4216	16.160	+0.107	2068.86	25.91	0.051	0.023
14	79	0.4620	16.348	+0.156	2267.32	26.21	0.046	0.024
15	210	0.4680	16.243	+0.042	2296.77	26.05	0.039	0.030
16	94	0.0906	13.169	+0.045	444.53	21.12	0.068	0.029
17	94	0.7922	14.704	+0.105	943.10	23.58	0.056	0.033
18	193	0.3870	15.882	-0.110	1899.30	25.46	0.048	0.029
19	210	0.4620	16.233	+0.041	2267.32	26.03	0.041	0.030

TABLE H-I-8

RUN 12

Solution of SEPARAN AP-30 0.01%

Q	= 28.4 USgal/min	τ_w	= 0.2318 psf
T	= 74.5°F	U^*	= 0.3462 ft/sec
N'_{Re}	= 95817	$\langle\bar{u}_x\rangle$	= 12.128 ft/sec
f	= 0.00193	$\langle\bar{u}_x\rangle_{max}$	= 13.80 ft/sec

	n	y inch	$\bar{u}_x$ ft/sec	$\bar{u}_r$ ft/sec	Y^+	U^+	I_x	I_r
1	15	0.0097	8.090	+0.075	22.3	23.37	0.0789	0.0099
2	18	0.0143	9.093	+0.096	32.8	26.26	0.0711	0.0135
3	28	0.0184	10.371	+0.173	42.2	29.96	0.0528	0.0106
4	55	0.0221	10.402	+0.105	50.8	30.04	0.0738	0.0099
5	90	0.0301	10.824	+0.152	69.1	31.27	0.0644	0.0115
6	107	0.0391	11.393	+0.099	89.7	32.91	0.0529	0.0129

RUN 12B

Q	= 28.4 USgal/min	τ_w	= 0.2514 psf
T	= 74.5 °F	U^*	= 0.3606 ft/sec
N'_{Re}	= 95817	$\langle\bar{u}_x\rangle$	= 12.128 ft/sec
f	= 0.00179	$\langle\bar{u}_x\rangle_{max}$	= 13.80 ft/sec

7	13	0.0232	10.520	+0.050	55.5	29.17	0.0514	0.0162
8	28	0.0311	10.750	+0.0192	74.4	29.81	0.0509	0.0145
9	76	0.0468	11.335	+0.022	112	31.43	0.0558	0.0137
10	100	0.0665	11.686	+0.027	159	32.41	0.0465	0.0198
11	100	0.1058	12.373	+0.054	253	34.31	0.0421	0.0209
12	107	0.1844	12.807	+0.059	441	35.52	0.0394	0.0181
13	97	0.2630	13.123	-0.040	629	36.39	0.0348	0.0208
14	75	0.3416	13.462	-0.047	817	37.33	0.0357	0.0236
15	85	0.4202	13.656	+0.053	1005	37.87	0.0251	0.0198

TABLE H-I-9

RUN 13

Solution of SEPARAN AP-30 at a conc. of 0.10%

Q	= 54.0 USgal/min	τ_w	= 0.4682 psf
T	= 75.0°F	U^*	= 0.4921 ft/sec
N'_{Re}	= 37600	$\langle\bar{u}_x\rangle$	= 21.616 ft/sec
f	= 0.00101	$\langle\bar{u}_x\rangle_{max}$	= 30.50 ft/sec

	n	y inch	$\bar{u}_x$ ft/sec	$\bar{u}_r$ ft/sec	Y^+	U^+	I_x	I_r
1	72	0.0101	5.770	+0.105	13.2	11.72	0.0491	0.0039
2	57	0.0140	7.535	+0.111	18.3	15.31	0.0349	0.0030
3	63	0.0180	9.607	+0.165	23.5	19.52	0.0458	0.0046
4	64	0.0258	11.848	+0.205	33.8	24.07	0.0432	0.0048
5	63	0.0337	12.913	+0.236	44.1	26.24	0.0346	0.0052
6	59	0.0415	14.550	+0.244	54.4	29.57	0.0413	0.0053
7	16	0.0058	5.027	+0.081	7.73	10.21	0.0398	0.0034
8	46	0.0245	10.679	+0.084	33.5	21.70	0.0466	0.0052
9	103	0.0447	15.237	+0.175	59.3	30.96	0.0403	0.0071
10	103	0.0650	17.555	+0.264	85.5	35.67	0.0422	0.0081
11	95	0.1057	21.131	+0.250	137	42.94	0.0438	0.0086
12	95	0.1452	22.799	+0.296	188	46.33	0.0396	0.0078
13	95	0.1837	24.714	+0.298	240	50.22	0.0381	0.0062
14	87	0.3005	28.249	-0.147	395	57.40	0.0427	0.0121
15	87	0.3796	29.538	+0.388	498	60.02	0.0477	0.0061

TABLE H-I-10

RUN 14

Solution of SEPARAN AP-30 at a conc. of 0.10%

Q	= 11.274 USgal/min	τ_w	= 0.860 psf
T	= 77°F	U^*	= 0.666 ft/sec
N'_{Re}	= 68450	$\langle\bar{u}_x\rangle$	= 33.40 ft/sec
f	= 0.00080	$\langle\bar{u}_x\rangle_{max}$	= 49.80 ft/sec

	n	y inch	$\bar{u}_r$ ft/sec	$\bar{u}_x$ ft/sec	Y^+	U^+	I_x	I_r
1	105	0.0119	+0.249	12.813	25.7	19.25	0.553	0.0048
2	102	0.0320	+0.302	20.796	68.8	31.24	0.0529	0.0054
3	98	0.0494	+0.344	24.623	106	36.99	0.0454	0.0073
4	103	0.0711	+0.310	27.931	153	41.96	0.0435	0.0067
5	106	0.1289	+0.533	34.248	277	51.45	0.0362	0.0072
6	102	0.2106	+0.496	39.365	452	59.14	0.0351	0.0077
7	12	0.2494	+0.421	40.366	536	60.64	0.0496	0.0085
8	100	0.2876	+0.494	42.465	619	63.79	0.0378	0.0074
9	98	0.3670	+0.541	44.83	789	63.75	0.0393	0.0080
10	100	0.4839	0.503	46.22	1041	69.44	0.0305	0.0092

TABLE H-I-11

RUN 15

water

Q	= 93.7 USgal/min	τ_w	= 0.105 psf
T	= 74°F	U^*	= 0.233 ft/sec
N'_{Re}	= 114083	$\langle\bar{u}_x\rangle$	= 5.00 ft/sec
f	= 0.00435	$\langle\bar{u}_x\rangle_{max}$	= 6.29 ft/sec

	n	y inch	$\bar{u}_x$ ft/sec	$\bar{u}_r$ ft/sec	Y^+	U^+	I_x	I_r
1	11	.0106	2.392	0.006	20.40	10.28	0.154	0.009
2	58	.0304	3.587	-0.043	58.51	15.42	0.067	0.038
3	78	.0550	3.969	-0.006	105.9	17.06	0.079	0.046
4	95	.0766	4.108	-0.002	147.4	17.66	0.078	0.038
5	95	.0947	4.391	+0.007	182.3	18.87	0.083	0.051
6	95	.1529	4.581	-0.013	294.3	19.69	0.064	0.049
7	95	.2051	4.818	+0.018	394.8	20.71	0.064	0.041
8	95	.3111	5.032	+0.016	598.8	21.63	0.064	0.038
9	95	.4099	5.320	+0.045	789.0	22.87	0.060	0.033
10	45	.6071	5.641	-0.014	1168	24.24	0.072	0.052
11	42	.8021	5.790	+0.008	1543	24.89	0.051	0.031
12	95	.702	5.977	+0.004	1351	25.69	0.053	0.036
13	55	1.00	6.285	-0.024	1925	27.01	0.056	0.030
14	26	1.20	6.240	-0.092	2310	26.82	0.058	0.028
15	38	1.40	6.290	+0.009	2695	27.03	0.053	0.022

TABLE H-I-12

RUN 16

Solution of SEPARAN AP-30 at a conc. of 0.01%

Q	= 95 USgal/min	τ_w	= 0.065 psf
T	= 74°F	U^*	= 0.183 ft/sec
N'_{Re}	= 97774	$\langle\bar{u}_x\rangle$	= 5.07 ft/sec
f	= 0.00258	$\langle\bar{u}_x\rangle_{max}$	= 5.87 ft/sec

	n	y inch	$\bar{u}_x$ ft/sec	$\bar{u}_r$ ft/sec	Y^+	U^+	I_x	I_r
1	89	.0252	3.458	0.032	31.2	18.88	0.112	0.012
2	95	.0528	3.695	0.023	85.4	20.17	0.089	0.024
3	95	.1017	4.368	0.048	126	23.84	0.067	0.027
4	95	.2014	4.806	0.034	249	26.23	0.057	0.027
5	95	.300	4.989	0.050	372	27.23	0.048	0.028
6	95	.505	5.340	0.068	626	29.15	0.046	0.033
7	95	.702	5.531	0.069	870	30.19	0.043	0.023
8	75	.905	5.715	-0.053	1121	31.19	0.033	0.024
9	70	1.101	5.798	0.060	1365	31.65	0.043	0.026
10	90	1.30	5.844	0.066	1611	31.90	0.033	0.022

TABLE H-I-13

RUN 17

Solution of SEPARAN AP-30 at a conc. of 0.10%

Q	= 163 USgal/min	τ_w	= 0.106 psf
T	= 74°F	U^*	= 0.234 ft/sec
N'_{Re}	= 21905	$\langle\bar{u}_x\rangle$	= 8.77 ft/sec
f	= 0.00146	$\langle\bar{u}_x\rangle_{max}$	=11.38 ft/sec

	n	y inch	$\bar{u}_x$ ft/sec	$\bar{u}_r$ ft/sec	Y^+	U^+	I_x	I_r
1	22	0.0204	1.671	0.049	6.27	7.12	0.041	0.0064
2	60	0.0514	3.117	0.038	15.4	13.29	0.064	0.0069
3	91	0.1018	5.069	0.074	30.4	21.61	0.065	0.0097
4	95	0.1565	6.714	0.100	47.0	28.62	0.074	0.0090
5	87	0.2043	7.364	0.087	61.3	31.39	0.072	0.0098
6	95	0.3023	8.863	0.088	90.6	37.78	0.059	0.0095
7	79	0.4004	9.7229	0.124	119	41.45	0.047	0.0109
8	84	0.6005	10.524	0.120	180	44.86	0.044	0.0108
9	30	0.7971	10.989	0.029	239	46.85	0.041	0.114
10	33	0.999	11.409	0.046	300	48.64	0.035	0.0084
11	35	1.1985	11.252	0.113	359	47.97	0.025	0.0110
12	35	1.298	11.360	0.086	389	48.43	0.034	0.0103

APPENDIX I

PRESSURE DROP MEASUREMENTS

Pressure drops over a range of flow rates were obtained for each of the experimental fluids and are tabulated in Tables I-I. For the Newtonian fluids the data serve to validate the apparatus while for the drag reducing solutions the data characterize the drag reduction over a range of flow rates of interest. The tables representing pressure drop measurements during a photographic run are specified so that degradation effects may be following.

TABLE I-I-1

FRICTION COEFFICIENT - GENERALIZED REYNOLDS NUMBER

Water
Pipe Diameter = 0.833 ft
Length Between Pressure Taps = 11 ft

Flow Gal/Min	T °F	Manometer Readings Inches Hg	Friction loss psf	Generalized Reynolds	Friction Factor
43.2	84.5	10.38	668.0	164200	0.00423
42.0	72.0	9.39	612.0	138000	0.00410
21.2	68.0	2.75	181.2	66000	0.00469
16.3	68.0	1.84	121.2	50700	0.00529
18.7	74.4	2.30	149.5	64000	0.00459
19.7	74.7	2.50	162.5	67400	0.00484
9.5	76.0	0.81	52.7	17200	0.00675

TABLE I-I-2

FRICTION COEFFICIENT - GENERALIZED REYNOLDS NUMBER

Water
Pipe Diameter = .2300 ft
Temperature = 70°F

Flow Gal/Min	Manometer Readings Inches ODB	Length (Taps) Ft	Generalized Reynolds	Friction Factor
113.2	39.60	23.60	131776	0.0043
113.2	29.45	17.50	132014	0.0043
113.2	19.12	11.69	132150	0.0042
96.5	29.65	23.60	112336	0.0044
96.5	21.90	17.50	112538	0.0044
96.5	14.42	11.69	112654	0.0043
83.5	22.65	23.60	97202	0.0045
83.5	16.81	17.50	97378	0.0045
83.5	11.10	11.69	97478	0.0044
70.5	16.86	23.60	82069	0.0047
70.5	12.55	17.50	82217	0.0047
70.5	8.30	11.69	82302	0.0046
61.2	12.73	23.60	71243	0.0047
61.2	9.52	17.50	71371	0.0047
61.2	6.32	11.69	71445	0.0047
51.2	9.70	23.60	59602	0.0052
51.2	7.25	17.50	59709	0.0052
51.2	4.89	11.69	59771	0.0052
43.3	7.10	23.60	50406	0.0053
43.3	5.27	17.50	50496	0.0053
34.0	4.62	23.60	39579	0.0056
34.0	3.54	17.50	39651	0.0057

Water
Pipe Diameter = .2300 ft
Temperature 74°F

Flow Gal/Min	Manometer Readings Inches Hg	Length (Taps) Ft	Generalized Reynolds	Friction Factor
92.0	0.66	23.60	112645	0.0045
92.0	0.50	17.50	112847	0.0045
126.0	1.16	23.60	154274	0.0042
126.0	0.87	17.50	154552	0.0042
142.5	1.45	23.60	174477	0.0041
142.5	1.10	17.50	174791	0.0041

TABLE-I-I- 3 FRICTION COEFFICIENT - GENERALIZED REYNOLDS NUMBER

DATE OF THE EXPERIMENT= 5/ 27/ 70
CONCENTRATION OF THE SEPARAN SOLUTION= 0.10
PIPE DIAMETER (FT) = 0.0833
TEMPERATURE (FAR.) = 78.0

FLOW GAL/MIN	MANOMETER READINGS INCHES HG	FRICTION LOSS PSF	LENGTH (TAPS) FT	SHEAR STRESS AT WALL PSF	K OR VISCOSITY LB-SEC/SF	N	GENERALIZED REYNOLDS	FRICTION FACTOR
82.50	14.94	976.29	22.00	0.924	0.81E-03	0.716	66054.8	0.00084
82.50	10.37	677.65	16.00	0.882	0.81E-03	0.715	65966.4	0.00080
82.50	6.93	452.86	11.00	0.857	0.82E-03	0.715	65914.5	0.00078
73.00	12.27	801.81	22.00	0.758	0.83E-03	0.713	56135.8	0.00088
73.00	8.57	560.03	16.00	0.728	0.84E-03	0.712	56076.0	0.00085
73.00	5.72	373.78	11.00	0.707	0.84E-03	0.712	56034.0	0.00082
62.50	9.70	633.87	22.00	0.600	0.86E-03	0.709	45681.9	0.00095
62.50	6.72	439.13	16.00	0.571	0.87E-03	0.708	45630.2	0.00091
62.50	4.50	294.06	11.00	0.556	0.87E-03	0.708	45603.1	0.00088
55.50	8.21	536.50	22.00	0.507	0.89E-03	0.706	39032.6	0.00102
55.50	5.72	373.78	16.00	0.486	0.89E-03	0.705	38996.6	0.00098
55.50	3.82	249.62	11.00	0.472	0.90E-03	0.705	38973.2	0.00095
46.00	6.23	407.11	22.00	0.385	0.92E-03	0.701	30432.1	0.00113
46.00	4.33	282.95	16.00	0.368	0.93E-03	0.701	30407.1	0.00108
46.00	2.93	191.46	11.00	0.362	0.93E-03	0.700	30398.7	0.00106
38.00	4.85	316.93	22.00	0.300	0.96E-03	0.697	23635.1	0.00129
38.00	3.41	222.83	16.00	0.290	0.96E-03	0.696	23622.6	0.00124
38.00	2.31	150.95	11.00	0.285	0.96E-03	0.696	23617.4	0.00123
27.50	3.24	211.72	22.00	0.200	0.10E-02	0.690	15407.0	0.00164
27.50	2.26	147.68	16.00	0.192	0.10E-02	0.689	15399.9	0.00158
27.50	1.57	102.59	11.00	0.194	0.10E-02	0.690	15401.6	0.00159

TABLE-I-I- 3 FRICTION COEFFICIENT - GENERALIZED REYNOLDS NUMBER

DATE OF THE EXPERIMENT= 5/ 27/ 70
CONCENTRATION OF THE SEPARAN SOLUTION= 0.10
PIPE DIAMETER (FT) = 0.0833
TEMPERATURE (FAR.) = 78.0

FLOW GAL/MIN	MANOMETER READINGS INCHES HG	FRICTION LOSS PSF	LENGTH (TAPS) FT	SHEAR STRESS AT WALL PSF	K OR VISCOSITY LB-SEC/SF	N	GENERALIZED REYNOLDS	FRICTION FACTOR
13.10	1.45	94.75	22.00	0.089	0.11E-02	0.676	5767.2	0.00325
13.10	1.00	65.34	16.00	0.085	0.11E-02	0.675	5766.1	0.00308
13.10	0.68	44.43	11.00	0.084	0.11E-02	0.675	5766.0	0.00304
11.50	0.89	58.15	22.00	0.055	0.11E-02	0.667	4853.8	0.00258
11.50	0.67	44.30	16.00	0.057	0.11E-02	0.668	4852.5	0.00271
11.50	0.48	31.43	11.00	0.059	0.11E-02	0.669	4851.7	0.00279
12.90	1.33	86.91	22.00	0.082	0.11E-02	0.674	5649.3	0.00307
12.90	1.03	67.30	16.00	0.087	0.11E-02	0.676	5650.4	0.00327
12.90	0.71	46.39	11.00	0.087	0.11E-02	0.676	5650.4	0.00328
27.20	3.20	209.11	22.00	0.197	0.10E-02	0.690	15185.2	0.00166
27.20	2.27	148.33	16.00	0.193	0.10E-02	0.689	15180.9	0.00162
27.20	1.57	102.59	11.00	0.194	0.10E-02	0.690	15181.9	0.00163
36.00	4.54	296.67	22.00	0.280	0.97E-03	0.696	22004.5	0.00134
36.00	3.18	207.80	16.00	0.270	0.97E-03	0.695	21992.3	0.00129
36.00	2.19	143.11	11.00	0.270	0.97E-03	0.695	21992.8	0.00130
47.00	6.51	425.41	22.00	0.402	0.92E-03	0.702	31319.6	0.00113
47.00	4.57	298.63	16.00	0.388	0.92E-03	0.701	31298.6	0.00109
47.00	3.05	199.31	11.00	0.377	0.93E-03	0.701	31281.7	0.00106
60.00	9.04	590.74	22.00	0.559	0.87E-03	0.708	43264.7	0.00096
60.00	6.33	413.65	16.00	0.538	0.88E-03	0.707	43227.9	0.00093
60.00	4.22	275.76	11.00	0.522	0.88E-03	0.706	43199.1	0.00090

TABLE-I-I- 3 FRICTION COEFFICIENT - GENERALIZED REYNOLDS NUMBER

DATE OF THE EXPERIMENT= 5/ 27/ 70
CONCENTRATION OF THE SEPARAN SOLUTION= 0.10
PIPE DIAMETER (FT) = 0.0833
TEMPERATURE (FAR.) = 78.0

FLOW GAL/MIN	MANOMETER READINGS INCHES HG	FRICTION LOSS PSF	LENGTH (TAPS) FT	SHEAR STRESS AT WALL PSF	K OR VISCOSITY LB-SEC/SF	N	GENERALIZED REYNOLDS	FRICTION FACTOR
76.00	13.08	854.74	22.00	0.809	0.82E-03	0.714	59222.5	0.00087
76.00	9.12	595.97	16.00	0.775	0.83E-03	0.713	59155.4	0.00083
76.00	6.07	396.66	11.00	0.750	0.83E-03	0.713	59105.2	0.00080
91.50	17.30	1130.51	22.00	1.070	0.79E-03	0.719	75764.7	0.00079
91.50	11.99	783.51	16.00	1.019	0.79E-03	0.718	75654.4	0.00075
91.50	8.04	525.39	11.00	0.994	0.80E-03	0.717	75598.9	0.00073

TABLE-I-I- 4 FRICTION COEFFICIENT - GENERALIZED REYNOLDS NUMBER

DATE OF THE EXPERIMENT= 5/ 30/ 70
CONCENTRATION OF THE SEPARAN SOLUTION= 0.01
PIPE DIAMETER (FT) = 0.0833
TEMPERATURE (FAR.) = 94.0

FLOW GAL/MIN	MANOMETER READINGS INCHES HG	FRICTION LOSS PSF	LENGTH (TAPS) FT	SHEAR STRESS AT WALL PSF	K OR VISCOSITY LB-SEC/SF	N	GENERALIZED REYNOLDS	FRICTION FACTOR
85.00	21.19	1380.69	22.00	1.306	0.23E-04	1.000	240496.8	0.00112
85.00	15.32	998.21	16.00	1.299	0.23E-04	1.000	240496.7	0.00111
85.00	10.49	683.50	11.00	1.293	0.23E-04	1.000	240496.7	0.00111
68.00	14.69	957.16	22.00	0.906	0.23E-04	1.000	192397.2	0.00121
68.00	10.69	696.53	16.00	0.906	0.23E-04	1.000	192397.1	0.00121
68.00	7.15	465.87	11.00	0.881	0.23E-04	1.000	192397.3	0.00118
57.00	11.13	725.20	22.00	0.686	0.23E-04	1.000	161274.1	0.00131
57.00	8.05	524.51	16.00	0.682	0.23E-04	1.000	161274.1	0.00130
57.00	5.53	360.32	11.00	0.682	0.23E-04	1.000	161274.0	0.00130
44.00	7.64	497.80	22.00	0.471	0.23E-04	1.000	124492.4	0.00150
44.00	5.56	362.27	16.00	0.471	0.23E-04	1.000	124492.4	0.00151
44.00	3.83	249.55	11.00	0.472	0.23E-04	1.000	124492.5	0.00151
34.00	5.30	345.33	22.00	0.326	0.23E-04	1.000	96198.7	0.00175
34.00	3.84	250.20	16.00	0.325	0.23E-04	1.000	96198.6	0.00174
34.00	2.67	173.97	11.00	0.329	0.23E-04	1.000	96198.7	0.00176
27.20	3.85	250.85	22.00	0.237	0.23E-04	1.000	76959.0	0.00199
27.20	2.81	183.09	16.00	0.238	0.23E-04	1.000	76959.0	0.00199
27.20	2.00	130.31	11.00	0.246	0.23E-04	1.000	76959.0	0.00206

TABLE-I-I- 4 FRICTION COEFFICIENT - GENERALIZED REYNOLDS NUMBER

DATE OF THE EXPERIMENT= 5/ 30/ 70
CONCENTRATION OF THE SEPARAN SOLUTION= 0.01
PIPE DIAMETER (FT) = 0.0833
TEMPERATURE (FAR.) = 94.0

FLOW GAL/MIN	MANOMETER READINGS INCHES HG	FRICTION LOSS PSF	LENGTH (TAPS) FT	SHEAR STRESS AT WALL PSF	K OR VISCOSITY LB-SEC/SF	N	GENERALIZED REYNOLDS	FRICTION FACTOR
21.70	2.80	182.44	22.00	0.172	0.23E-04	1.000	61397.4	0.00227
21.70	2.01	130.96	16.00	0.170	0.23E-04	1.000	61397.4	0.00224
21.70	1.45	94.47	11.00	0.178	0.23E-04	1.000	61397.4	0.00235
14.70	1.62	105.57	22.00	0.099	0.23E-04	1.000	41591.7	0.00286
14.70	1.23	80.15	16.00	0.104	0.23E-04	1.000	41591.8	0.00299
14.70	0.88	57.34	11.00	0.108	0.23E-04	1.000	41591.8	0.00311
12.90	1.34	87.32	22.00	0.082	0.23E-04	1.000	36498.9	0.00308
12.90	0.98	63.86	16.00	0.083	0.23E-04	1.000	36498.9	0.00309
12.90	0.72	46.92	11.00	0.088	0.23E-04	1.000	36498.9	0.00331
9.20	0.85	55.39	22.00	0.052	0.23E-04	1.000	26030.2	0.00384
9.20	0.62	40.40	16.00	0.052	0.23E-04	1.000	26030.2	0.00385
9.20	0.48	31.28	11.00	0.059	0.23E-04	1.000	26030.2	0.00434
27.20	3.87	252.20	22.00	0.238	0.23E-04	1.000	76958.9	0.00200
27.20	2.81	183.12	16.00	0.238	0.23E-04	1.000	76959.0	0.00199
27.20	1.95	127.08	11.00	0.240	0.23E-04	1.000	76959.0	0.00201
43.50	7.62	496.58	22.00	0.470	0.23E-04	1.000	123077.6	0.00154
43.50	5.55	361.68	16.00	0.470	0.23E-04	1.000	123077.7	0.00154
43.50	3.83	249.59	11.00	0.472	0.23E-04	1.000	123077.8	0.00154
93.00	24.63	1605.11	22.00	1.519	0.23E-04	1.000	263131.5	0.00108
93.00	17.78	1158.70	16.00	1.508	0.23E-04	1.000	263131.6	0.00108
93.00	12.19	794.41	11.00	1.503	0.23E-04	1.000	263131.4	0.00107

TABLE-I-I- 5 FRICTION COEFFICIENT - GENERALIZED REYNOLDS NUMBER

DATE OF THE EXPERIMENT= 5/ 30/ 70
CONCENTRATION OF THE SEPARAN SOLUTION= 0.10
PIPE DIAMETER (FT) = 0.0833
TEMPERATURE (FAR.) = 67.0

FLOW GAL/MIN	MANOMETER READINGS INCHES HG	FRICTION LOSS PSF	LENGTH (TAPS) FT	SHEAR STRESS AT WALL PSF	K OR VISCOSITY LB-SEC/SF	N	GENERALIZED REYNOLDS	FRICTION FACTOR
74.00	12.97	848.71	22.00	0.803	0.82E-03	0.714	57192.9	0.00091
74.00	8.96	586.31	16.00	0.763	0.83E-03	0.713	57112.9	0.00086
74.00	6.01	393.27	11.00	0.744	0.83E-03	0.712	57076.0	0.00084
54.00	8.21	537.23	22.00	0.508	0.89E-03	0.706	37659.5	0.00108
54.00	5.72	374.29	16.00	0.487	0.89E-03	0.705	37623.9	0.00104
54.00	3.83	250.62	11.00	0.474	0.89E-03	0.705	37602.9	0.00101
27.50	3.50	229.02	22.00	0.216	0.10E-02	0.691	15415.8	0.00178
27.50	2.47	161.62	16.00	0.210	0.10E-02	0.691	15409.7	0.00173
27.50	1.70	111.24	11.00	0.210	0.10E-02	0.691	15409.9	0.00173
13.35	1.54	100.77	22.00	0.095	0.11E-02	0.677	5912.4	0.00333
13.35	1.12	73.28	16.00	0.095	0.11E-02	0.677	5912.4	0.00333
13.35	0.79	51.69	11.00	0.097	0.11E-02	0.678	5913.3	0.00342

TABLE-I-I- 6 FRICTION COEFFICIENT - GENERALIZED REYNOLDS NUMBER

DATE OF THE EXPERIMENT= 6/ 15/ 70
CONCENTRATION OF THE SEPARAN SOLUTION= 0.10
PIPE DIAMETER (FT) = 0.0833
TEMPERATURE (FAR.) = 90.0

FLOW GAL/MIN	MANOMETER READINGS INCHES HG	FRICTION LOSS PSF	LENGTH (TAPS) FT	SHEAR STRESS AT WALL PSF	K OR VISCOSITY LB-SEC/SF	N	GENERALIZED REYNOLDS	FRICTION FACTOR
12.10	1.10	71.73	22.00	0.067	0.11E-02	0.671	5192.5	0.00287
12.10	0.85	55.43	16.00	0.072	0.11E-02	0.672	5192.2	0.00305
12.10	0.61	39.91	11.00	0.075	0.11E-02	0.673	5192.3	0.00320
12.10	1.93	126.04	22.00	0.119	0.10E-02	0.681	5206.6	0.00506
12.10	1.52	99.26	16.00	0.129	0.10E-02	0.682	5212.3	0.00548
12.10	1.32	86.20	11.00	0.163	0.10E-02	0.686	5234.1	0.00692

TABLE-I-I- 7 FRICTION COEFFICIENT - GENERALIZED REYNOLDS NUMBER

DATE OF THE EXPERIMENT= 8/ 12/ 70
CONCENTRATION OF THE SEPARAN SOLUTION= 0.01
PIPE DIAMETER (FT) = 0.0833
TEMPERATURE (FAR.) = 77.0

FLOW GAL/MIN	MANOMETER READINGS INCHES HG	FRICTION LOSS PSF	LENGTH (TAPS) FT	SHEAR STRESS AT WALL PSF	K OR VISCOSITY LB-SEC/SF	N	GENERALIZED REYNOLDS	FRICTION FACTOR
12.15	1.04	67.97	22.00	0.064	0.23E-04	1.000	34376.9	0.00271
12.15	1.16	75.81	22.00	0.071	0.23E-04	1.000	34376.8	0.00302
12.15	0.76	49.67	16.00	0.064	0.23E-04	1.000	34376.9	0.00272
12.15	0.90	58.82	16.00	0.076	0.23E-04	1.000	34376.9	0.00322
12.15	0.48	31.37	11.00	0.059	0.23E-04	1.000	34376.9	0.00250
12.15	0.60	39.21	11.00	0.074	0.23E-04	1.000	34376.9	0.00312

TABLE-I-I- 8 FRICTION COEFFICIENT - GENERALIZED REYNOLDS NUMBER

DATE OF THE EXPERIMENT= 9/ 14/ 70
CONCENTRATION OF THE SEPARAN SOLUTION= 0.01
PIPE DIAMETER (FT) = 0.0833
TEMPERATURE (FAR.) = 74.5

FLOW GAL/MIN	MANOMETER READINGS INCHES HG	FRICTION LOSS PSF	LENGTH (TAPS) FT	SHEAR STRESS AT WALL PSF	K OR VISCOSITY LB-SEC/SF	N	GENERALIZED REYNOLDS	FRICTION FACTOR
28.40	3.74	244.51	22.00	0.231	0.23E-04	1.000	80354.2	0.00178
28.40	2.73	178.47	16.00	0.232	0.23E-04	1.000	80354.2	0.00179
28.40	1.88	122.90	11.00	0.232	0.23E-04	1.000	80354.2	0.00179
28.40	4.00	261.50	22.00	0.247	0.23E-04	1.000	80354.1	0.00191
28.40	2.94	192.20	16.00	0.250	0.23E-04	1.000	80354.1	0.00193
28.40	2.03	132.71	11.00	0.251	0.23E-04	1.000	80354.2	0.00193

TABLE-I-I- 9 FRICTION COEFFICIENT - GENERALIZED REYNOLDS NUMBER

DATE OF THE EXPERIMENT= 9/ 16/ 70
CONCENTRATION OF THE SEPARAN SOLUTION= 0.10
PIPE DIAMETER (FT) = 0.0833
TEMPERATURE (FAR.) = 75.0

FLOW GAL/MIN	MANOMETER READINGS INCHES HG	FRICTION LOSS PSF	LENGTH (TAPS) FT	SHEAR STRESS AT WALL PSF	< OR VISCOSITY LB-SEC/SF	N	GENERALIZED REYNOLDS	FRICTION FACTOR
54.00	7.95	519.38	22.00	0.491	0.89E-03	0.705	37649.3	0.00104
54.00	5.71	373.03	16.00	0.485	0.89E-03	0.705	37639.1	0.00103
54.00	3.85	251.52	11.00	0.476	0.89E-03	0.705	37623.6	0.00101
54.00	7.93	518.40	22.00	0.490	0.89E-03	0.705	37640.7	0.00104
54.00	5.65	369.35	16.00	0.480	0.89E-03	0.705	37624.1	0.00102
54.00	3.76	245.80	11.00	0.465	0.90E-03	0.705	37598.6	0.00099
54.00	7.91	517.10	22.00	0.489	0.89E-03	0.705	37638.6	0.00104
54.00	5.55	362.82	16.00	0.472	0.90E-03	0.705	37610.0	0.00100
54.00	3.71	242.53	11.00	0.459	0.90E-03	0.704	37588.3	0.00097

TABLE-I-I-10 FRICTION COEFFICIENT - GENERALIZED REYNOLDS NUMBER

DATE OF THE EXPERIMENT= 9/ 17/ 70
CONCENTRATION OF THE SEPARAN SOLUTION= 0.10
PIPE DIAMETER (FT) = 0.0833
TEMPERATURE (FAR.) = 77.0

FLOW GAL/MIN	MANOMETER READINGS INCHES HG	FRICTION LOSS PSF	LENGTH (TAPS) FT	SHEAR STRESS AT WALL PSF	K OR VISCOSITY LB-SEC/SF	N	GENERALIZED REYNOLDS	FRICTION FACTOR
81.50	15.18	992.10	22.00	0.939	0.80E-03	0.716	65014.7	0.00088
81.50	10.33	675.12	16.00	0.879	0.81E-03	0.715	64889.7	0.00082
81.50	6.95	454.22	11.00	0.860	0.81E-03	0.715	64850.4	0.00080
81.50	15.07	984.91	22.00	0.932	0.80E-03	0.716	65000.7	0.00087
81.50	10.35	676.43	16.00	0.880	0.81E-03	0.715	64893.1	0.00082
81.50	6.96	454.87	11.00	0.861	0.81E-03	0.715	64853.0	0.00080

TABLE-I-I-11 FRICTION COEFFICIENT - GENERALIZED REYNOLDS NUMBER

DATE OF THE EXPERIMENT= 3/ 10/ 71
CONCENTRATION OF THE SEPARAN SOLUTION= 0.01
PIPE DIAMETER (FT) = 0.0833
TEMPERATURE (FAR.) = 75.0

FLOW GAL/MIN	MANOMETER READINGS INCHES HG	FRICTION LOSS PSF	LENGTH (TAPS) FT	SHEAR STRESS AT WALL PSF	K OR VISCOSITY LB-SEC/SF	N	GENERALIZED REYNOLDS	FRICTION FACTOR
31.00	2.08	135.97	12.00	0.235	0.23E-04	1.000	87710.6	0.00152
31.00	1.05	68.64	6.00	0.238	0.23E-04	1.000	87710.6	0.00154
33.00	2.75	179.77	12.00	0.311	0.23E-04	1.000	93369.3	0.00178
33.00	1.37	89.56	6.00	0.310	0.23E-04	1.000	93369.3	0.00177
40.50	3.75	245.14	12.00	0.425	0.23E-04	1.000	114589.7	0.00161
40.50	1.81	118.32	6.00	0.410	0.23E-04	1.000	114589.7	0.00155
47.00	4.52	295.48	12.00	0.512	0.23E-04	1.000	132980.4	0.00144
47.00	2.20	143.82	6.00	0.499	0.23E-04	1.000	132980.4	0.00140
56.00	5.69	371.97	12.00	0.645	0.23E-04	1.000	158445.0	0.00128
56.00	2.90	189.58	6.00	0.658	0.23E-04	1.000	158444.7	0.00130

TABLE-I-I-12 FRICTION COEFFICIENT - GENERALIZED REYNOLDS NUMBER

DATE OF THE EXPERIMENT= 3/ 10/ 71
CONCENTRATION OF THE SEPARAN SOLUTION= 0.01
PIPE DIAMETER (FT) = 0.2298
TEMPERATURE (FAR.) = 75.0

FLOW GAL/MIN	MANOMETER READINGS INCHES HG	FRICTION LOSS PSF	LENGTH (TAPS) FT	SHEAR STRESS AT WALL PSF	K OR VISCOSITY LB-SEC/SF	N	GENERALIZED REYNOLDS	FRICTION FACTOR
26.50	2.67	4.22	23.60	0.010	0.23E-04	1.000	27178.9	0.00527
32.00	3.59	5.67	23.60	0.013	0.23E-04	1.000	32819.8	0.00486
38.50	4.61	7.29	23.60	0.017	0.23E-04	1.000	39486.3	0.00431
50.50	6.57	10.39	23.60	0.025	0.23E-04	1.000	51793.7	0.00357
65.00	9.12	14.42	23.60	0.035	0.23E-04	1.000	66665.2	0.00299
82.00	12.90	20.40	23.60	0.049	0.23E-04	1.000	84100.7	0.00266
104.50	18.30	28.94	23.60	0.070	0.23E-04	1.000	107177.2	0.00232
133.00	26.78	42.36	23.60	0.103	0.23E-04	1.000	136407.1	0.00210
133.00	27.25	43.10	23.60	0.104	0.23E-04	1.000	136407.1	0.00213
96.00	17.09	27.03	23.60	0.065	0.23E-04	1.000	98459.4	0.00257
73.00	11.78	18.63	23.60	0.045	0.23E-04	1.000	74870.1	0.00306
65.00	10.07	15.92	23.60	0.038	0.23E-04	1.000	66665.2	0.00330
44.50	6.02	9.52	23.60	0.023	0.23E-04	1.000	45640.0	0.00421

TABLE-I-I-12 FRICTION COEFFICIENT - GENERALIZED REYNOLDS NUMBER

DATE OF THE EXPERIMENT= 3/ 10/ 71
CONCENTRATION OF THE SEPARAN SOLUTION= 0.01
PIPE DIAMETER (FT) = 0.2300
TEMPERATURE (FAR.) = 75.0

FLOW GAL/MIN	MANOMETER READINGS INCHES HG	FRICTION LOSS PSF	LENGTH (TAPS) FT	SHEAR STRESS AT WALL PSF	K OR VISCOSITY LB-SEC/SF	N	GENERALIZED REYNOLDS	FRICTION FACTOR
26.50	2.13	3.36	17.50	0.011	0.23E-04	1.000	27155.3	0.00570
32.00	2.67	4.23	17.50	0.013	0.23E-04	1.000	32791.3	0.00490
38.50	3.49	5.52	17.50	0.018	0.23E-04	1.000	39452.0	0.00443
50.50	4.91	7.76	17.50	0.025	0.23E-04	1.000	51748.7	0.00361
65.00	6.88	10.88	17.50	0.035	0.23E-04	1.000	66607.2	0.00306
82.00	9.67	15.29	17.50	0.050	0.23E-04	1.000	84027.5	0.00270
104.50	13.62	21.54	17.50	0.070	0.23E-04	1.000	107083.9	0.00234
133.00	19.85	31.40	17.50	0.103	0.23E-04	1.000	136288.6	0.00210
133.00	20.13	31.84	17.50	0.104	0.23E-04	1.000	136288.4	0.00213
96.00	12.67	20.04	17.50	0.065	0.23E-04	1.000	98373.8	0.00258
73.00	8.32	13.16	17.50	0.043	0.23E-04	1.000	74805.0	0.00293
65.00	7.35	11.62	17.50	0.038	0.23E-04	1.000	66607.2	0.00327
44.50	4.63	7.32	17.50	0.024	0.23E-04	1.000	45600.3	0.00439

TABLE-I-I-12 FRICTION COEFFICIENT - GENERALIZED REYNOLDS NUMBER

DATE OF THE EXPERIMENT= 3/ 10/ 71
CONCENTRATION OF THE SEPARAN SOLUTION= 0.01
PIPE DIAMETER (FT) = 0.2304
TEMPERATURE (FAR.) = 75.C

FLOW GAL/MIN	MANOMETER READINGS INCHES HG	FRICTION LOSS PSF	LENGTH (TAPS) FT	SHEAR STRESS AT WALL PSF	K OR VISCOSITY LB-SEC/SF	N	GENERALIZED REYNOLDS	FRICTION FACTOR
26.50	1.41	2.23	11.68	0.010	0.23E-04	1.000	27108.1	0.00569
32.00	1.81	2.86	11.68	0.014	0.23E-04	1.000	32734.3	0.00501
38.50	2.37	3.74	11.68	0.018	0.23E-04	1.000	39383.5	0.00453
50.50	3.35	5.29	11.68	0.026	0.23E-04	1.000	51658.8	0.00372
65.00	4.50	7.11	11.68	0.035	0.23E-04	1.000	66491.6	0.00302
82.00	6.31	9.98	11.68	0.049	0.23E-04	1.000	83881.6	0.00266
104.50	8.74	13.82	11.68	0.068	0.23E-04	1.000	106898.0	0.00227
133.00	12.73	20.13	11.68	0.099	0.23E-04	1.000	136051.8	0.00204
96.00	8.17	12.92	11.68	0.063	0.23E-04	1.000	98202.9	0.00251
73.00	5.70	9.01	11.68	0.044	0.23E-04	1.000	74675.2	0.00303
65.00	4.99	7.89	11.68	0.038	0.23E-04	1.000	66491.6	0.00335
44.50	3.25	5.14	11.68	0.025	0.23E-04	1.000	45521.1	0.00465

TABLE-I-I-13 FRICTION COEFFICIENT - GENERALIZED REYNOLDS NUMBER

DATE OF THE EXPERIMENT= 3/ 12/ 71
CONCENTRATION OF THE SEPARAN SOLUTION= 0.10
PIPE DIAMETER (FT) = 0.0833
TEMPERATURE (FAR.) = 76.0

FLOW GAL/MIN	MANOMETER READINGS INCHES HG	FRICTION LOSS PSF	LENGTH (TAPS) FT	SHEAR STRESS AT WALL PSF	K OR VISCOSITY LB-SEC/SF	N	GENERALIZED REYNOLDS	FRICTION FACTOR
13.00	0.15	9.80	12.00	0.017	0.13E-02	0.646	5885.5	0.00062
27.50	1.33	86.93	12.00	0.150	0.10E-02	0.685	15370.6	0.00124
32.20	1.68	109.81	12.00	0.190	0.10E-02	0.689	18933.5	0.00114
32.20	1.05	68.63	6.00	0.238	0.99E-03	0.693	18977.5	0.00142
36.30	2.61	170.60	12.00	0.296	0.96E-03	0.697	22260.6	0.00139
36.30	1.21	79.09	6.00	0.274	0.97E-03	0.695	22234.6	0.00129
40.50	3.17	207.20	12.00	0.359	0.93E-03	0.700	25757.4	0.00136
40.50	1.40	91.51	6.00	0.317	0.95E-03	0.698	25700.9	0.00120
45.50	3.70	241.84	12.00	0.419	0.91E-03	0.703	30052.0	0.00126
45.50	1.79	117.00	6.00	0.406	0.92E-03	0.702	30031.7	0.00122
50.30	4.35	284.33	12.00	0.493	0.89E-03	0.706	34343.0	0.00121
50.30	2.10	137.26	6.00	0.476	0.89E-03	0.705	34315.7	0.00117
58.50	6.55	428.13	12.00	0.742	0.83E-03	0.712	42188.1	0.00135
58.50	3.13	204.59	6.00	0.710	0.84E-03	0.712	42131.9	0.00129
66.00	7.35	480.42	12.00	0.833	0.82E-03	0.714	49440.1	0.00119
66.00	3.57	233.35	6.00	0.809	0.82E-03	0.714	49396.9	0.00115
55.00	5.42	354.27	12.00	0.614	0.86E-03	0.709	38755.6	0.00126
55.00	2.75	179.75	6.00	0.623	0.86E-03	0.709	38770.8	0.00128

TABLE-I-I-13 FRICTION COEFFICIENT - GENERALIZED REYNOLDS NUMBER

DATE OF THE EXPERIMENT= 3/ 12/ 71
CONCENTRATION OF THE SEPARAN SOLUTION= 0.10
PIPE DIAMETER (FT) = 0.0833
TEMPERATURE (FAR.) = 76.0

FLOW GAL/MIN	MANOMETER READINGS INCHES HG	FRICTION LOSS PSF	LENGTH (TAPS) FT	SHEAR STRESS AT WALL PSF	K OR VISCOSITY LB-SEC/SF	N	GENERALIZED REYNOLDS	FRICTION FACTOR
44.00	3.57	233.35	12.00	0.404	0.92E-03	0.702	28752.0	0.00130
44.00	1.71	111.77	6.00	0.387	0.92E-03	0.701	28727.2	0.00124
33.50	2.42	158.18	12.00	0.274	0.97E-03	0.695	20024.9	0.00152
33.50	1.22	79.74	6.00	0.276	0.97E-03	0.696	20027.5	0.00153
26.50	1.73	113.08	12.00	0.196	0.10E-02	0.690	14672.7	0.00173
26.50	0.91	59.48	6.00	0.206	0.10E-02	0.691	14681.9	0.00182
21.00	1.32	86.28	12.00	0.149	0.10E-02	0.689	10782.7	0.00211
17.20	1.11	72.55	12.00	0.125	0.10E-02	0.682	8279.4	0.00264
29.50	1.95	127.46	12.00	0.221	0.10E-02	0.692	16908.6	0.00158
29.50	0.98	64.05	6.00	0.222	0.10E-02	0.692	16909.7	0.00158
36.20	2.86	186.94	12.00	0.324	0.95E-03	0.698	22216.4	0.00154
36.20	1.30	84.97	6.00	0.294	0.96E-03	0.697	22179.4	0.00140
42.40	3.45	225.50	12.00	0.391	0.92E-03	0.702	27383.5	0.00135
42.40	1.69	110.46	6.00	0.383	0.92E-03	0.701	27372.1	0.00132
50.00	4.37	285.64	12.00	0.495	0.89E-03	0.706	34081.8	0.00123
50.00	2.15	140.53	6.00	0.487	0.89E-03	0.705	34069.1	0.00121

TABLE-I-I-14 FRICTION COEFFICIENT - GENERALIZED REYNOLDS NUMBER

DATE OF THE EXPERIMENT= 3/ 12/ 71
CONCENTRATION OF THE SEPARAN SOLUTION= 0.10
PIPE DIAMETER (FT) = 0.2298
TEMPERATURE (FAR.) = 76.0

FLOW GAL/MIN	MANOMETER READINGS INCHES HG	FRICTION LOSS PSF	LENGTH (TAPS) FT	SHEAR STRESS AT WALL PSF	K OR VISCOSITY LB-SEC/SF	N	GENERALIZED REYNOLDS	FRICTION FACTOR
29.50	5.10	8.06	23.60	0.019	0.13E-02	0.649	2204.6	0.00813
69.00	11.95	18.90	23.60	0.046	0.12E-02	0.664	6945.6	0.00348
96.50	16.95	26.81	23.60	0.065	0.11E-02	0.670	10908.1	0.00252
145.50	30.20	47.76	23.60	0.116	0.10E-02	0.681	18987.4	0.00197
121.50	22.90	36.22	23.60	0.088	0.11E-02	0.676	14879.9	0.00215
97.00	17.35	27.44	23.60	0.066	0.11E-02	0.671	10987.1	0.00255
76.30	13.45	21.27	23.60	0.051	0.11E-02	0.666	7954.3	0.00320
60.20	9.93	15.70	23.60	0.038	0.12E-02	0.661	5776.7	0.00380
46.80	7.75	12.25	23.60	0.029	0.12E-02	0.656	4113.6	0.00490
35.80	6.05	9.56	23.60	0.023	0.12E-02	0.652	2864.5	0.00654
29.00	5.04	7.97	23.60	0.019	0.13E-02	0.648	2154.2	0.00831

TABLE-I-I-14 FRICTION COEFFICIENT - GENERALIZED REYNOLDS NUMBER

DATE OF THE EXPERIMENT= 3/ 12/ 71
CONCENTRATION OF THE SEPARAN SOLUTION= 0.10
PIPE DIAMETER (FT) = 0.2300
TEMPERATURE (FAR.) = 76.0

FLOW GAL/MIN	MANOMETER READINGS INCHES HG	FRICTION LOSS PSF	LENGTH (TAPS) FT	SHEAR STRESS AT WALL PSF	K OR VISCOSITY LB-SEC/SF	N	GENERALIZED REYNOLDS	FRICTION FACTOR
29.50	3.90	6.16	17.50	0.020	0.12E-02	0.649	2200.9	0.00842
69.00	8.50	13.44	17.50	0.044	0.12E-02	0.663	6930.5	0.00335
96.50	12.05	19.05	17.50	0.062	0.11E-02	0.670	10883.0	0.00243
145.50	21.85	34.56	17.50	0.113	0.10E-02	0.680	18945.4	0.00193
121.50	16.52	26.12	17.50	0.085	0.11E-02	0.675	14847.4	0.00210
97.00	12.30	19.45	17.50	0.063	0.11E-02	0.670	10961.1	0.00245
76.30	9.60	15.18	17.50	0.049	0.11E-02	0.666	7936.9	0.00309
60.20	6.98	11.04	17.50	0.036	0.12E-02	0.660	5764.2	0.00361
46.80	5.53	8.74	17.50	0.028	0.12E-02	0.656	4105.4	0.00474
35.80	4.40	6.95	17.50	0.022	0.12E-02	0.651	2859.2	0.00645
29.00	3.75	5.93	17.50	0.019	0.13E-02	0.648	2150.4	0.00838

TABLE-I-I-14 FRICTION COEFFICIENT - GENERALIZED REYNOLDS NUMBER

DATE OF THE EXPERIMENT= 3/ 12/ 71
CONCENTRATION OF THE SEPARAN SOLUTION= 0.10
PIPE DIAMETER (FT) = 0.2304
TEMPERATURE (FAR.) = 76.0

FLOW GAL/MIN	MANOMETER READINGS INCHES HG	FRICTION LOSS PSF	LENGTH (TAPS) FT	SHEAR STRESS AT WALL PSF	K OR VISCOSITY LB-SEC/SF	N	GENERALIZED REYNOLDS	FRICTION FACTOR
29.50	2.68	4.23	11.68	0.020	0.12E-02	0.650	2193.4	0.00874
69.00	5.52	8.73	11.68	0.043	0.12E-02	0.663	6904.5	0.00329
96.50	7.60	12.02	11.68	0.059	0.11E-02	0.669	10837.7	0.00231
145.50	14.15	22.38	11.68	0.110	0.10E-02	0.680	18869.4	0.00189
121.50	10.17	16.08	11.68	0.079	0.11E-02	0.674	14777.0	0.00195
97.00	7.70	12.17	11.68	0.060	0.11E-02	0.669	10914.3	0.00232
76.30	6.20	9.80	11.68	0.048	0.12E-02	0.665	7906.5	0.00302
60.20	4.48	7.08	11.68	0.034	0.12E-02	0.659	5742.5	0.00350
46.80	3.67	5.80	11.68	0.028	0.12E-02	0.655	4090.8	0.00475
35.80	2.98	4.71	11.68	0.023	0.12E-02	0.652	2849.3	0.00660
29.00	2.52	3.98	11.68	0.019	0.13E-02	0.649	2142.8	0.00850

TABLE-1-1-22 FRICTION COEFFICIENT - GENERALIZED REYNOLDS NUMBER

DATE OF THE EXPERIMENT= 3/ 22/ 71
CONCENTRATION OF THE SEPARAN SOLUTION= 0.01
PIPE DIAMETER (FT) = 0.0833
TEMPERATURE (FAR.) = 75.0

FLOW GAL/MIN	MANOMETER READINGS INCHES HG	FRICTION LOSS PSF	LENGTH (TAPS) FT	SHEAR STRESS AT WALL PSF	K OR VISCOSITY LB-SEC/SF	N	GENERALIZED REYNOLDS	FRICTION FACTOR
27.00	1.66	108.51	12.00	0.188	0.23E-04	1.000	76393.0	0.00160
27.00	0.74	48.37	6.00	0.167	0.23E-04	1.000	76393.1	0.00143
41.30	2.85	186.31	12.00	0.323	0.23E-04	1.000	116853.2	0.00117
41.30	1.54	100.67	6.00	0.349	0.23E-04	1.000	116853.1	0.00127
58.50	5.90	385.70	12.00	0.669	0.23E-04	1.000	165518.3	0.00121
58.50	2.82	184.35	6.00	0.639	0.23E-04	1.000	165518.2	0.00116
45.00	3.90	254.95	12.00	0.442	0.23E-04	1.000	127321.7	0.00135
45.00	1.88	122.90	6.00	0.426	0.23E-04	1.000	127321.9	0.00131
40.00	3.19	208.53	12.00	0.361	0.23E-04	1.000	113175.0	0.00140
40.00	1.68	109.82	6.00	0.381	0.23E-04	1.000	113174.9	0.00148
33.20	2.39	156.24	12.00	0.271	0.23E-04	1.000	93935.2	0.00153
33.20	1.20	78.44	6.00	0.272	0.23E-04	1.000	93935.1	0.00153

TABLE-I-I-16 FRICTION COEFFICIENT - GENERALIZED REYNOLDS NUMBER

DATE OF THE EXPERIMENT= 3/ 23/ 71
CONCENTRATION OF THE SEPARAN SOLUTION= 0.01
PIPE DIAMETER (FT) = 0.2290
TEMPERATURE (FAR.) = 74.0

FLOW GAL/MIN	MANOMETER READINGS INCHES HG	FRICTION LOSS PSF	LENGTH (TAPS) FT	SHEAR STRESS AT WALL PSF	K OR VISCOSITY LB-SEC/SF	N	GENERALIZED REYNOLDS	FRICTION FACTOR
95.00	16.57	26.21	23.60	0.063	0.23E-04	1.000	97774.1	0.00250
95.00	12.25	19.38	17.50	0.063	0.23E-04	1.000	97774.1	0.00249
95.00	7.97	12.60	11.68	0.061	0.23E-04	1.000	97774.1	0.00243
95.00	16.80	26.57	23.60	0.064	0.23E-04	1.000	97774.1	0.00253
95.00	12.49	19.76	17.50	0.064	0.23E-04	1.000	97774.2	0.00254
95.00	8.18	12.94	11.68	0.063	0.23E-04	1.000	97774.1	0.00249
95.00	17.20	27.21	23.60	0.066	0.23E-04	1.000	97774.1	0.00259
95.00	12.90	20.40	17.50	0.066	0.23E-04	1.000	97774.2	0.00262
95.00	8.46	13.38	11.68	0.065	0.23E-04	1.000	97774.1	0.00258

TABLE-I-I-17 FRICTION COEFFICIENT - GENERALIZED REYNOLDS NUMBER

DATE OF THE EXPERIMENT= 3/ 25/ 71
CONCENTRATION OF THE SEPARAN SOLUTION= 0.10
PIPE DIAMETER (FT) = 0.2290
TEMPERATURE (FAR.) = 74.0

FLOW GAL/MIN	MANOMETER READINGS INCHES HG	FRICTION LOSS PSF	LENGTH (TAPS) FT	SHEAR STRESS AT WALL PSF	K OR VISCOSITY LB-SEC/SF	N	GENERALIZED REYNOLDS	FRICTION FACTOR
27.50	4.70	7.43	23.60	0.018	0.13E-02	0.647	2018.8	0.00847
97.00	16.82	26.61	23.60	0.064	0.11E-02	0.670	11057.1	0.00243
163.00	32.42	51.29	23.60	0.124	0.10E-02	0.682	22236.2	0.00166
163.00	31.87	50.42	23.60	0.122	0.10E-02	0.681	22228.1	0.00163
163.00	32.42	51.29	23.60	0.124	0.10E-02	0.682	22236.2	0.00166
180.00	37.06	58.63	23.60	0.142	0.10E-02	0.684	25414.8	0.00156
26.40	4.80	7.59	23.60	0.018	0.13E-02	0.647	1910.5	0.00939
11.00	2.90	4.58	23.60	0.011	0.13E-02	0.638	581.2	0.03269
5.00	1.75	2.76	23.60	0.006	0.13E-02	0.628	197.4	0.09548
27.50	3.78	5.98	17.50	0.019	0.13E-02	0.648	2019.3	0.00919
97.00	11.93	18.87	17.50	0.061	0.11E-02	0.669	11050.5	0.00233
163.00	22.24	35.18	17.50	0.115	0.10E-02	0.680	22200.6	0.00154
163.00	22.22	35.15	17.50	0.115	0.10E-02	0.680	22200.3	0.00153
163.00	22.60	35.75	17.50	0.116	0.10E-02	0.681	22207.7	0.00156
180.00	26.02	41.16	17.50	0.134	0.10E-02	0.683	25383.6	0.00147
26.40	3.52	5.56	17.50	0.018	0.13E-02	0.647	1910.4	0.00929
11.00	2.19	3.46	17.50	0.011	0.13E-02	0.638	581.2	0.03330
5.00	1.41	2.23	17.50	0.007	0.13E-02	0.630	197.5	0.10377
97.00	7.32	11.58	11.68	0.056	0.11E-02	0.668	11039.7	0.00214
163.00	13.77	21.78	11.68	0.106	0.11E-02	0.679	22169.3	0.00142

TABLE-I-I-17 FRICTION COEFFICIENT - GENERALIZED REYNOLDS NUMBER

DATE OF THE EXPERIMENT= 3/ 25/ 71
CONCENTRATION OF THE SEPARAN SOLUTION= 0.10
PIPE DIAMETER (FT) = 0.2290
TEMPERATURE (FAR.) = 74.0

FLOW GAL/MIN	MANOMETER READINGS INCHES HG	FRICTION LOSS PSF	LENGTH (TAPS) FT	SHEAR STRESS AT WALL PSF	K OR VISCOSITY LB-SEC/SF	N	GENERALIZED REYNOLDS	FRICTION FACTOR
163.00	13.77	21.78	11.68	0.106	0.11E-02	0.679	22169.3	0.00142
163.00	13.78	21.80	11.68	0.106	0.11E-02	0.679	22169.6	0.00142
180.00	15.81	25.01	11.68	0.122	0.10E-02	0.681	25334.1	0.00134
26.40	2.50	3.95	11.68	0.019	0.13E-02	0.648	1910.9	0.00988

TABLE-I-I-18 FRICTION COEFFICIENT - GENERALIZED REYNOLDS NUMBER

DATE OF THE EXPERIMENT= 3/ 25/ 71
CONCENTRATION OF THE SEPARAN SOLUTION= 0.10
PIPE DIAMETER (FT) = 0.2298
TEMPERATURE (FAR.) = 74.0

FLOW GAL/MIN	MANOMETER READINGS INCHES HG	FRICTION LOSS PSF	LENGTH (TAPS) FT	SHEAR STRESS AT WALL PSF	K OR VISCOSITY LB-SEC/SF	N	GENERALIZED REYNOLDS	FRICTION FACTOR
27.50	4.60	7.27	23.60	0.017	0.13E-02	0.647	2004.3	0.00844
97.00	16.72	26.45	23.60	0.064	0.11E-02	0.670	10980.3	0.00246
163.00	32.32	51.13	23.60	0.124	0.10E-02	0.682	22085.4	0.00168
163.00	31.77	50.26	23.60	0.122	0.10E-02	0.681	22077.3	0.00165
163.00	32.32	51.13	23.60	0.124	0.10E-02	0.682	22085.4	0.00168
180.00	36.96	58.47	23.60	0.142	0.10E-02	0.684	25243.4	0.00158
26.40	4.70	7.43	23.60	0.018	0.13E-02	0.647	1896.7	0.00936
11.00	2.80	4.42	23.60	0.010	0.13E-02	0.637	576.9	0.03212
5.00	1.65	2.61	23.60	0.006	0.13E-02	0.627	195.9	0.09161

TABLE-I-I-18 FRICTION COEFFICIENT - GENERALIZED REYNOLDS NUMBER

DATE OF THE EXPERIMENT= 3/ 25/ 71
CONCENTRATION OF THE SEPARAN SOLUTION= 0.10
PIPE DIAMETER (FT) = 0.2300
TEMPERATURE (FAR.) = 74.0

FLOW GAL/MIN	MANOMETER READINGS INCHES HG	FRICTION LOSS PSF	LENGTH (TAPS) FT	SHEAR STRESS AT WALL PSF	K OR VISCOSITY LB-SEC/SF	N	GENERALIZED REYNOLDS	FRICTION FACTOR
27.50	3.68	5.82	17.50	0.019	0.13E-02	0.648	2001.1	0.00915
97.00	11.83	18.71	17.50	0.061	0.11E-02	0.669	10954.5	0.00236
163.00	22.14	35.02	17.50	0.115	0.10E-02	0.680	22012.1	0.00156
163.00	22.12	34.99	17.50	0.114	0.10E-02	0.680	22011.7	0.00156
163.00	22.50	35.59	17.50	0.116	0.10E-02	0.681	22019.2	0.00159
180.00	25.92	41.00	17.50	0.134	0.10E-02	0.683	25169.3	0.00150
26.40	3.42	5.41	17.50	0.017	0.13E-02	0.647	1893.2	0.00922
11.00	2.09	3.30	17.50	0.010	0.13E-02	0.637	575.9	0.03248
5.00	1.31	2.07	17.50	0.006	0.13E-02	0.629	195.6	0.09853

TABLE-I-I-18 FRICTION COEFFICIENT - GENERALIZED REYNOLDS NUMBER

DATE OF THE EXPERIMENT= 3/ 25/ 71
CONCENTRATION OF THE SEPARAN SOLUTION= 0.10
PIPE DIAMETER (FT) = 0.2304
TEMPERATURE (FAR.) = 74.0

FLOW GAL/MIN	MANOMETER READINGS INCHES HG	FRICTION LOSS PSF	LENGTH (TAPS) FT	SHEAR STRESS AT WALL PSF	K OR VISCOSITY LB-SEC/SF	N	GENERALIZED REYNOLDS	FRICTION FACTOR
97.00	7.22	11.42	11.68	0.056	0.11E-02	0.668	10905.4	0.00217
163.00	13.67	21.62	11.68	0.106	0.11E-02	0.679	21905.4	0.00146
163.00	13.67	21.62	11.68	0.106	0.11E-02	0.679	21905.4	0.00146
163.00	13.68	21.64	11.68	0.106	0.11E-02	0.679	21905.6	0.00146
180.00	15.71	24.85	11.68	0.122	0.10E-02	0.681	25034.1	0.00137
26.40	2.40	3.79	11.68	0.018	0.13E-02	0.648	1886.8	0.00977

FIN